A Relativistic Treatment of Atoms and Molecules

From Relativity to Electroweak Interaction

A thesis submitted in partial fulfillment of the requirements
of the degree of
Doctor of Philosophy

in

Theoretical Physics

at

Massey University Auckland
New Zealand

Christian Thierfelder
2009

Abstract

Relativistic quantum chemistry is the relativistic formulation of quantum mechanics applied to many-electron systems, that is to atoms, molecules and solids. It combines the principles of special relativity, which are obeyed by any fundamental physical theory, with the basic rules of quantum mechanics. By construction, it represents the most fundamental theory of all molecular sciences, which describes matter by the action, interaction and motion of the elementary particles. This science is of vital importance to physicists, chemists, material scientists, and biologists with a molecular view of the world.

A full relativistic treatment of atoms and molecules which includes the quantization of the electromagnetic field is currently one of the most challenging tasks in electronic structure theory. Therefore, relativistic effects in atoms and molecules were studied computationally. A combination of wave function and density functional based methods within a correct relativistic framework proved necessary to achieve accurate results of various atomic and molecular properties. The first part of this thesis deals with investigations in atomic systems including quantum electrodynamic effects in the ionization potentials of a large number of elements. K-shell and L-shell ionizations potentials for ^{268}Mt were calculated and static dipole polarizabilities of the neutral group 14 elements were investigated. The second part concentrates on molecular systems including superheavy element monohydrides up to 120H^{+}). In particular, the chemical bonding of the superheavy elements 119 and 120 are investigated for the first time. Electric field gradients of a number of gold and copper compounds were also calculated and the nuclear quadrupole moment of gold and copper determined in good agreement with experiment. Finally, the parity violation energy difference in the chiral molecule bromochlorofluoromethane (CHFClBr) was investigated by relativistic coupled-cluster theory to provide benchmark results for all future investigations in this field.

Acknowledgements

First and foremost, I would like to thank my supervisor Prof. Peter Schwerdtfeger for his multi-level support over the last four years, which were filled with scientific discussions, a lot of work and Friday afternoon BBQs.

My special thanks goes to Prof. Wolf Gero Schmidt for his interesting idea of doing a PhD on the opposite side of the world.

I wish to thank all the members of the Centre for Theoretical Chemistry and Physics for fruitful discussions and nice coffee breaks. Furthermore I thank Detlev for nice discussions, the awesome quiz-nights and all the useful trivia knowledge I learned there. I would like to thank Dr. Ben Jebus for sharing his wisdom and reminding me to observe things always from different angles. Anton and Philip I thank for the best Thursday and Saturday nights in town ever.

I am grateful for the hospitality provided by Prof. Trond Saue, Prof. Luuk Visscher and Dr. Jacinda Ginges during my research stays in Strasbourg, Amsterdam and Sydney.

Finally I wish to thank my family, my friends, and Martina, without you I am nothing - I silently thank you for your support and understanding!

Table of Contents

Abbreviations

BI	Breit interaction
BSSE	basis set superposition error
CC	coupled-cluster
CCSD	coupled-cluster singles and doubles
CI	configuration interaction
CIS	configuration interaction singles
CISD	configuration interaction singles and doubles
DFT	density functional theory
DHF	Dirac-Hartree-Fock
DK	Douglas-Kroll
DKS	Dirac-Kohn-Sham
EFG	electric field gradient
FCI	full configuration interaction
FSCC	Fock-space coupled-cluster
GGA	generalized gradient approximation
GTO	Gaussian-type orbitals
HF	Hartree-Fock
LDA	local density approximation
MCSCF	multi-configurational Hartree-Fock
MP2	second-order Møller-Plesset perturbation theory
NR	non-relativistic
NQM	nuclear quadrupole moment
NQCC	nuclear quadrupole coupling constant
PNC	parity non-conservation
PV	parity violation
PVED	parity violation energy difference
QED	quantum electrodynamics

RKB	restricted kinetic balance
SE	self-energy
SHE	superheavy element
TDDFT	time-dependent density functional theory
UKB	unrestricted kinetic balance
VP	vacuum polarization
XC	exchange-correlation

Chapter 1

Introduction and Overview

Although Dirac himself, at the time he published his famous relativistic wave equation, wrote that [1],

> "The general theory of quantum mechanics is now almost complete, the imperfections that still remain being in connection with the exact fitting in of the theory with relativity ideas. This give rise to difficulties only when high-speed particles are involved, and are *therefore of no importance in the consideration of atomic and molecular structure and ordinary chemical reactions*, in which it is, indeed, usually sufficiently accurate if one neglects relativity variation of mass with the velocity and assumes only Coulomb forces between the various electrons and atomic nuclei."

it is now a well established fact [2–4], that one often needs to account for relativistic effects in quantum theoretical calculations of atoms and molecules. For molecules containing heavy atoms, non-relativistic calculations will not even give qualitatively correct results [4], and even for molecules containing light atoms relativity is needed for very precise calculations [5].

With the term "*relativistic effect*" one means the difference between the approximative physical description using a non-relativistic model and the more correct relativistic description. This difference is just the result of applying different physical models and has no connection to reality, as there is no non-relativistic molecule, but there are molecules which can be described sufficiently by a non-relativistic model.

The goal of this thesis was to study relativistic effects in heavy and superheavy elements. For example in chapter 5, the influence of relativistic effects on the static dipole-polarizability of group 14 elements is discussed. It is shown that the spin-orbit effect is negligible for the lighter elements but becomes essential for Pb as spin-orbit coupling reduces the polarizability by 20%. And in chapter 7, the electrical-field gradients of copper- and gold-halides were calculated, showing the importance of relativistic effects.

The relativistic effects in superheavy elements ($Z > 90$) are even more dramatic. Superheavy element (SHE) research faces currently one of the biggest experimental and theoretical challenges [6]. This multidisciplinary field combines nuclear physics, atomic physics, theoretical physics, chemistry and quantum chemistry with state-of-the-art computational and engineering methods. The earliest studies of the atomic and chemical properties of the heaviest actinides led to unmatched scientific discoveries: chemical analysis of the first attempts to create superheavy elements led - at first - to the discovery of nuclear fission [7,8]. Later, systematic investigations of fission fragments led - in turn - to the discovery of the first trans-uranium elements [9, 10] and opened up the way for the synthesis of superheavy elements. The production of ever heavier elements and the investigation of their nuclear structure are unique tools to improve the understanding of nuclear matter and nuclear forces under extreme conditions. In addition valuable information is added to the knowledge of stellar nuclear synthesis - the mechanism for the creation of the chemical elements found on earth.

Chemical characterization of the nuclear reaction products was at first crucial for the element identification. Later, it was replaced by the observation of correlations between recoil-nuclei and subsequent α-decay chains. Today, both approaches are being combined and are supported by relativistic nuclear and electronic structure calculations to face the demanding challenge of unambiguous isotope identification, as has been demonstrated very recently for superheavy elements up to nuclear charge 114 [11]. Due to the development of powerful laser systems during the last decades, atomic physics methods have also gained importance in this field as well. These investigations aim for a better understanding of the electronic structure in the strong nuclear fields of the heaviest elements and yield information on their atomic and nuclear properties.

Superheavy elements can only be produced in nuclear fusion reactions at heavy ion accelerators at rates around one atom a day [12]. Typical half life times in the order of milliseconds hamper any attempt to produce macroscopic- and thus visible amounts of the heaviest members of the periodic table. Combining methods for production, stopping and cooling of single superheavy ions may not only render these elements visible but may also pave the way for precision spectroscopy with ultracold ions which have been inaccessible so far. But for the interpretation of the spectroscopic data, accurate relativistic structure calculations are essential to assist and improve the experiment.

In chapter 4 calculated, K- and L-shell ionization potentials of the superheavy element Meitnerium are shown and discussed. This was motivated by the observation of a 155 keV photon in a nuclear decay chain at the GSI in Darmstadt. Experimentalists explained this by a possible X-ray transition during the decay process. Therefore a Dirac-Hartree-Fock study was performed to gain more insight into the X-ray transitions of Meitnerium. Properties of superheavy hydrides are discussed in detail in chapter 6.

To obtain extremely high precision results for atomic properties one has to go beyond relativistic quantum mechanics and use quantum electrodynamics (QED), the relativistic quantum field theory of the interaction of charged particles and photons. The predictions of the theory are in remarkably good agreement with the results of experiments [13–15].

The basic structure of QED is quite the same as it was soon after the initial formulation of renormalization methods in the late 1940s [16–18], and applications to bound-state problems in the 1950s [19–23]. Since then, QED has been well established and has provided the underpinnings of the theory of a wide range of phenomena ranging from properties of single particles [14] to complex atoms [24], materials [25] and even chemical problems [26]. However, practical computational difficulties have limited direct applications of the theory to only the most simple systems. Even in one-electron atoms, the calculations based on QED are formidable tasks, but often necessary to make predictions that are correct at the level of precision of current experiments.

In recent years, this situation has been changing, and the domain of practical applications of QED has been expanding rapidly. New techniques in non-perturbative studies of QED have been successful not only in improving the precision of cal-

culations, but also in expanding the practical range of applicability, particularly to highly ionized atoms and inner levels of heavy neutral atoms, where predictions are necessary to interpret experimental results quantitatively.

Quantum electrodynamics is one of the most well tested theories in physics. However, despite the enormous success of QED in predicting the properties of electrons in weak external fields, the theory is not tested very well in the strong field limit. Thus, one of the primary goals in future research is to explore the behavior of electrons in some of the strongest electromagnetic fields accessible to experimental investigation. For instance, the electric field strength at the surface of a uranium nucleus with a radius of 7.42 fm, which amounts to $E \simeq 2 \times 10^{19}$ V/cm, or the field of the magnetic moment of the nucleus $^{209}_{83}$Bi at the nuclear surface that gives a maximum magnetic field strength of about $B = 10^{12}$ Gauss.

Electrons in innermost bound states experience the largest overlap with this strong field domain. Precision measurements of electron binding energies and transition rates are best suited to deduce characteristic QED phenomena in intense fields. The binding energy of a single K-shell electron in the Coulomb field of a uranium nucleus amounts to about 132 keV, which corresponds to roughly one third of the electron rest mass. In this case, the radial expectation value of the 1s wave function, $\langle r \rangle_{1s} = 715$ fm, is the same order of magnitude as the Compton wavelength of the electron.

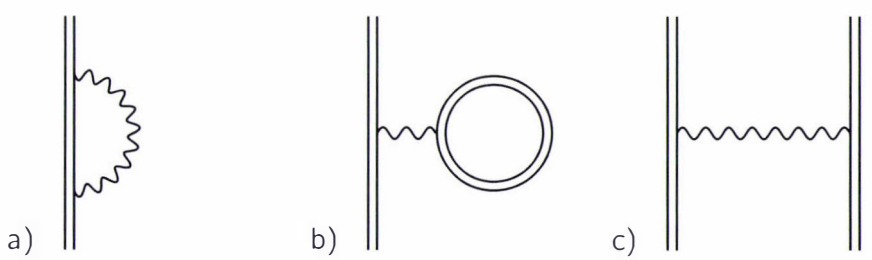

Figure 1.1: Lowest order Feynman diagrams for the self-energy (a), vacuum polarization (b) and the Breit interaction (c) of bound electrons.

The fundamental processes under consideration are depicted by the Feynman diagrams in Fig. 1.1. The double lines denote the motion of the electron in the external Coulomb field of the nucleus. Here the Furry picture [27] is adopted in which the interaction with the external potential is incorporated in the wave function and the propagator from the very beginning. Hence, plane waves or free

propagators, which do not account for the external potential, are avoided.

Part (a) in Fig. 1.1 indicates the self-energy, where a photon is emitted and reabsorbed again by the bound electron. Due to the relatively small mass of the electron, this virtual process of the bound particle dominates the QED level shift in hydrogen-like atoms. Part (b) reflects the vacuum polarization where the photon mediating the interaction between the electron and the nucleus virtually generates an electron-positron pair. For an impression concerning the importance of both radiative processes one considers the associated energy shift for a K-shell electron in hydrogen-like uranium. The sum of the vacuum polarization and self-energy correction amounts to 266 eV which should be compared with the total 1s binding energy of 132 keV. The current experimental uncertainty sums up to 16 eV [28], while future precision measurements may lower this boundary down to 0.1 eV.

Traditionally, QED corrections are treated in a perturbation expansion in the fine structure constant $\alpha \simeq 1/137$ representing the number of virtual photons. Superimposed on this, one considers in every order in α an additional expansion in $Z\alpha$, the coupling constant to the external field with nuclear charge number Z. An essential aspect of strong-field bound state quantum electrodynamics is the avoidance of any expansion in $Z\alpha$ in order to incorporate the external field exactly.

The determination of radiative corrections in atomic states started in 1935 when Uehling published his calculation of the lowest-order vacuum polarization [29]. In 1947 Lamb and Retherford detected the splitting of the $2p_{1/2}$ and the $2s_{1/2}$ states in hydrogen which initiated extensive developments in theoretical research on QED corrections in atoms [30].

The investigation of QED effects in many electron atoms was another goal of this thesis used later in the work for Meitnerium. In chapter 3, a semi-empirical radiative potential for the self-energy is discussed, which was implemented into the program package GRASP. The vacuum-polarization and self-energy contribution as well as the Breit interaction to the ionization potential were calculated for all group 1, 2, 11, 12, 13 and 18 atoms.

For an understanding of chemistry, fundamental forces other than the electromagnetic force (namely the gravitational, strong, and weak force) can usually be safely neglected. It is nevertheless very tempting, albeit extremely challenging,

to try to observe the influence of the weak interaction on molecular systems directly, as this would enable low energy tests of the weak interaction [31]. This extremely weak and short-ranged interaction is of particular interest since it shows preference for particle helicity, for instance involving almost exclusively left-handed electrons [32]. As nicely shown by Wu et al. in the β-decay of cobalt radionuclides [33] the weak interaction breaks parity symmetry as first proposed by Lee and Yang [34]. As a consequence of this parity symmetry breakdown, commonly called parity-violation (PV), the two "enantiomers" of a chiral molecule become strictly speaking diastereomers, thus causing a small energy difference between them.

The main obstacle for the observation of PV effects is its tininess. For instance, in the case of aminoacids, the theoretical PV energy difference (PVED) between the two enantiomers is on the order of 10^{-16}kJ mol^{-1} [35, 36] which, combined with its significant variation as a function of molecular structure, precludes any direct link between PV and biohomochirality unless a convincing amplification mechanism can be found [37–39]. To measure such minute energy differences furthermore calls for very accurate experiments which have to be dedicated solely to its observation. Only a few scientific groups in the world have performed experiments aiming at detecting PV effects in molecular systems, but with no clear-cut success so far [40–42].

A promising new experimental setup has been proposed by Chardonnet and coworkers [42,43]. It aims at detecting PV vibrational transition frequency difference by molecular beam spectroscopy using a two-photon Ramsey-fringes experiment. A sensitivity of 0.01 Hz is expected, but the choice of the candidate molecule and the preparation of its enantiomers are crucial for any successful experiment. The ideal candidate chiral molecule for the experiment should: (i) be available in large enantiomeric excess or, ideally, in enantiopure form; (ii) show a large PV frequency difference of an intense fundamental transition ideally within the CO_2 laser operating range (850 -1120 cm^{-1}); (iii) not be too bulky since the sensitivity of the experiment will be largely determined by the partition function of the molecules in a supersonic beam where the internal degrees of freedom are frozen down to about 1 K; (iv) avoid nuclei with quadrupolar moments; and (v) preferably sublimate without decomposition for injection into the Fabry-Perot cavity of the experiment, although laser ablation techniques may also be envisaged.

Prior to 2002 small organic chiral molecules such as aminoacids, chiral conformations of hydroperoxides [44, 45] or heterohalogenomethanes [43, 46–48] were extensively studied. Among the latter, bromochlorofluoromethane (CHFClBr) has drawn particular attention due to its structural simplicity [49]. However, such a chiral molecule, although a good model, shows a calculated PV too small [48, 50, 51] (a few mHz) to be clearly observed considering today's best experimental resolution of around 1 Hz [52]. Recently, chiral halogenated adamantanes and cubanes have been synthesized, but they were found to show very low PV effects [53].

Since 2002, chiral metal transition complexes bearing heavy atoms have attracted particular interest. Considering that the PVED scales approximately as Z^5 (where Z is the atomic number) [54–57], theoretical studies clearly favor chiral compounds with a heavy atom at or near the stereochemical center for large PV effects. Indeed, chiral gold, mercury, iridium, osmium and rhenium complexes were calculated to be favorable candidates for PV observation by Schwerdtfeger and co-workers [58–60], as well as bismuth compounds by Lazzeretti and coworkers [61]. The aim of the last chapter is actually to calculate the PVED of the molecule CHFClBr at the coupled-cluster level of theory, which will serve as a future benchmark reference value.

Layout of this thesis

The thesis presented here is divided into three parts:

1. The first part gives an introduction to the methodology, starting from relativistic quantum mechanics (chapter 2.1), followed by a detailed discussion of quantum theoretical approximations (chapter 2.4).

2. The second part deals with atomic systems. In chapter 3, calculations of the K-shell and L-shell ionizations potentials of Meitnerium are presented. Then results of quantum-electrodynamic calculations of bound state QED, obtained by implementing a new effective potential for the electron self-energy into the program package GRASP, (chapter 4) are shown. In chapter 5, the spin-orbit effects of the static dipole polarizability of group 14 elements are investigated by relativistic coupled-cluster calculations.

3. The third part is assigned to molecular systems. In chapter 6, molecular properties of superheavy hydrides are calculated by density functional theory and the influence of relativistic effects are discussed. Electrical field gradients of coinage metal halides, which were used to calculate precise nuclear quadrupole moments of ^{63}Cu and ^{197}Au, are presented in chapter 7. Finally, in chapter 8, parity violation effects due to electroweak interactions in the molecule CHFClBr are calculated at the coupled-cluster level of theory by utilizing the finite-field method for the parity violation operator.

Chapter 2

Theory and Methodology

In this thesis, electronic properties of atoms and molecules are studied by theoretical methods within a relativistic framework. For a correct but yet computationally feasible description of these quantum systems, a variety of different methods and approximations have to be applied. This chapter gives a short overview on the applied methods. A more detailed description can be found in standard references and textbooks on electronic structure theory [62–67].

2.1 The Dirac Equation

The quantum mechanical equation describing the relativistic motion of a single electron of mass m in a stationary state and a fixed external field V may be written as

$$\hat{H}\psi = E\psi, \tag{2.1}$$

where $\hat{H}$ is the Dirac Hamiltonian (in SI units)

$$\hat{H} = c\vec{\alpha} \cdot \vec{p} + mc^2\beta + V \tag{2.2}$$

In equation (2.1), the eigenfunction ψ is a four-component spinor that contains two large components (L), which passes to the corresponding non-relativistic wave functions for the two possible spin orientations in the limit $c \to \infty$ for the velocity

of light, and two small components (S) which vanish in the non-relativistic limit.

$$\psi = \begin{pmatrix} \psi^L \\ \psi^S \end{pmatrix} = \begin{pmatrix} \psi_1^L \\ \psi_2^L \\ \psi_1^S \\ \psi_2^S \end{pmatrix}. \tag{2.3}$$

The Hamiltonian given in (2.2) is a matrix operator in which $\vec{p}$ is a three-vector whose elements corresponds to the components of the momentum $p_i = -i\hbar\partial_i$ $(i = x, y, z)$. Thus, in coordinate representation, $\vec{\alpha}$ is a three-vector whose elements are the matrices

$$\alpha_x = \begin{pmatrix} 0 & 0 & 0 & 1 \\ 0 & 0 & 1 & 0 \\ 0 & 1 & 0 & 0 \\ 1 & 0 & 0 & 0 \end{pmatrix} = \begin{pmatrix} 0 & \sigma_x \\ \sigma_x & 0 \end{pmatrix}, \tag{2.4}$$

$$\alpha_y = \begin{pmatrix} 0 & 0 & 0 & -i \\ 0 & 0 & i & 0 \\ 0 & -i & 0 & 0 \\ i & 0 & 0 & 0 \end{pmatrix} = \begin{pmatrix} 0 & \sigma_y \\ \sigma_y & 0 \end{pmatrix}, \tag{2.5}$$

$$\alpha_z = \begin{pmatrix} 0 & 0 & 1 & 0 \\ 0 & 0 & 0 & -1 \\ 1 & 0 & 0 & 0 \\ 0 & -1 & 0 & 0 \end{pmatrix} = \begin{pmatrix} 0 & \sigma_z \\ \sigma_z & 0 \end{pmatrix}. \tag{2.6}$$

The components of $\vec{\alpha}$ may be written in terms of the Pauli spin matrices

$$\sigma_x = \begin{pmatrix} 0 & 1 \\ 1 & 0 \end{pmatrix}, \tag{2.7}$$

$$\sigma_y = \begin{pmatrix} 0 & -i \\ i & 0 \end{pmatrix}, \tag{2.8}$$

$$\sigma_z = \begin{pmatrix} 1 & 0 \\ 0 & -1 \end{pmatrix}. \tag{2.9}$$

which satisfy the commutation relations

$$[\sigma_i, \sigma_j] = 2i\epsilon_{ijk}\sigma_k \tag{2.10}$$

β is the matrix

$$\beta = \begin{pmatrix} \sigma_0 & 0 \\ 0 & -\sigma_0 \end{pmatrix} = \begin{pmatrix} 1 & 0 & 0 & 0 \\ 0 & 1 & 0 & 0 \\ 0 & 0 & -1 & 0 \\ 0 & 0 & 0 & -1 \end{pmatrix}. \tag{2.11}$$

where σ_0 is the 2×2 unit matrix. The Dirac equation reads than

$$\begin{aligned} V\psi^L &+ c(\vec{\sigma}\cdot\vec{p})\psi^S &= E\psi^L \\ c(\vec{\sigma}\cdot\vec{p})\psi^L &+ (V - 2mc^2)\psi^S &= E\psi^S. \end{aligned} \tag{2.12}$$

The eigenvalue spectrum (shifted by $-mc^2$) is shown schematically in Fig. 2.1. It is made up of two parts. The first, in the interval $(-\infty, -2mc^2)$, corresponds to the negative energy states, and the second, in the interval $(0, +\infty)$, to the positive energy states.

The solutions with a positive energy describe the electronic continuum. The states with an energy below $-2mc^2$ describe the "positronic" continuum. However, their presence is intolerable, as they make all positive energy states unstable in the final analysis. The presence of negative energy states has been discussed intensively in the literature and a proper description is only obtained in the framework of quantum-electrodynamics.

2.1.1 The Dirac-Coulomb problem

In a first approximation, the energy levels of one-electron atoms are given by the solutions of the Schrödinger equation for an electron in the field of an infinitely heavy Coulomb center with charge Z

$$E_n = -\frac{1}{2}mc^2\frac{(Z\alpha)^2}{n^2}, \tag{2.13}$$

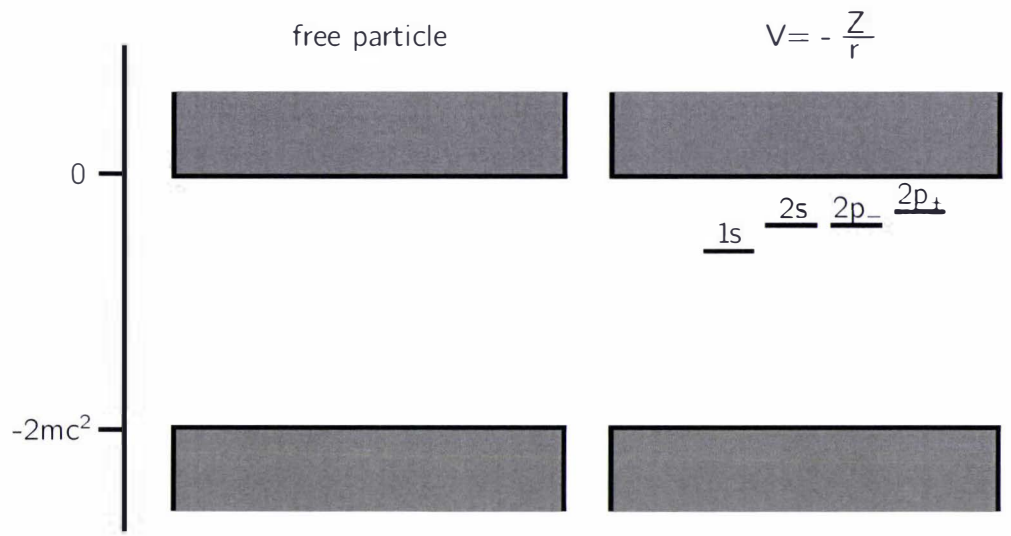

Figure 2.1: Spectrum of a free Dirac particle and the Dirac-Coulomb problem

where n is called the principal quantum number. Each state is completely described by the principal quantum number, the value of the angular momentum l and the projection of the angular momentum m_l. In the non-relativistic Coulomb problem all states with the same principal quantum number have exactly the same energy which means that the energy levels of the Schrödinger equation in the Coulomb field are n-fold degenerate with respect to the angular momentum quantum number. As in any spherically symmetric problem, the energy levels in a Coulomb field do not depend on the projection of the orbital angular momentum, and each energy level with given l is additionally $2l + 1$-fold degenerate. The relativistic dependence of the energy of a free classical particle on its momentum is given by the relativistic square root

$$\sqrt{m^2c^4 + p^2c^2} = mc^2 + \frac{p^2}{2m} - \frac{p^4}{8m^3c^2} + \ldots \tag{2.14}$$

The kinetic energy operator in the Schrödinger equation corresponds to the second term of this non-relativistic series expansion, and thus the Schrödinger equation describes only the leading non-relativistic approximation to the hydrogen energy levels.

A proper description of all relativistic corrections to the energy levels is given by the Dirac equation with a Coulomb source. All relativistic corrections may easily

be obtained from the exact solution of the Dirac equation in an external Coulomb field

$$
\begin{aligned}
E_{nj} &= mc^2 \left(1 + \frac{(Z\alpha)^2}{(\sqrt{(j+\frac{1}{2})^2 - (Z\alpha)^2} + n - j - \frac{1}{2})^2} \right)^{-\frac{1}{2}} \\
&= mc^2 - \frac{mc^2(Z\alpha)^2}{2n^2} - \frac{mc^2(Z\alpha)^4}{2n^3} \left(\frac{1}{j+\frac{1}{2}} - \frac{3}{4n} \right) \\
&\quad - \frac{mc^2(Z\alpha)^6}{2n^4} \left(\frac{1}{(j+\frac{1}{2})^3} + \frac{3}{n(j+\frac{1}{2})^2} + \frac{5}{2n^3} + \frac{6}{n^2(j+\frac{1}{2})} \right) + \ldots,
\end{aligned}
\tag{2.15}
$$

where $j = 1/2, 3/2, \ldots, n - 1/2$ is the total angular momentum of the state.

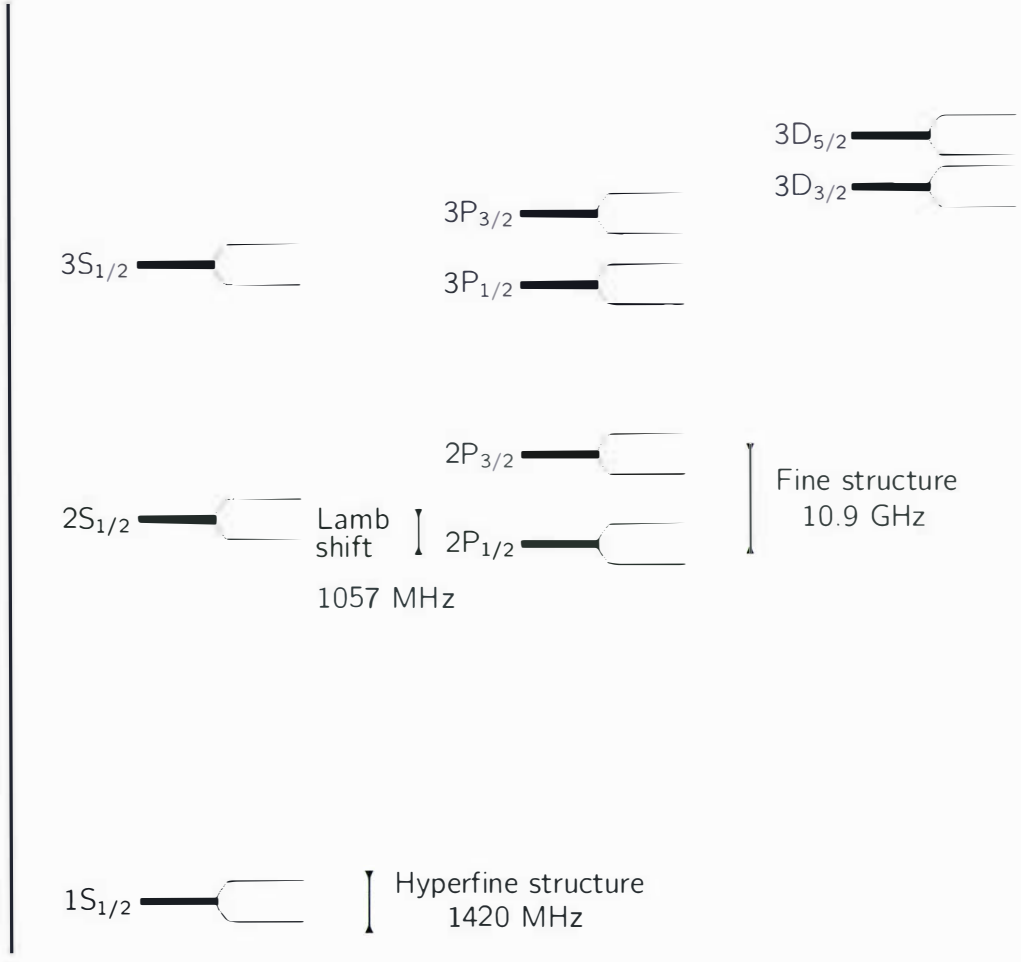

Figure 2.2: Low-lying energy levels of hydrogen

The main difference of the Dirac spectrum (Fig. 2.2) compared to the non-relativistic one is that the energy levels with the same principal quantum number but different total angular momentum are split into n components of the fine structure. However, not all degeneracy is lifted: the energy levels corresponding to the same n and j but different $l = j \pm 1/2$ values remain doubly degenerated.

This degeneracy is lifted by the corrections connected to the finite size of the Coulomb source, recoil contributions and by the dominating QED loop contributions. The respective energy shifts are called Lamb shift.

The magnetic moment of the heavy nucleus is completely ignored in the Dirac equation and hence the hyperfine splitting of the energy levels is missing in this spectrum.

2.2 The Many-Electron Problem

As atoms and molecules are composed of electrons and atomic nuclei, a correct description of such systems requires a complete picture of all mutual interactions, but it is clear that such a description can only be approximate. Let us briefly review the approximations involved.

First, the Born-Oppenheimer approximation is inherently incompatible with the theory of special relativity since it singles out a preferred reference frame, namely the frame in which nuclei can be treated as stationary sources of external fields. Relativistic corrections to the nuclear motion are, however, expected to be very small. The advantage of the Born-Oppenheimer approximation is that it reduces the complexity of the molecular description and allows to focus on the electronic degrees of freedom. The eigenvalues of the electronic Hamiltonian defined by the Born-Oppenheimer approximation are assumed to vary smoothly as a function of nuclear coordinates. This leads to the concept of molecular potential energy surfaces.

Second, all hyperfine effects are neglected, which leads to a time reversal symmetric Hamiltonian.

Third, the description of even a single electron in the molecular field leads to a many-body problem due to the possible creation of virtual electron-positron pairs. The proper treatment of the problem can only be obtained within the

framework of QED, which allows the number of particles in the system to vary. One can avoid to work with the full mathematical machinery of QED by invoking the no-pair approximation, which means to neglect all pair creations. Therefore one remains within the framework of Dirac's hole theory with the Dirac sea of negative energy electrons at all times completely filled. It corresponds to working with classical fields and implies neglect of QED effects, such as self energy and vacuum polarization, which represent the interaction of the electron with the zero-point fluctuations of the quantized electromagnetic and Dirac fields, respectively.

The use of the Dirac Hamiltonian as a relativistic substitute for the one electron terms in the non-relativistic many-body Hamiltonian yields the Dirac-Coulomb Hamiltonian [68]. This Hamiltonian can be utilized in conjunction with a Hartree-Fock like wave-function in what is known as the Dirac-Hartree-Fock (DHF) method, which has a special status in quantum chemistry. It is often used to benchmark relativistic effects in the absence of electron correlation. Such benchmark calculations provide an estimate of accuracy of more approximate methods, which attempt to include relativistic effects as a perturbation of the non-relativistic Hartree-Fock case, as well as methods which employ transformed, simplified versions of the Dirac-Coulomb Hamiltonian [69].

The capability of the Dirac equation to describe the relativistic interaction of electrons with nuclei makes it a good starting point for a relativistic many-body Hamiltonian. The relativistic electron interaction can be approximated by the non-relativistic Coulomb operator $\hat{g}_{ij} = 1/r_{ij}$, although the higher order Breit corrections become important in high-precision atomic calculations. The Dirac-Coulomb Hamiltonian for a molecular system of n electrons in the field of N fixed nuclei is then given by (in atomic units)

$$\begin{aligned} \hat{H}_{DC} &= \sum_{i}^{n} \hat{h}_i^D + \sum_{i<j} \frac{1}{r_{ij}} + V_{\mathrm{NN}} \\ &= \sum_{i}^{n} (c(\vec{\alpha}_i \cdot \vec{p}_i) + mc^2\beta_i + V_{\mathrm{nuc}}) + \sum_{i<j} \frac{1}{r_{ij}} + V_{\mathrm{NN}}, \end{aligned} \tag{2.16}$$

where the last term is the Coulomb interaction of the nuclei

$$V_{\mathrm{NN}} = \sum_{ab} \frac{Z_a Z_b}{r_{ab}} \tag{2.17}$$

and the Dirac matrices in the standard Dirac-Pauli representation for particle i

$$\vec{\alpha}_i = \begin{pmatrix} 0 & \vec{\sigma} \\ \vec{\sigma} & 0 \end{pmatrix}, \quad \beta_i = \begin{pmatrix} \sigma_0 & 0 \\ 0 & -\sigma_0 \end{pmatrix}. \tag{2.18}$$

The electron-nucleus interaction V_{nuc} is in general represented by

$$V_{\text{nuc}}(\vec{r}_i) = -\sum_a \frac{\rho_{\text{N}}(\vec{r}_a)}{|\vec{r}_i - \vec{r}_a|} d\vec{r}_i, \tag{2.19}$$

where ρ_{N} in the nuclear charge distribution. The associated wave equation $\hat{H}_{DC}\Psi = E\Psi$ is not Lorentz invariant, and as a result $\hat{H}_{DC}$ does not represent a proper relativistic Hamiltonian. In order to obtain a two-electron interaction term which is consistent with special relativity, it is necessary to utilize quantum electrodynamics (QED).

2.3 The Dirac-Hartree-Fock Approach

Analogous to Hartree-Fock theory, the Dirac-Hartree-Fock (DHF) model begins with the assumption that an n-electron wave-function Ψ can be approximated by a trial function corresponding to a Slater determinant of orthonormal orbitals:

$$\begin{aligned} \Psi &= \mathcal{A}\left(\prod_{i=0}^{n} \psi_i(\vec{r}_j)\right) \\ &= \frac{1}{\sqrt{n!}} \begin{vmatrix} \psi_1(\vec{r}_1) & \psi_2(\vec{r}_1) & \cdots & \psi_n(\vec{r}_1) \\ \psi_1(\vec{r}_2) & \psi_2(\vec{r}_2) & \cdots & \psi_n(\vec{r}_2) \\ \vdots & \vdots & & \vdots \\ \psi_1(\vec{r}_n) & \psi_2(\vec{r}_n) & \cdots & \psi_n(\vec{r}_n) \end{vmatrix}, \end{aligned} \tag{2.20}$$

where $\mathcal{A}$ is the antisymmetrizer operator and the ψ_k are molecular 4-spinors of the form (2.3). The expectation value of the total energy is

$$\begin{aligned} E &= \langle \Psi | \hat{H}_{DC} | \Psi \rangle \\ &= \sum_i^n \langle \psi_i | \hat{h}_D | \psi_i \rangle + \frac{1}{2} \sum_{i,j}^n \left(\langle \psi_i \psi_i | \psi_j \psi_j \rangle - \langle \psi_i \psi_j | \psi_j \psi_i \rangle \right). \end{aligned} \tag{2.21}$$

where the Mulliken notation for the two-electron integrals is used

$$\langle \psi_i \psi_j | \psi_k \psi_l \rangle = \iint d^3\vec{r}_1 d^3\vec{r}_2 \, \psi_i^\dagger(\vec{r}_1)\psi_j(\vec{r}_1)\frac{1}{r_{12}}\psi_k^\dagger(\vec{r}_2)\psi_l(\vec{r}_2). \tag{2.22}$$

The single-particle 4-spinors are expanded in separate scalar function basis sets for the large $\{\chi^L\}$ and small $\{\chi^S\}$ component parts,

$$\psi_k = \begin{pmatrix} \psi_k^{L\alpha} \\ \psi_k^{L\beta} \\ \psi_k^{S\alpha} \\ \psi_k^{S\beta} \end{pmatrix} = \begin{pmatrix} \sum_\mu \chi_\mu^L c_{\mu k}^{L\alpha} \\ \sum_\mu \chi_\mu^L c_{\mu k}^{L\beta} \\ \sum_\nu \chi_\nu^S c_{\nu k}^{S\alpha} \\ \sum_\nu \chi_\nu^S c_{\nu k}^{S\beta} \end{pmatrix}. \tag{2.23}$$

This method has been adopted from non-relativistic molecular theory, where it was first introduced by Roothaan. The energy is thus parameterized in terms of the complex expansion coefficients $\{c\}$. Utilizing the variational principle leads, as in non-relativistic theory, to a pseudoeigenvalue equation

$$\mathbf{Fc} = \epsilon \, \mathbf{Sc}. \tag{2.24}$$

A major difference, however, is that matrices and vectors may be complex. In a real basis, the overlap matrix $\mathbf{S}$ is real and block diagonal with elements

$$S_{\mu\nu}^{X,Y} = \langle \chi_\mu^X | \chi_\nu^Y \rangle \delta_{XY}; \qquad X, Y = L\alpha, L\beta, S\alpha, S\beta, \tag{2.25}$$

The Fock-matrix $\mathbf{F}$ is conveniently split up into two parts. The one-electron Fock matrix $\mathbf{F}^{[1]}$ is the matrix representation of the Dirac operator in the current basis

$$\mathbf{F}^{[1]} = \begin{bmatrix} \mathbf{V}^{LL} & -ic\mathbf{d}_z^{LS} & 0 & -ic\mathbf{d}_-^{LS} \\ -ic\mathbf{d}_z^{SL} & \mathbf{W}^{SS} & -ic\mathbf{d}_-^{SL} & 0 \\ 0 & -ic\mathbf{d}_+^{LS} & \mathbf{V}^{LL} & ic\mathbf{d}_z^{LS} \\ -ic\mathbf{d}_+^{SL} & 0 & ic\mathbf{d}_z^{SL} & \mathbf{W}^{SS} \end{bmatrix} \tag{2.26}$$

where

$$V_{\mu\nu}^{XY} = \langle \chi_\mu^X | V | \chi_\nu^Y \rangle \tag{2.27}$$

$$W_{\mu\nu}^{XY} = \langle \chi_\mu^X | V - 2mc^2 | \chi_\nu^Y \rangle \tag{2.28}$$

$$d_{z,\mu\nu}^{XY} = \langle \chi_\mu^X | \frac{\partial}{\partial z} | \chi_\nu^Y \rangle \tag{2.29}$$

$$d_{\pm,\mu\nu}^{XY} = \langle \chi_\mu^X | \frac{\partial}{\partial x} \pm i \frac{\partial}{\partial y} | \chi_\nu^Y \rangle \tag{2.30}$$

The two-electron Fock matrix is given by

$$\mathbf{F}^{[2]} = \mathbf{F}^J + \mathbf{F}^K \tag{2.31}$$

$$\mathbf{F}^J = \begin{bmatrix} \mathbf{J}^{L\alpha} & 0 & 0 & 0 \\ 0 & \mathbf{J}^{S\alpha} & 0 & 0 \\ 0 & 0 & \mathbf{J}^{L\beta} & 0 \\ 0 & 0 & 0 & \mathbf{J}^{S\beta} \end{bmatrix} \tag{2.32}$$

$$\mathbf{F}^K = -\begin{bmatrix} \mathbf{K}^{L\alpha L\alpha} & \mathbf{K}^{L\alpha S\alpha} & \mathbf{K}^{L\alpha L\beta} & \mathbf{K}^{L\alpha L\beta} \\ \mathbf{K}^{S\alpha L\alpha} & \mathbf{K}^{S\alpha S\alpha} & \mathbf{K}^{S\alpha L\beta} & \mathbf{K}^{S\alpha L\beta} \\ \mathbf{K}^{L\beta L\alpha} & \mathbf{K}^{L\beta S\alpha} & \mathbf{K}^{L\beta L\beta} & \mathbf{K}^{L\beta L\beta} \\ \mathbf{K}^{S\beta L\alpha} & \mathbf{K}^{S\beta S\alpha} & \mathbf{K}^{S\beta L\beta} & \mathbf{K}^{S\beta L\beta} \end{bmatrix}. \tag{2.33}$$

As in the non-relativistic theory it can be divided into a Coulomb contribution

$$J_{\mu\nu}^{XY} = \sum_X \sum_{\lambda,\kappa} D_{\lambda\kappa}^{YY} (\chi_\mu^X \chi_\nu^X | \chi_\kappa^Y \chi_\lambda^Y) \tag{2.34}$$

and an exchange contribution

$$K_{\mu\nu}^{XY} = \sum_{\lambda,\kappa} D_{\lambda\kappa}^{XY} (\chi_\mu^X \chi_\lambda^X | \chi_\kappa^Y \chi_\nu^Y). \tag{2.35}$$

The contributions are defined in terms of the back-transformed density matrix

$$D_{\lambda\kappa}^{XY} = \sum_i c_{\lambda i}^X c_{\kappa i}^{Y*}. \tag{2.36}$$

The generalized matrix eigenvalue problem (2.24) is the solution to the DHF problem utilizing a finite basis set. It has to be solved iteratively in a self-consistent manner for a given set of positions of the atomic centers. With this electronic

solution, the forces on the nuclei resulting from the electron distribution can be calculated. Hence after each electronic convergence step the atoms are moved along the forces following by a new electronic step. This is repeated until the forces are below a certain threshold. By this outlined procedure, the geometry and the electronic structure of a molecule can be obtained at the DHF level. It is obvious that for large basis sets the dimensions of the matrices become quite large, which results in the need of enormous computational resources to diagonalize the equations.

2.4 Basis Sets

The 4-spinor wave function is usually parametrized in molecular calculations by expanding the single-particle solutions in a set of analytic basis functions. The choice of basis set is almost exclusively given by a set of atomic centered Slater or Gaussian functions. Gaussian basis sets have become particularly popular. With this choice, the most time-consuming integrals in molecular calculations, the two-electron integrals, can be calculated extremely efficiently.

In DIRAC [70], the 4-spinors are expanded in scalar basis functions (2.23). Atomic centered cartesian Gaussians

$$G^{\alpha}_{ijk}(\vec{r}_A) = \mathcal{N} x_A^i y_A^j z_A^k \exp(-\alpha r_A^2) \tag{2.37}$$

are used, where $i + j + k = l$ is the angular quantum number, A refers to the nuclear center and $\mathcal{N}$ is a normalization constant. For a given quantum number l there are $\frac{1}{2}(l+1)(l+2)$ cartesian Gaussians. This basis set for a given l value may be transformed to a set of $(2l+1)$ spherical Gaussians,

$$G^{\alpha}_{nlm}(\vec{r}_A) = \mathcal{N} r_A^{n-1} \exp(-\alpha r_A^2)\, Y_{lm}(\theta_A, \phi_A) \tag{2.38}$$

with the restriction $n = l + 1$, where $Y_{lm}(\theta, \phi)$ are the spherical harmonics. It is also possible to transform directly to a set of 2-spinor Gaussians of the form

$$G^{\alpha}_{n\kappa m_j}(\vec{r}_A) = \mathcal{N} r_A^{n-1} \exp(-\alpha r_A^2)\, \chi_{\kappa, m_j}(\theta_A, \phi_A) \tag{2.39}$$

where χ_{κ, m_j} is the angular part of the hydrogenic solution to the Dirac equation.

It is tempting to assume that the basis for the large component should be quite close to the non-relativistic basis. While this holds for lighter elements, it is normally not accurate enough for heavy elements. Usually higher exponents are required for an accurate description of the relativistically contracted inner shells. Furthermore orbitals with $l > 0$ are spin-orbit split into two components, which may have their maxima quite apart from each other.

An important feature in 4-component calculations is that the basis sets for the large and the small component should not be chosen independently due to the apparent coupling between both components. The relationship between the large and small components of the bound state 4-spinor solutions may for a one-electron atom be written as

$$2mc\psi^S = B(E)(\vec{\sigma}\cdot\vec{p})\psi^L; \qquad B(E) = \left[1 + \frac{E-V}{2mc^2}\right]^{-1}. \tag{2.40}$$

In the non-relativistic limit, the operator $B(E)$ tends toward unity, so that

$$\lim_{c\to\infty} 2mc\psi^S = (\vec{\sigma}\cdot\vec{p})\psi^L. \tag{2.41}$$

This observation forms the basis for the kinetic balance conditions [71]. The operator $(\vec{\sigma}\cdot\vec{p})$ acting on a large basis function generates a linear combination of basis functions. In the unrestricted kinetic balance (URK) approach no such fixed combinations are assumed, and all Gaussians generated (2.41) are independently used as basis functions

$$\chi^L = \{G^\alpha_l\} \rightarrow \chi^S = \{G^\alpha_{l-1}, G^\alpha_{l+1}\}. \tag{2.42}$$

From this it is obvious that the number of small component basis functions is approximately twice the number of large component basis functions. In a basis of 2-spinor Gaussians, the restricted kinetic balance (RKB) leads to a one-to-one matching of the large and the small component basis due to their κ-dependence. In a scalar basis, however, the ratio between the number of small and large basis functions will be exactly two for all l values. The resulting basis set is best expressed in terms of spherical Gaussians

$$\chi^L = \{G^\alpha_{l+1,lm}\} \rightarrow \chi^S = \{G^\alpha_{l+2,l+1,m}, \left(\frac{2\alpha r^2}{2l+1} - 1\right) G^\alpha_{l,l-1,m}\}. \tag{2.43}$$

In summary, kinetically balanced basis sets give energy eigenvalue spectra for molecular and atomic systems that consist of continuum solutions below $-2mc^2$ and above $2mc^2$ as well as bound state solutions in the gap below $2mc^2$ There is a strict separation of positive and negative energy states for any reasonble chemical system, and the electrons of the system are allowed to occupy only positive energy states. The calculated energies converge towards the exact solutions when the basis set is increased towards completeness. The convergence may be from above or below, and this is the only difference from the non-relativistic case.

The scalar small component basis can be reduced by using dual family basis sets. Exponents for the primitive large component basis for a given atomic center are then selected from two lists, one for even-l and one for odd-l functions. That means that for instance the large d exponents will be a subset of the set of large s exponents, so that the small p exponents generated from the d functions is already included in the p exponents generated from s and may therefore be discarded.

2.5 Electron Correlation

In the Hartree-Fock approximation, the electron-electron interaction is considered to be represented by only one Slater determinant. Generally, this solution recovers about 99% of the total energy, but for many applications the remainder is crucial to get an accurate description of the properties for the system. In the HF Ansatz, the motion of the electrons are said to be uncorrelated and the state corresponding to this configuration is often called the "vacuum".

In real systems, electrons interact with the field generated by all the other electrons through the manifestation of instantaneous excitations from occupied to unoccupied spin-orbitals. The correlation energy E_{corr} is then defined as the difference between the total exact non-relativistic (or relativistic) energy E_{tot} of the system and the Hartree-Fock energy E_{HF} in a complete basis-set expansion [62]

$$E_{\text{corr}} = E_{\text{tot}} - H_{\text{HF}}. \tag{2.44}$$

Since the HF wave function is the best single-determinant that can be obtained, it is clear that any approach aiming at introducing electron correlation has to re-

lax this constraint by considering more than one Slater determinant. A common strategy is to include a number of determinants, managable by the computational resources, that reproduce a large portion of the electron correlation. A customary procedure to expand the determinantal space is to generate determinants that involve unoccupied (virtual) one-electron states. This implies that one has to consider determinants in which an electron has been promoted from an occupied state in the HF wave function into an unoccupied state. This can be done for single electrons in any of the occupied states into any of the unoccupied states. Such a type of determinant receives the name of single-excitation determinant (S). In the same manner, determinants in which two electrons have been promoted from the occupied into the unoccupied states are called double excitation-determinants (D).

2.5.1 Configuration Interaction

The simplest multi-determinantal method consists of adding Slater determinants constructed from the occupied and unoccupied orbitals of the HF wave function [63]

$$\begin{aligned} |\Psi_{\mathrm{CI}}\rangle &= |\Psi_{\mathrm{HF}}\rangle + \sum_{a}^{\mathrm{occ}} \sum_{r}^{\mathrm{virt}} c_a^r |\Psi_a^r\rangle + \sum_{ab}^{\mathrm{occ}} \sum_{rs}^{\mathrm{virt}} c_{ab}^{rs} |\Psi_{ab}^{rs}\rangle + \cdots \\ &= |\Psi_{\mathrm{HF}}\rangle + \sum_{S} c_S |\Psi_S\rangle + \sum_{D} c_D |\Psi_D\rangle + \cdots \end{aligned} \tag{2.45}$$

This method is called configuration interaction (CI), which stems from the fact that electron correlation is retrieved from contributions to the electronic energy arising from Hamiltonian matrix elements between different Slater determinants, i.e. different electronic configurations. The ground-state is obtained by minimization of the CI energy

$$E_{\mathrm{CI}} = \min_{\{c_S, c_D, \ldots\}} \frac{\langle \Psi_{\mathrm{CI}} | \hat{H} | \Psi_{\mathrm{CI}} \rangle}{\langle \Psi_{\mathrm{CI}} | \Psi_{\mathrm{CI}} \rangle} \tag{2.46}$$

with respect to the coefficients $\{c_i\}$. This is equivalent to solving the secular equation

$$\mathbf{Hc} = E_{\mathrm{CI}}\mathbf{c}, \tag{2.47}$$

where **H** is the Hamiltonian matrix with the matrix elements $H_{ij} = \langle \Psi_i | \hat{H} | \Psi_j \rangle$. Here the HF orbitals remain frozen and only the coefficients are optimized. The lowest eigenvalue E_{CI} found is the electronic ground-state energy. Higher eigenvalues correspond to electronic excited states.

The method, in which all available determinants resulting from an expansion in a finite set of orbitals are included in the calculation, receives the name of full CI. Despite its formal and conceptual simplicity, it is only applicable to the simplest systems as the number of determinants is growing rapidly with the size of the system and cannot be handled computationally. It is therefore necessary to truncate the CI expansion so that only a small subset of determinants of the full set is included. The truncated CI expansion should preferably recover a large part of the correlation energy.

Usually, the singly and doubly excited configurations are retained, and the truncated CI is therefore called CISD. In general this scheme can recover about 90% of the dynamic correlation which arises from the mutual Coulomb repulsion. However, in some situations the quasi degeneracy of a few states makes the single reference state approach less sound, and a multi-reference (MRCI) approach is required to evaluate the static and dynamic correlation arising from the simultaneous excitation of more than one determinant.

An important problem of truncated CI methods is size-inconsistency. This means that the energy of two infinitely separated fragments is not the sum of the energy of the individually treated fragments. Therefore CISD is not suitable for the correct description of dissociations in molecules.

2.5.2 Coupled-Cluster Methods

Since its introduction to quantum chemistry in the late 1960s by Cizek and Paldus [72–74], coupled cluster (CC) theory has emerged as perhaps the most reliable, yet computationally affordable method for the approximate solution of the electronic many-electron problem and the prediction of molecular properties. Compared to CI methods, it has the advantage of being size-consistent by construction. The CC wave function is written in a product from as an infinite

expansion of a single determinant by considering excitations to infinite order

$$|\Psi_{CC}\rangle = \left[\prod_{a,r}(1 + t_a^r a_r^\dagger a_a)\right]\left[\prod_{ab,rs}(1 + t_{rs}^{ab} a_s^\dagger a_r^\dagger a_b a_a)\right]\cdots|\Psi_{HF}\rangle. \tag{2.48}$$

It should be stressed that the CI and the CC wave functions are entirely equivalent provided all excitations are included in the expression, and only differ in their parameterization. Their nonequivalence becomes apparent only when some of the excitation operators are omitted from the wave function.

Since $(1 + t_a^r a_r^\dagger a_a) = \exp(t_a^r a_r^\dagger a_a)$, it can be shown that the CC wave function can alternatively by written as an exponential ansatz

$$|\Psi_{CC}\rangle = \exp T|\Psi_{HF}\rangle, \tag{2.49}$$

with the excitation operator

$$T = T_1 + T_2 + \cdots + T_N, \tag{2.50}$$

where the T_n denote the set of all possible excitations of n electrons

$$T_1 = \sum_{a,r} t_a^r a_r^\dagger a_a \tag{2.51}$$

$$T_2 = \sum_{ab,rs} t_{ab}^{rs} a_s^\dagger a_r^\dagger a_b a_a. \tag{2.52}$$

The coefficients $t_{ab\ldots}^{rs\ldots}$ are called coupled cluster amplitudes. A Taylor expansion of the exponential operator leads to the following CC wave function

$$\begin{aligned}|\Psi_{CC}\rangle =& |\Psi_{HF}\rangle + T_1|\Psi_{HF}\rangle + \left(T_2 + \frac{1}{2!}T_1^2\right)|\Psi_{HF}\rangle + \left(T_3 + T_2T_1 + \frac{1}{3!}T_1^3\right)|\Psi_{HF}\rangle \\ &+ \left(T_4 + T_3T_1 + \frac{1}{2}T_2T_1^2 + \frac{1}{2}T_2^2 + \frac{1}{4!}T_1^4\right)|\Psi_{HF}\rangle + \cdots,\end{aligned} \tag{2.53}$$

which contains triple and higher excitations as products of lower order excitations.

The CC wave function has to fulfill the electronic Schrödinger equation

$$\hat{H}|\Psi_{CC}\rangle = E_{CC}|\Psi_{CC}\rangle, \tag{2.54}$$

and is equivalent to the optimization of the coupled-cluster amplitudes $t_{ab\ldots}^{rs\ldots}$. The

nonlinear parametrization of the wave function (2.48) means that the derivatives of the coupled cluster state become complicated functions of the amplitudes. Therefore, the variational minimum conditions on the amplitudes give rise to an intractable set of nonlinear equations for all amplitudes

$$\langle \Psi_{ab\ldots}^{rs\cdots} | e^T \hat{H} | \Psi_{CC} \rangle = E_{CC} \langle \Psi_{ab\ldots}^{rs\cdots} | e^T \Psi_{CC} \rangle. \tag{2.55}$$

Solving these equations is impossible for all but the smallest systems which makes the variational principle unsuitable but not impossible for the coupled cluster method. Instead, the cluster amplitudes are determined by projecting the Schrödinger equation in the form

$$e^{-T} \hat{H} e^T | \Psi_{HF} \rangle = E_{CC} | \Psi_{HF} \rangle \tag{2.56}$$

against a set of configurations $\langle \Psi_{ab\ldots}^{rs\cdots} |$ that span the space of all states that can be reached by applying the cluster operator T linearly to the reference state $|\Psi_{HF}\rangle$:

$$\langle \Psi_{HF} | e^{-T} \hat{H} e^T | \Psi_{HF} \rangle = E_{CC} \tag{2.57}$$

$$\langle \Psi_{ab\ldots}^{rs\cdots} | e^{-T} \hat{H} e^T | \Psi_{HF} \rangle = 0 \tag{2.58}$$

This set of equations for the coupled cluster energy E_{CC} and the coupled cluster amplitudes $t_{ab\ldots}^{rs\cdots}$ are called linked coupled-cluster equations. The term linked is used, because in diagrammatic coupled-cluster theory the energy independent equations give rise to only linked diagrams [75].

A Baker-Campbell-Hausdorff (BCH) expansion of the similarity-transformed Hamiltonian is no higher than quartic in the amplitudes:

$$\begin{aligned} e^{-T} \hat{H} e^T =& \hat{H} + [\hat{H}, T] + \frac{1}{2!}[[\hat{H}, T], T] + \frac{1}{3!}[[[\hat{H}, T], T], T] \\ &+ \frac{1}{4!}[[[[\hat{H}, T], T], T], T] \end{aligned} \tag{2.59}$$

The projected coupled cluster Schrödinger equation (2.58) therefore yields at most quartic equations in the cluster amplitudes - even for the full cluster expansion. The BCH expansion terminates because of the special structure of the cluster operators, which are linear combinations of commuting excitation operators of the form (2.52). Since the Hamilton operator $\hat{H}$ contains only one- and two electron operators it leads to a rather simple expression for the coupled

cluster energy:

$$E_{CC} = \langle \Psi_{HF} | e^{-T} \hat{H} e^{T} | \Psi_{HF} \rangle \tag{2.60}$$
$$= E_{HF} + \sum_{a,r} t_a^r \langle \Psi_{HF} | \hat{H} | \Psi_a^r \rangle + \frac{1}{4} \sum_{ab,rs} (t_{ab}^{rs} + t_a^r t_b^s - t_a^s t_b^r) \langle \Psi_{HF} | \hat{H} | \Psi_{ab}^{rs} \rangle.$$

The coupled cluster correlation energy is therefore determined completely by the singles and doubles amplitudes.

In practical calculations, the cluster operator T must be truncated at some excitation level due to the growing number of excited determinants. By truncating, some of the terms in amplitude equations will become zero and the amplitudes derived from these approximate equations will no longer be exact. The energy calculated from these approximate singles and doubles amplitudes will therefore be approximate. How severe these are, depends on how many terms are included in T. Taking only the T_1 operator into account does not give any improvement over HF, as matrix elements between HF and singly excited states are zero. The lowest level of approximation is therefore $T = T_2$; referred to as CCD. Compared to doubles, there are relatively few singly excited determinants. Using $T = T_1 + T_2$ gives the more complete CCSD model. Both CCD and CCSD scales like M^6 in the limit of a large basis set. Including triple excitations , $T = T_1 + T_2 + T_3$, results in the CCSDT approximation (M^8, where M is the number of basis functions). The most frequently used method is the perturbative treatment of the triple excitations on top of a CCSD calculation, CCSD(T) (M^7).

The extension of the coupled cluster method to the relativistic case is very technical but rather straight forward. First, one has to examine the role of the negative energy states in the N-particle wave function. Here, the no-pair approximation is frequently used, meaning that all determinants contain only positive-energy spinors. In a second step, the time reversal symmetry of a closed shell system is used to introduce a Kramers-pair basis. The time-reversal operator is applied to the excitation operators T_i and leads to symmetry relations between the amplitudes of Kramers pairs and furthermore to new expressions for the T_i. Finally, the reference determinant is replaced by the DHF wave function. This procedure is the basis of the Kramers-restricted CCSD (KRCCSD) method [76]. Since all integrals are complex and due to the lack of spin symmetry in the relativistic theory, an increase in computation time by a factor of 32 compared to the non-relativistic

CCSD method is caused.

2.6 Density Functional Theory

The traditional methods in electronic structure theory, in particular Hartree-Fock theory and its successors, are based on a complex multi-valued many-electron wave-function. The main objective of density functional theory, which originates from the Thomas-Fermi model, is to replace the many-body electronic wave function with the one-particle electronic density as the basic quantity. Whereas the many-body wave function is dependent on $3n$ variables, three spatial variables for each of the N electrons, the density is only a function of spatial three variables, and is therefore a simpler quantity to deal with both conceptually and practically.

Density functional theory is founded on the Hohenberg-Kohn theorem and the Kohn-Sham equations which will be reviewed shortly. The time independent Hamiltonian of an n-electron system can be written as

$$\hat{H} = \hat{T} + \hat{V}_{ee} + \hat{V}_{nuc}, \tag{2.61}$$

where $\hat{T}$ is the contribution from the kinetic energy, $\hat{V}_{ee}$ the interaction potential of the n electrons, and $\hat{V}_{nuc}$ the external potential, which is in the Born-Oppenheimer approximation the sum of the nuclear Coulomb potentials.

$$\hat{V}_{nuc} = \sum_{i}^{n} v(\vec{r}_i) = \sum_{i}^{n} \sum_{\alpha}^{N} \frac{Z_\alpha}{r_{i\alpha}}, \tag{2.62}$$

For an n-electron system, the potential $\hat{V}_{nuc}$ defines its identity. This means that the V-term determines if for example we have a 68 electron system denoted an Er atom, a Mt^{41+} ion or a CHFClBr molecule.

The first Hohenberg-Kohn theorem [77] legitimizes the use of the density $\rho(\vec{r})$ as a basic variable. It states that: *The time-independent external potential $v(\vec{r}_i)$ is completely determined by the electron density $\rho(\vec{r})$ to within an additive constant*. In other words, from a given electron density the external potential, i.e. the positions of the nuclei are determined. Furthermore, the wave-function and hence all properties of the ground state can be obtained at least in principle from the density. By inserting the external potential, determined by the density into the

Schrödinger equation, the Hamiltonian and therefore the wave-function is determined. It is important to note that the theorem states just the existence of this connection, but does not give a recipe or a way to construct the wave-function.

The second Hohenberg-Kohn theorem [77] establishes a variational principle for the energy as a functional of the density: *If $\rho(\vec{r})$ is the density arising from the solution of the N-electron Schrödinger equation*

$$\hat{H}|\Psi\rangle = E[\rho]|\Psi\rangle \tag{2.63}$$

and for any density $\rho'(\vec{r}) \neq \rho(\vec{r})$ that satisfies

$$\int \rho'(\vec{r}) d^3\vec{r} = n, \tag{2.64}$$

it follows $E'(\vec{r}) > E(\vec{r})$.

This theorem is derived from the Rayleigh-Ritz variational principle and the correspondence between the wave function and the one-particle density. By using the Lagrange multiplier the stationarity condition is given by

$$\delta \left\{ E[\rho] - \mu \left[\int \rho(\vec{r}) d\vec{r} - n \right] \right\} = 0. \tag{2.65}$$

Utilizing the energy functional,

$$\begin{aligned} E[\rho] &= \langle \Psi | \hat{H} | \Psi \rangle = \langle \Psi | \hat{T} + \hat{V}_{ee} + \hat{V}_{nuc} | \Psi \rangle \\ &= \langle \Psi | \hat{T} + \hat{V}_{ee} | \Psi \rangle + \int \rho(\vec{r}) v(\vec{r}) d\vec{r} \\ &= F[\rho] + \int \rho(\vec{r}) v(\vec{r}) d\vec{r}, \end{aligned} \tag{2.66}$$

the stationarity condition can be expressed in the Euler-Lagrange form

$$\mu = \frac{\delta E[\rho]}{\delta \rho(\vec{r})} = v(\vec{r}) + \frac{\delta F[\rho]}{\delta \rho(\vec{r})}, \tag{2.67}$$

where $F[\rho]$ is a universal functional (independent from the external potential) for all n-electron systems with Coulomb fields. The simple form of this equation hides the fact that this universal functional is not available in explicit form.

Kohn and Sham found a practical scheme to map a many-electron system to a

non-interacting system of quasi-particles which has the same ground state density as the interacting system. By using single-particle orbitals $\{\phi_i\}$, the wave function of the non-interacting system may be written as a single determinant, although the Kohn-Sham orbitals are only trial functions to construct the one-particle density. The electron density and the total energy are

$$\rho(\vec{r}) = \sum_i^n |\langle \vec{r}|\phi_i\rangle|^2, \tag{2.68}$$

$$E = -\frac{1}{2}\sum_i^n \langle\phi_i|\nabla^2|\phi_i\rangle + \frac{1}{2}\iint d^3\vec{r}\,d^3\vec{r}'\,\rho(\vec{r})\frac{1}{|\vec{r}-\vec{r}'|}\rho(\vec{r}') + \sum_i^n \langle\phi_i|V_{\text{nuc}}|\phi_i\rangle + E_{\text{xc}}[\rho]. \tag{2.69}$$

The unknown exchange-correlation functional $E_{\text{xc}}[\rho]$ contains all contributions beyond the Hartree energy. The orbitals $\{\phi_i\}$, are solutions of the Kohn-Sham equations

$$\left[-\frac{1}{2}\nabla^2 + v^{\text{eff}}\right]|\phi_i\rangle = \epsilon_i|\phi_i\rangle \tag{2.70}$$

$$v^{\text{eff}} = v + \int d^3\vec{r}'\,\frac{\rho(\vec{r}')}{|\vec{r}-\vec{r}'|} + \frac{\delta E_{\text{xc}}}{\delta\rho(\vec{r})}. \tag{2.71}$$

The canonical Kohn-Sham equations have the same form as the Hartree equations, except that they contain a more general local potential $v^{\text{eff}}(\vec{r})$. The computational effort to solve the Kohn-Sham equations is not much more than to solve the Hartree equations - and less than for the Hartree-Fock equations. The Hartree-Fock equations contain a nonlocal potential operator in the two-electron Hamiltonian and hence are not a special case of the Kohn-Sham equations. Nevertheless, all three theories - Hartree, Hartree-Fock and Kohn-Sham - provide one-electron equations describing many electron systems. The Kohn-Sham theory, exact in principle, is distinguished from the Hartree-Fock theory in its capacity to fully incorporate the exchange-correlation effect for electrons. But the success of DFT depends on finding an accurate exchange-correlation potential $v_{\text{xc}}(\vec{r}) = \delta E_{\text{xc}}/\delta\rho(\vec{r})$. There is an extensive literature discussing the merits of various potentials, and good accounts may be found elsewhere [78].

The extension of the Hohenberg-Kohn theorems to relativistic systems was first given by Rajagopol and Callaway [79–81]. The main idea is that in the relativistic

model, the four-current j plays the same role as the density does in the non-relativistic case. The generalization is straight forward but rather technical and some subtleties have to be addressed. The relativistic Kohn-Sham equations are given by

$$\left[c(\vec{\alpha}\cdot\vec{p}) + mc^2(\beta - 1) + v^{\text{eff}}[j]\right]\psi_i(\vec{x}) = \epsilon_i\psi_i(\vec{x}) \tag{2.72}$$

where the effective potential may be written in the form

$$\begin{aligned} v^{\text{eff}}[\vec{j},\rho] = &-\left(e\phi(\vec{r}) + e^2\int\frac{\rho(\vec{r}')}{|\vec{r}-\vec{r}'|}d\vec{r}' + \frac{\delta E^{\text{xc}}}{\delta\rho(\vec{r})}\right) \\ &- c\vec{\alpha}\left(e\vec{A}(\vec{r}) + e^2\int\frac{\vec{j}(\vec{r}')}{|\vec{r}-\vec{r}'|}d\vec{r}' + \frac{\delta E^{\text{xc}}}{\delta\vec{j}(\vec{r})}\right) \end{aligned} \tag{2.73}$$

Here ϕ denotes the electrostatic and $\vec{A}$ the vector potential. Equation (2.73) explicitly shows the contributions from the charge density and current density parts of the four-current. These equations are also known as Dirac-Kohn-Sham equations.

For the majority of quantum chemical problems suitable for a DFT treatment, the accuracy ambitions are compatible with the use of the Dirac-Coulomb Hamiltonian. It was shown [82–84] that in those cases one can use the exchange-correlation form from ordinary non-relativistic DFT without much loss of accuracy. This includes the use of gradient-corrected and hybrid functional which are easily implemented in the relativistic formalism.

Chapter 3

QED Effects in Atoms

Considerable progress has been made in the past decades to accurately describe few-electron systems in strong Coulomb-fields [85,86]. For example, calculations for Li-like uranium using relativistic many-body perturbation theory gives 322.33 eV for the $^2S_{1/2}/^2P_{1/2}$ level splitting [87], which corrects to 280.56 eV upon inclusion of lowest order vacuum polarization and electron self-energy [88, 89]. This is already in excellent agreement with the experimental value of 280.59(9) eV of Schweppe et al. [90]. Higher-order quantum electrodynamic (QED) corrections including mass polarization and recoil contributions from the nucleus are not negligible, but approximately cancel out [85]. Even more impressive, QED effects to the electronic g-factor are now so precise that hadronic contributions need to be considered to achieve higher accuracy [91–93].

The situation completely changes for multi-electron systems as accurate relativistic electronic structure calculations including QED effects become more demanding in computer time with increasing number of electrons involved if electron correlation is taken into account. Moreover, one changes from the simple free-particle Feynman-Dyson picture to the bound-state Furry picture which modifies the electron propagator involving the actual one-particle functions from the Dirac-Hamiltonian. Nevertheless, in the last decade great progress has been made in relativistic quantum calculations of heavy atoms or molecules with high nuclear charge [64], in particular at the Dirac-Breit level applying Fock-space coupled-cluster theory to atoms [94, 95]. These calculations now reach accuracies of a few tenths of an eV for ionization potentials and excitation energies. Hence, they are now in the region where one has to consider self-energy (SE) and vacuum

polarization (VP) contributions to correct for valence properties.

To lowest order, QED effects consist of the one-photon Breit interaction (BI) [96], the Uehling form of the vacuum polarization [29] and the one-loop self-energy contribution [19, 97], with Breit interaction being the dominant term, followed by the electron SE. The VP is usually much smaller than the SE and of opposite sign. While the BI and the VP (including higher order in the fine structure constant α) are easily implemented into atomic program codes, the evaluation of the SE term requires a complete set of one-particle Dirac states within the Furry picture of QED, which becomes rather tedious even in the lowest order. In a recent paper, Labzowsky and co-workers presented estimates for the Lamb shift of the valence *ns*-electron levels in the alkali (Li-Fr) and coinage metal atoms (Cu-Au) [98]. In a subsequent paper they confirmed these estimates by using the multiple-commutator method for SE calculations within a Dirac-Slater approach [99].

In this work the Dirac-Hartree-Fock approach within an interaction picture of bound state QED [24] is used. The QED corrections to valence-shell ionization potentials for the group 1, 2, 11, 12, 13 and 18 elements of the periodic table down to the heaviest atoms with nuclear charge Z=120 are calculated.

3.1 The Breit Interaction

The interaction between two electrons is covariantly described by the exchange of virtual photons (Fig. 3.1). This interaction can be interpreted by a potential $\Phi(r)$ which simplifies to the Coulomb potential in the static limit. Here a derivation of the frequency independent Breit interaction within the framework of modern QED is given.

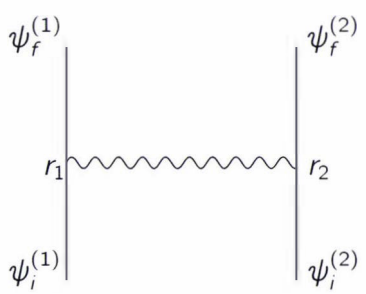

Figure 3.1: Feynman diagram of the lowest order Breit interaction

The S-matrix element for the process is given by

$$S_{fi} = -i \int d^4 r_1 \int d^4 r_2 j_{fi}^{(2)}(r_2) D_F(r_2 - r_1) j_{fi}^{(1)}(r_1), \tag{3.1}$$

with the photon propagator D_F and the transition currents

$$\begin{aligned} j_{fi}^{(n)}(r_1) &= \bar{\psi}_f^{(n)}(r_1)\gamma\psi_i^{(n)}(r_1) \\ &= j_{fi}^{(n)}(\vec{r}_1) e^{i\omega_{fi}^{(n)} t_{r_1}}. \end{aligned} \tag{3.2}$$

The time-dependence has been separated and the transition frequency is defined by $\omega_{fi}^{(n)} = E_f^{(n)} - E_i^{(n)}$. To distinguish 4-vectors from spatial vectors, the vector-arrow is omitted. By inserting the Fourier representation of the currents and the photon propagator (in the Feynman gauge) into (3.1) one obtains

$$S_{fi} = -i \int d^4 r_1 \int d^4 r_2 \int \frac{d^4 k}{(2\pi)^4} j_{fi}^{(2)}(\vec{r}_2) e^{i\omega_{fi}^{(2)} t_{r_2}} \frac{-4\pi e^{ik\cdot(r_2 - r_1)}}{k^2 + i\varepsilon} j_{fi}^{(1)}(\vec{r}_1) e^{i\omega_{fi}^{(1)} t_{r_1}}. \tag{3.3}$$

The following t_{r_2}-integration reduces the four dimensional momentum integral to a three dimensional integral. After transformation to spherical coordinates, the angular part of the k-integral can be integrated trivially and the remaining radial integration can be solved by using the residual theorem.

$$S_{fi} = -i \int d^3 r_2 \int dt \underbrace{j_{fi}^{(2)}(\vec{r}_2) e^{i\omega_{fi}^{(2)} t}}_{j_{fi}^{(2)}(\vec{r}_2, t)} \underbrace{\int d^3 r_1 \frac{e^{i\omega_{fi}^{(1)}(t - |\vec{r}_1 - \vec{r}_2|)}}{|\vec{r}_1 - \vec{r}_2|} j_{fi}^{(1)}(\vec{r}_1)}_{A_{fi}^{(1)}(\vec{r}_2, t)}. \tag{3.4}$$

From this one can see, that the vector potential $A_{fi}^{(1)}(\vec{r}_2, t)$ can be rewritten as a retarded potential

$$A_{fi}^{(1)}(\vec{r}_2, t) = \int d^3 r_1 \frac{j_{fi}^{(1)}(\vec{r}_1, t - |\vec{r}_1 - \vec{r}_2|)}{|\vec{r}_1 - \vec{r}_2|}, \tag{3.5}$$

and the transition current $j_{fi}^{(2)}(\vec{r}_2)$ interacts with the electromagnetic field emitted by the other current $j_{fi}^{(1)}(\vec{r}_1)$ at an earlier time with time difference $|\vec{r}_1 - \vec{r}_2| \equiv |\vec{r}_1 - \vec{r}_2|/c$ (from now on the c is kept for the purpose of approximations which have to be made).

The transition currents can now be inserted into (3.4), where the identity $\bar{\psi} =$

$\psi^\dagger\gamma^0$ is used and the exponential function is replaced by a Taylor expansion in powers of $1/c$. The time integration can thus be carried out

$$S_{fi} \simeq -2\pi i\delta(\omega_{fi}^{(1)} + \omega_{fi}^{(2)}) \int d^3r_2 \int d^3r_1\, \psi_i^{(2)\dagger}(\vec{r}_2)\psi_i^{(1)\dagger}(\vec{r}_1)\left(1^{(1)}1^{(2)} - \vec{\alpha}^{(1)}\cdot\vec{\alpha}^{(2)}\right) \times \left(\frac{1}{|\vec{r}_1-\vec{r}_2|} + \frac{i|\omega_{fi}|}{c} - \frac{\omega_{fi}^2|\vec{r}_1-\vec{r}_2|}{2c^2}\right)\psi_i^{(2)}(\vec{r}_2)\psi_i^{(1)}(\vec{r}_1). \tag{3.6}$$

With $\omega_{fi}^{(1)} = -\omega_{fi}^{(2)}$ and the assumption that the $\psi_m^{(n)}$ are eigenfunctions of the Hamiltonians $H^{(n)}\psi_m^{(n)} = E^{(n)}\psi_m^{(n)}$ one can show that

$$\omega_{fi}^2|\vec{r}_1-\vec{r}_2| = [H^{(1)},[H^{(2)},|\vec{r}_1-\vec{r}_2|]]. \tag{3.7}$$

This expression can be calculated by using the explicit form of the Dirac Hamiltonian $H^{(1)} = c\vec{\alpha}^{(1)}\cdot\hat{\vec{p}}_1 + \beta^{(1)}c^2 + H_{\text{ext}}^{(1)}(\vec{r}_1)$, where the momentum operator does not commute with $|\vec{r}_1-\vec{r}_2|$

$$\omega_{fi}^2|\vec{r}_1-\vec{r}_2| = c^2\left[\frac{\vec{\alpha}^{(1)}\cdot\vec{\alpha}^{(2)}}{|\vec{r}_1-\vec{r}_2|} - \frac{\vec{\alpha}^{(1)}\cdot(\vec{r}_1-\vec{r}_2)\vec{\alpha}^{(2)}\cdot(\vec{r}_1-\vec{r}_2)}{|\vec{r}_1-\vec{r}_2|^3}\right]. \tag{3.8}$$

By inserting this result into (3.6) one obtains ($\vec{n} = \vec{r}/r$)

$$S_{fi} \simeq -2\pi i\delta(\omega_{fi}^{(1)} + \omega_{fi}^{(2)}) \int d^3r_2 \int d^3r_1\, \psi_i^{(2)\dagger}(\vec{r}_2)\psi_i^{(1)\dagger}(\vec{r}_1) \times \left[\frac{1}{|\vec{r}_1-\vec{r}_2|} - \frac{\vec{\alpha}^{(1)}\cdot\vec{\alpha}^{(2)} + (\vec{\alpha}^{(1)}\cdot\vec{n})(\vec{\alpha}^{(2)}\cdot\vec{n})}{2|\vec{r}_1-\vec{r}_2|}\right]\psi_i^{(2)}(\vec{r}_2)\psi_i^{(1)}(\vec{r}_1). \tag{3.9}$$

The term in the brackets is the desired effective interaction potential. The second term, within the brackets, is the frequency independent Breit term. This correction to the electron-electron interaction accounts for the magnetic interaction and retardation to the order α^2, and only includes the exchange of a single virtual photon as shown in Fig. 3.1.

Therefore, the effective interaction operator has the form

$$\begin{aligned}\Phi(r_{12}) &= \frac{e^2}{r_{12}} - \frac{e^2}{2}\frac{\vec{\alpha}^{(1)}\cdot\vec{\alpha}^{(2)} + (\vec{\alpha}^{(1)}\cdot\vec{n})(\vec{\alpha}^{(2)}\cdot\vec{n})}{r_{12}} \\ &= \Phi_{\text{C}}(r_{12}) + \Phi_{\text{Breit}}(r_{12}).\end{aligned} \tag{3.10}$$

As expected the first term denotes the Coulomb potential between the particles.

In addition there is a correction term Φ_{Breit}, quadratic in the velocity, which is known as Breit interaction. In a non-relativistic approximation (also for the wave-function $\psi_{i,f}^{(n)}$) the potential can be reduced to a sum of contributions that can be recognized as two-electron spin-orbit and spin-spin interactions [21].

3.2 Radiative potentials

The momentum representation of the high-frequency contribution to the radiative potential is equal to [100]

$$\begin{aligned}\Phi_{\text{rad}}(\vec{p}) &= Q_{\text{rad}}(\vec{p})\Phi(\vec{p}) \\ &= \left(-\frac{1}{\vec{p}^2}\mathcal{P}(-\vec{p}^2) + \frac{g(-\vec{p}^2)}{2m}\vec{\gamma}\cdot\vec{p} + f(-\vec{p}^2) - 1\right)\Phi(\vec{p}) \\ &= \Phi_{\text{U}} + \Phi_{\text{mag}} + \Phi_{\text{el}}^{\lambda},\end{aligned} \tag{3.11}$$

where Φ is the atomic potential that at small distances is equal to the unscreened nuclear electrostatic potential. Here, the first term contains the polarization operator $\mathcal{P}(-\vec{p}^2)$ and leads to the Uehling potential. The actual problem is the calculation of the self-energy, represented by the terms containing the electric $f(\vec{p}^2)$ and the magnetic $g(\vec{p}^2)$ formfactor of the electron.

The Uehling correction is derived first because of the simplicity of its calculation. The field of a fixed charge (nucleus) is given by the Coulomb potential $\Phi_{\text{C}}(r) = A_0 = Ze/r$ (relativistic units). The components of its three-dimensional Fourier expansion are

$$\Phi(\vec{p}) = A_0(\vec{p}) = \frac{4\pi Ze}{\vec{p}^2}. \tag{3.12}$$

Including the radiative corrections, this field is replaced by the effective field

$$\mathcal{A}_0 = A_0 + \mathcal{D}_{0\rho}\frac{\mathcal{P}_{\rho\lambda}}{4\pi}A_\lambda. \tag{3.13}$$

The second term gives the required change in the scalar potential. In the first approximation of perturbation theory for $\mathcal{P}(\vec{p}^2)$, the exact photon-propagator

$\mathcal{D}(\vec{p}^2)$ can be replaced by the free photon-propagator $D(\vec{p}^2)$

$$\mathcal{D}(\vec{p}^2) \approx D(\vec{p}^2) = -\frac{4\pi}{\vec{p}^2}. \tag{3.14}$$

Thus, the radiative correction to the field potential is

$$\delta\Phi(\vec{p}) = -\frac{4\pi Ze}{(\vec{p}^2)^2}\mathcal{P}(-\vec{p}^2). \tag{3.15}$$

To determine the form of this correction in the coordinate representation, the inverse Fourier transform has to be calculated

$$\delta\Phi(\vec{r}) = \int e^{i\vec{p}\cdot\vec{r}}\delta\Phi(\vec{p})\,\frac{d^3\vec{p}}{(2\pi)^3}. \tag{3.16}$$

Since $\delta\Phi(\vec{p})$ is a function of $z = -\vec{p}^2$ only, integration over angles gives

$$\begin{aligned}\delta\Phi(\vec{r}) &= \frac{1}{4\pi^2}\int_0^\infty \delta\Phi(t)\frac{\sin r\sqrt{-z}}{r}d(-z) \\ &= \frac{1}{4\pi^2 r}\,\mathrm{Im}\int_{-\infty}^{\infty}\delta\Phi(-y^2)e^{-iry}y\,dy\end{aligned} \tag{3.17}$$

where was used that the integrand is an even function of $y = \sqrt{-z}$. The contour integration can now be moved into the upper half-plane of y, and coincides with the branch cut of the function $\mathcal{P}(-\vec{p}^2)$. This cut extends along the imaginary axis from the point $2im$, the physical sheet corresponding to the left side of the cut. Replacing y by a new variable $x = iy$, one obtains

$$\delta\Phi(r) = \frac{1}{(2\pi)^2 r}\int_{2m}^{\infty}\mathrm{Im}\,\delta\Phi(x^2)e^{-rx}x\,dx. \tag{3.18}$$

Integration over $\xi = x^2$, yields

$$\delta\Phi(r) = \frac{1}{(2\pi)^2 r}\int_{4m^2}^{\infty}\mathrm{Im}\,\delta\Phi(\xi)e^{-r\sqrt{\xi}}\,d\xi. \tag{3.19}$$

The imaginary part

$$\begin{aligned}\mathrm{Im}\,\delta\Phi(\xi) &= -\frac{4\pi e}{\xi^2}\mathrm{Im}\,\mathcal{P}(\xi) \\ &= -\frac{4\pi\alpha Ze}{3\xi^2}\sqrt{\frac{\xi-4m^2}{\xi}}(\xi+2m^2)\end{aligned} \tag{3.20}$$

can be found in standard textbooks [101], and after an obvious change of variable one obtains

$$\begin{aligned} \Phi_U(r) &= \delta\Phi(r) \\ &= \frac{2\alpha}{3\pi}\Phi_C(r)\int_1^\infty e^{-2mrt}\left(1+\frac{1}{2t^2}\right)\frac{\sqrt{t^2-1}}{t^2}\,dt, \end{aligned} \tag{3.21}$$

the well-known Uehling potential [29].

In analogy, the potential $\Phi_{mag}(r)$ for the magnetic interaction can be derived

$$\begin{aligned} \Phi_{mag}(r) &= \frac{1}{2m}\int e^{i\vec{p}\cdot\vec{r}}g(-\vec{p}^2)\vec{p}\cdot\vec{\gamma}\,\Phi_C(\vec{p})\frac{d^3\vec{p}}{(2\pi)^3} \\ &= \frac{4\pi Ze}{2m}\int e^{i\vec{p}\cdot\vec{r}}g(-\vec{p}^2)\vec{p}\cdot\vec{\gamma}\,\frac{1}{\vec{p}^2}\frac{d^3\vec{p}}{(2\pi)^3} \\ &= \frac{2\pi Ze}{2m}(-i\vec{\gamma}\cdot\vec{\nabla})\int e^{i\vec{p}\cdot\vec{r}}g(-\vec{p}^2)\frac{1}{\vec{p}^2}\frac{d^3\vec{p}}{(2\pi)^3}. \end{aligned} \tag{3.22}$$

After angular integration one obtains

$$\begin{aligned} \Phi_{mag}(r) &= \frac{Ze}{2\pi m}(-i\vec{\gamma}\cdot\vec{\nabla})\frac{1}{r}\mathrm{Im}\int_{-\infty}^\infty \frac{g(-\vec{p}^2)}{\vec{p}^2}e^{ipr}\,p\,dp \\ &= \frac{Ze}{2\pi m}(-i\vec{\gamma}\cdot\vec{\nabla})\frac{1}{r}\int_0^\infty \mathrm{Im}\,\frac{g(\xi)}{\xi}e^{\sqrt{\xi}r}\,d\xi \end{aligned} \tag{3.23}$$

where the new variable $\xi = -p^2$ was introduced. With the imaginary part of the magnetic form factor of the electron [101]

$$\mathrm{Im}\,g(\xi) = \frac{\alpha m^2}{\sqrt{\xi(\xi-4m^2)}} \tag{3.24}$$

and another change of variable $\xi = 4m^2t^2$, one obtains

$$\Phi_{mag}(r) = \frac{\alpha}{4\pi m}(-i\vec{\gamma}\cdot\vec{\nabla})\left[\Phi_C(r)\int_1^\infty\left(\frac{1}{t^2\sqrt{t^2-1}}e^{-2mrt}\,dt-1\right)\right].$$

The last term leads due to the electric interaction to the potential $\Phi_{el}(r)$ which

is given by

$$\begin{aligned}\Phi_{\mathrm{el}}^{\lambda}(r) &= \int e^{i\vec{p}\cdot\vec{r}}\left(f(-\vec{p}^2)-1\right)\,\Phi_{\mathrm{C}}(\vec{p})\frac{d^3\vec{p}}{(2\pi)^3} \\ &= \frac{Ze}{\pi r}\,\mathrm{Im}\int_{-\infty}^{\infty}\frac{f(-\vec{p}^2)-1}{\vec{p}^2}e^{ipr}\,p\,dp \\ &= \frac{Ze}{\pi r}\int_0^{\infty}\mathrm{Im}\,\frac{f(\xi)-1}{\xi}e^{\sqrt{\xi}r}\,d\xi\end{aligned} \tag{3.25}$$

After angular integration and sufficient changes of variables, the imaginary part of the electric form factor of the electron [101]

$$\mathrm{Im}\,f(\xi) = \frac{\alpha}{4\sqrt{t(t-4m^2)}}\left[-3\xi+8m^2+2(\xi-2m^2)\log\frac{\xi-4m^2}{\lambda^2}\right] \tag{3.26}$$

can be inserted. The final integration gives

$$\begin{aligned}\Phi_{\mathrm{el}}^{\lambda}(r) = &-\frac{\alpha}{\pi}\Phi_{\mathrm{C}}(r)\int_1^{\infty}\frac{1}{\sqrt{t^2-1}}\left[\left(1-\frac{1}{2t^2}\right)\right. \\ &\left.\times\left[\log(t^2-1)+\log\left(\frac{4m^2}{\lambda^2}\right)\right]-\frac{3}{2}+\frac{1}{t^2}\right]e^{-2rmt}\end{aligned} \tag{3.27}$$

Here, λ is a low-frequency cut-off parameter. To reproduce the results of ref. [102, 103], a suitable replacement for the second logarithm is $4\log(1/Z\alpha+0.5)$ where λ was selected [24] of the order of the electron binding energy $\lambda\sim(Z\alpha)^2m$. The electrical potential is furthermore not applicable for very small distances $r \ll Z\alpha r_c$. This is taken into account by a small distance cut-off coefficient $mr/(mr+0.07Z^2\alpha^2)$. The final expression for the electric form-factor reads

$$\begin{aligned}\Phi_{\mathrm{el}}(r) = &-A(Z,r)\frac{\alpha}{\pi}\Phi_{\mathrm{C}}(r)\int_1^{\infty}dt\frac{e^{-2trm}}{\sqrt{t^2-1}}\left[\left(1-\frac{1}{2t^2}\right)\right. \\ &\left.\times\left[\log(t^2-1)+4\log\left(\frac{1}{Z\alpha}+0.5\right)\right]-\frac{3}{2}+\frac{1}{t^2}\right],\end{aligned} \tag{3.28}$$

with

$$A(Z,r) = A_n(Z)\frac{mr}{mr+0.07Z^2\alpha^2}. \tag{3.29}$$

A consistent calculation of the low-frequency contribution to the nonlocal self-energy operator using Coulomb or parametric Green's functions is a complicated task [24]. It is much easier and also sufficient to fit this contribution using a

parametric potential $\Phi_{low}(r)$. To reproduce the p-level radiative energy shifts [102, 103], the following expression can be used

$$\Phi_{low} = -\frac{B(Z)}{e} Z^4 \alpha^5 mc^2 e^{-Z\alpha/a_B}. \tag{3.30}$$

Here a_B is the Bohr radius and is given by $B(Z) = 0.074 + 0.35Z\alpha$.

3.3 Computational details

Dirac-Hartree-Fock (DHF) calculations were carried out using the Dirac-Coulomb Hamiltonian (in atomic units), as described before

$$H = \sum_i \left(c\vec{\alpha}_i \cdot \vec{p}_i + c^2\beta_i + V_{nuc} \right) + \sum_{i<j} \frac{1}{r_{ij}} \tag{3.31}$$

with $\vec{\alpha}$ and β denoting the Dirac matrices in the standard Dirac representation. The equations were solved numerically using a modified code of the program system GRASP [104]. For heavy elements, the $1s$-shell radius is very small ($\langle r \rangle_{1s} \approx 500$ fm) and as a consequence, the influence of the finite nuclear size is an important contribution to the total energy. The electrostatic potential of the nucleus V_{nuc} was therefore modeled by a two-parameter Fermi-type charge distribution [105, 106]

$$\varrho(r) = \frac{\varrho_0}{1 + \exp\left[(r-a)/b\right]}, \tag{3.32}$$

where a and b were extracted from ref. [105].

Due to the small size of the quantum electrodynamic (QED) corrections, they are treated as a perturbation [107]. A fully self-consistent implementation of these effects within the GRASP code is currently in progress. The major correction to the non-relativistic Coulomb term stems from the Breit operator, which was treated within the Coulomb-gauge [96, 108, 109]

$$g_{\omega,C}(1,2) = -\frac{\vec{\alpha}_1 \cdot \vec{\alpha}_2}{r_{12}} \exp(i\omega_{12} r_{12}) - (\vec{\alpha}_1 \cdot \vec{\nabla}_1)(\vec{\alpha}_2 \cdot \vec{\nabla}_2) \frac{\exp(i\omega_{12} r_{12}) - 1}{\omega_{12}^2 r_{12}} \tag{3.33}$$

where ω_{12} is the energy of the virtual (transversal) exchange photon. The first term is the retarded Gaunt term (GI) and the second term arises from the choice of the Coulomb gauge instead of the Feynman gauge. This is known as the retarded gauge term. This correction to the electron-electron interaction accounts for magnetic interaction and retardation to the order α^2, and only includes the exchange of a single (left-right), virtual photon as depicted in Fig. 3.1.

The (other) radiative corrections are calculated by a nonlocal radiative potential, which is split into an self-energy and a vacuum polarization part

$$\begin{aligned}\Delta E_{\mathrm{VP}} &= \langle\Psi|\Phi_{\mathrm{VP}}(r)|\Psi\rangle \\ &\simeq \langle\Psi|\Phi_{\mathrm{U}}(r) + \Phi_{\mathrm{WK}}(r) + \Phi_{\mathrm{KS}}(r)|\Psi\rangle. \end{aligned} \tag{3.34}$$

This implies that the energy shift is calculated as an expectation value of a radiative one-electron potential using the eigenfunctions of the DHF operator. In general the radiative perturbation is a series expansion in the two parameters α and $Z\alpha$, where the powers of α describe the order of the QED corrections and $Z\alpha$ describes the order of relativistic corrections to the energy levels [107]. It is known that the latter expansion works quite well for lighter elements, but it is less than clear how well it works for elements with high nuclear charge such as the superheavy elements where $Z\alpha \lesssim 1$.

For the vacuum polarization the potential is well known. By utilizing perturbation theory for the polarization operator $\mathcal{P}(-p^2)$, the energy contribution of lowest order ($\alpha(Z\alpha)$) is given by the Uehling potential (3.22), where the virtual electron-positron pair is allowed to propagate freely (Fig. 3.2). The Uehling term gives typically more than 90% of the VP in hydrogen-like atoms. In presence of the nuclear Coulomb field the electron and positron wave functions become distorted. Wichmann and Kroll [110] have considered the vacuum polarization of order α in a strong Coulomb field (Fig. 3.2) and have shown that the polarization charge density is an analytic function of $Z\alpha$ for $|Z\alpha| \leq 1$,

$$\begin{aligned}\Phi_{\mathrm{WK}}(r) =& \frac{\alpha(Z\alpha)^3}{\pi}\left[\left(-\frac{3}{2}\zeta(3) + \frac{\pi^2}{6} - \frac{7}{9}\right)\frac{1}{r} + 2\pi\zeta(3)\right. \\ & \left. -\frac{\pi^3}{4} + \left(-6\zeta(3) + \frac{\pi^4}{16} - \frac{\pi^2}{6}\right)r + O(r^2)\right]. \end{aligned} \tag{3.35}$$

The Källen-Sabry correction [111] cannot be written in such a short analytical

form. Therefore, just the crucial Feynman diagrams are presented in Fig. 3.3.

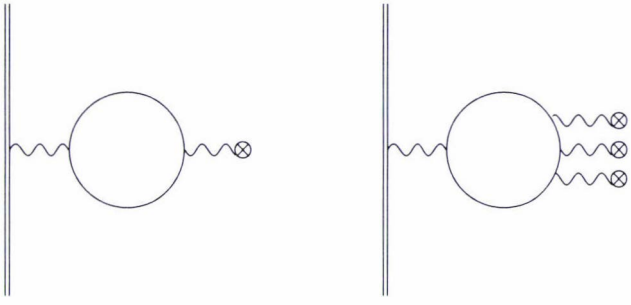

Figure 3.2: Feynman diagrams for vacuum polarization of order $\alpha(Z\alpha)$ Uehling (left) and of order $\alpha(Z\alpha)^3$ Wichmann and Kroll (right).

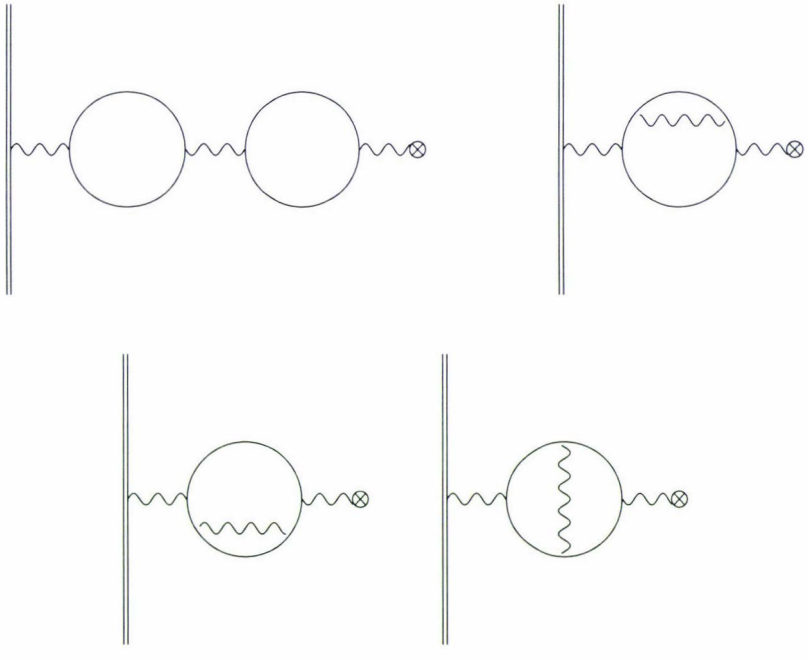

Figure 3.3: Vacuum polarization of order $\alpha^2(Z\alpha)$ (Källen-Sabry).

The calculation of the self-energy operator $\Sigma(r, r', E)$ shown in Fig. 3.4 is more complicated and rather tedious. The problem can, however, be divided into two parts. In the first part the electron interacts with a high frequency virtual photon where the nuclear Coulomb field needs to be included only in first order. The second part represents the interaction with a low frequency photon.

The radiative potential for the self-energy is given by a sum of three terms

$$\Phi_{SE}(r) = \Phi_{mag}(r) + \Phi_{el}(r) + \Phi_{low}(r), \tag{3.36}$$

which were derived in chapter 3.2. All three self-energy potentials Φ_{em}, Φ_{mag} and

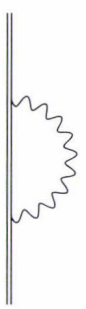

Figure 3.4: Feynman diagram of the electron self-energy

Φ_{low} were implemented into GRASP. For the numerical t-integration a modified Simpson-rule on a logarithmic grid was used to handle the pole of the integrands.

The function $A_n(Z)$ in the electric interaction term (3.28) was obtained by adjusting the obtained values to accurate calculations of self-energy contributions in hydrogen-like atoms for *ns* electrons by Mohr [102, 103, 112, 113]. A suitable choice for $A_n(Z)$ is

$$A_n(Z) = A_{n0} + A_{n1}\frac{Z}{1 + \exp[(Z/A_{n2})^5]}. \tag{3.37}$$

Adjusted coefficients A_{ni} for the different main quantum numbers are given in Table 3.1. For higher principal quantum numbers n, the coefficients A_{ni} can be derived from a least squares fit to the data in Table 3.1

$$A_{ni} = c_{i0}\left(1 + c_{i1}n^{c_{i2}}\right). \tag{3.38}$$

The coefficients are listed in Table 3.2.

n	A_{n0}	A_{n1}	A_{n2}
1	0.7645	0.00230	112.930
2	0.7912	0.00629	101.636
3	0.7980	0.00738	101.611
4	0.8009	0.00779	101.047
5	0.8023	0.00799	100.632
6	0.8032	0.00813	100.607
7	0.8037	0.00824	100.591
∞	0.8061	0.00860	100.765

Table 3.1: Adjusted coefficients $A_n(Z)$ for the electric interaction term in eq. (3.37).

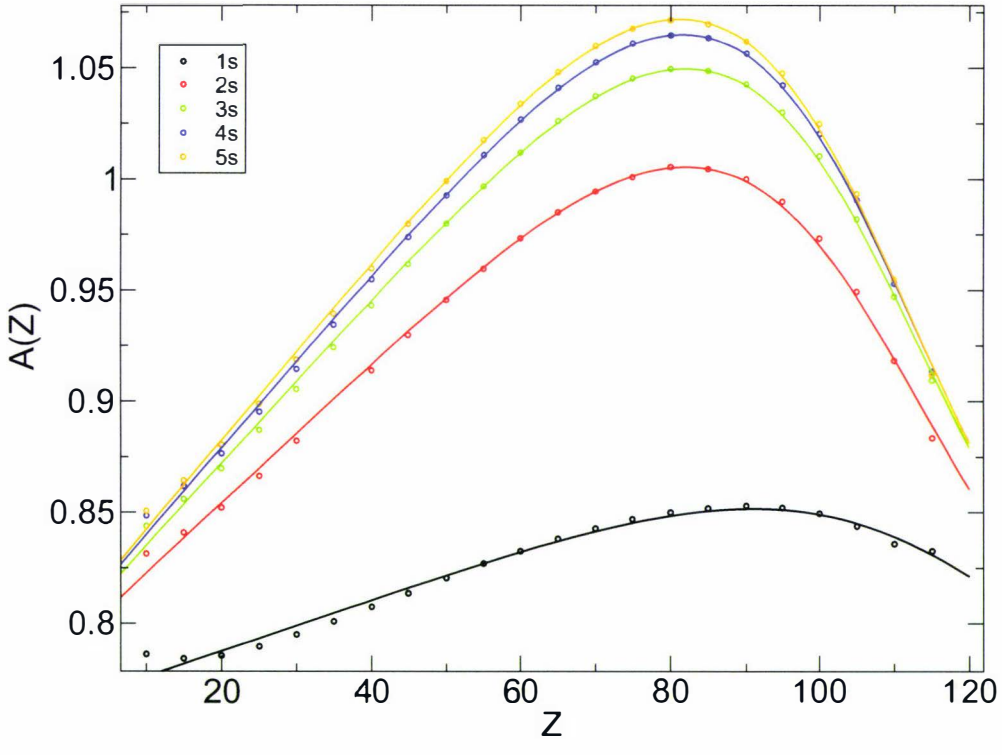

Figure 3.5: Adjusted coefficients $A_n(Z)$ for different ns orbitals for the electric interaction term in eq. (3.37)

i	c_{i0}	c_{i1}	c_{i2}
0	0.80608	-0.0516	1.489
1	0.00860	-0.7329	1.465
2	100.76488	0.1207	3.473

Table 3.2: Adjusted coefficients c_i for the coefficients A_{ni}

3.4 Results and Discussion

The calculated contributions from the VP, the SE and the BI to the ionization potential for Group 1, 2, 11, 12, 13 and 18 elements of the periodic table are given in Table 3.3.

The SE contribution is approximately an order of magnitude larger than the VP and has the opposite sign as one expects. However, the total VP contribution is increasing over several orders of magnitude for the heavier elements and becomes comparable to the SE term with increasing nuclear charge Z. This originates from the strong Coulomb field that the inner tail of the valence electrons experience with increasing nuclear charge. This is most important for the short-range Uehling potential. In fact the VP and SE contributions for the valence shell ionization potentials approximately fit a simple power law,

$$E(Z) = CZ^{\gamma} \tag{3.39}$$

as shown in Fig. 3.6. The coefficients C and γ are obtained from a linear regression and given in Table 3.4. It is worth mentioning that the exponent γ for the vacuum polarization as well as the self-energy of groups 11 and 12 is roughly 70% larger than for the others investigated groups. All three SE terms in (3.36) are important for the total SE contribution. A nice example is the $^2S_{1/2} \rightarrow {}^1S_0$ ionization of gold. The magnetic form-factor contribution to the total SE is 71 %, the electric form-factor contributes for 22 %, and the (long-range) low-frequency contribution is 7 %.

A comparison of the SE values to the results obtained by Labzowsky et al. [114] for group 1 and 11 valence-shell ionization potentials shows good agreement (Table 3.5). Note that for Rg and Cp, the relativistic 7s contraction is so large that ionization occurs out of the $6d_{5/2}$ shell instead of the $7s$ shell [115]. This is in contrast to the lighter group 1 and 11 elements where ionization occurs out of the valence ns shell. This explains the changing trend in all QED contributions down the group 11 and 12 in the periodic table. Note that Labzowsky et al. [114] only considered removal of an electron out of the ns shell. A recent paper by Indelicato et al. [116] also investigated QED effects in superheavy elements. Their total SE term within the Welton model [117] at the DHF level of theory for Rg is 0.084 eV, which is in good agreement with the presented value.

system	SE	VP	SC-GI ($\omega = 0$)	SC-BI ($\omega = 0$)	PT-BI ($\omega = 0$)	PT-BI($\omega - \omega_{=0}$)
Group 1 ($^2S_{1/2} \rightarrow {}^1S_0$)						
Li	-3.366×10^{-5}	1.189×10^{-6}	-1.418×10^{-4}	-1.279×10^{-4}	-1.279×10^{-4}	-9.450×10^{-9}
Na	-1.366×10^{-4}	1.639×10^{-5}	-2.734×10^{-4}	-2.799×10^{-4}	-2.088×10^{-4}	-7.250×10^{-7}
K	-5.414×10^{-4}	3.729×10^{-5}	-2.482×10^{-4}	-2.751×10^{-4}	-2.753×10^{-4}	-3.530×10^{-6}
Rb	-9.720×10^{-4}	1.440×10^{-4}	-2.630×10^{-4}	-3.568×10^{-4}	-3.580×10^{-4}	-2.770×10^{-5}
Cs	-2.376×10^{-3}	3.296×10^{-4}	-2.247×10^{-4}	-3.711×10^{-4}	-3.736×10^{-4}	-8.800×10^{-5}
Fr	-6.150×10^{-3}	1.651×10^{-3}	-4.816×10^{-4}	-7.454×10^{-4}	-7.457×10^{-4}	-5.130×10^{-4}
E119	-2.120×10^{-2}	1.212×10^{-2}	-4.244×10^{-3}	-4.650×10^{-3}	-4.639×10^{-3}	-3.070×10^{-3}
Group 2 ($^1S_0 \rightarrow {}^2S_{1/2}$)						
Be	-8.998×10^{-5}	3.450×10^{-6}	-3.763×10^{-4}	-3.460×10^{-4}	-3.460×10^{-4}	-2.550×10^{-8}
Mg	-4.436×10^{-4}	2.469×10^{-5}	-5.319×10^{-4}	-5.206×10^{-4}	-5.208×10^{-4}	-1.136×10^{-6}
Ca	-6.976×10^{-4}	4.860×10^{-5}	-4.602×10^{-4}	-4.690×10^{-4}	-4.693×10^{-4}	-4.600×10^{-6}
Sr	-1.705×10^{-4}	1.728×10^{-4}	-5.628×10^{-4}	-6.297×10^{-4}	-6.318×10^{-4}	-3.170×10^{-5}
Ba	-2.729×10^{-3}	3.814×10^{-4}	-5.679×10^{-4}	-6.793×10^{-4}	-6.814×10^{-4}	-9.700×10^{-5}
Ra	-6.982×10^{-3}	1.786×10^{-3}	-1.060×10^{-3}	-1.254×10^{-3}	-1.256×10^{-3}	-5.370×10^{-4}
E120	-2.278×10^{-2}	1.321×10^{-2}	-5.341×10^{-3}	-5.591×10^{-3}	-5.593×10^{-3}	-3.120×10^{-3}
Group 11 ($^2S_{1/2} \rightarrow {}^1S_0$)						
Cu	-3.328×10^{-3}	2.765×10^{-4}	-3.686×10^{-3}	-3.437×10^{-3}	-3.448×10^{-3}	-4.900×10^{-6}
Ag	-7.377×10^{-3}	8.495×10^{-4}	-5.432×10^{-3}	-5.188×10^{-3}	-5.210×10^{-3}	-4.630×10^{-5}
Au	-2.643×10^{-2}	5.284×10^{-3}	-1.274×10^{-2}	-1.224×10^{-2}	-1.232×10^{-2}	-4.660×10^{-4}
Rg	-8.958×10^{-2}	3.648×10^{-2}	-3.643×10^{-2}	-3.423×10^{-2}	-3.444×10^{-2}	-3.400×10^{-3}
Rg[a]	3.290×10^{-2}	-1.276×10^{-2}	2.958×10^{-2}	2.791×10^{-2}	2.796×10^{-2}	-6.000×10^{-4}
Group 12 ($^1S_0 \rightarrow {}^2S_{1/2}$)						
Zn	-3.366×10^{-3}	2.864×10^{-4}	-3.414×10^{-3}	-3.217×10^{-3}	-3.236×10^{-3}	-1.090×10^{-5}
Cd	-7.287×10^{-3}	8.559×10^{-4}	-5.110×10^{-3}	-4.905×10^{-3}	-4.926×10^{-3}	-6.100×10^{-5}
Hg	-2.575×10^{-2}	5.262×10^{-3}	-1.208×10^{-2}	-1.162×10^{-2}	-1.169×10^{-2}	-5.230×10^{-4}
Cp	-9.076×10^{-2}	3.790×10^{-2}	-3.682×10^{-2}	-3.457×10^{-2}	-3.478×10^{-2}	-3.640×10^{-3}
Cp[b]	3.520×10^{-2}	-1.397×10^{-2}	3.072×10^{-2}	2.898×10^{-2}	2.900×10^{-2}	-6.700×10^{-4}
Group 13 ($^2P_{1/2} \rightarrow {}^1S_0$)						
B	2.381×10^{-4}	-9.695×10^{-6}	-8.681×10^{-4}	-6.847×10^{-4}	-6.848×10^{-4}	1.305×10^{-7}
Al	5.776×10^{-4}	-3.210×10^{-5}	-1.291×10^{-3}	-1.071×10^{-3}	-1.071×10^{-3}	3.100×10^{-7}
Ga	2.018×10^{-3}	-1.707×10^{-4}	-4.157×10^{-3}	-3.482×10^{-3}	-3.490×10^{-3}	7.600×10^{-6}
In	3.466×10^{-3}	-4.010×10^{-4}	-7.249×10^{-3}	-6.184×10^{-3}	-6.213×10^{-3}	1.943×10^{-4}
Tl	6.226×10^{-3}	-1.230×10^{-3}	-1.673×10^{-2}	-1.488×10^{-2}	-1.502×10^{-2}	-2.180×10^{-4}
E113	-3.143×10^{-3}	2.860×10^{-3}	-4.877×10^{-2}	-4.615×10^{-2}	-4.479×10^{-2}	-4.679×10^{-3}
Group 18 ($^1S_0 \rightarrow {}^2P_{3/2}$)						
He	-1.781×10^{-4}	5.871×10^{-6}	-1.735×10^{-3}	-1.736×10^{-3}	-1.735×10^{-3}	0.000×10^{-0}
Ne	1.037×10^{-3}	-6.090×10^{-5}	-2.152×10^{-3}	-1.473×10^{-3}	-1.473×10^{-3}	1.217×10^{-5}
Ar	1.240×10^{-3}	-9.531×10^{-5}	-1.488×10^{-3}	-7.247×10^{-3}	-7.235×10^{-4}	3.993×10^{-5}
Kr	2.374×10^{-3}	-2.986×10^{-4}	-3.056×10^{-3}	-1.675×10^{-3}	-1.674×10^{-3}	2.897×10^{-4}
Xe	3.183×10^{-3}	-6.060×10^{-4}	-4.149×10^{-3}	-2.370×10^{-3}	-2.373×10^{-3}	8.240×10^{-4}
Rn	6.142×10^{-3}	-2.290×10^{-3}	-4.828×10^{-3}	-2.336×10^{-3}	-2.357×10^{-3}	3.129×10^{-3}
E118	1.192×10^{-2}	-8.441×10^{-3}	-1.631×10^{-3}	9.422×10^{-4}	8.613×10^{-4}	6.350×10^{-3}

Table 3.3: The self-energy (SE), vacuum polarization (VP) and frequency-dependent Breit contributions (BI) (in eV) and sum over all QED contributions to the ionization potential $E \rightarrow E^+$ of each element E at the DHF level of theory. Notation: SC: self-consistent treatment; PT: Perturbative treatment; GI: Gaunt term only; ω=0: low frequency limit. The last term PT-BI($\omega - \omega_{=0}$) denotes the correction to the Breit interaction due to the finite frequency of the transversal exchange photon. [a] The $^2D_{5/2} \rightarrow {}^3D_3$ transition is taken. [b] The $^1S_0 \rightarrow {}^2D_{5/2}$ transition is taken.

group	C_{SE} [eV]	γ_{SE}	C_{VP} [eV]	γ_{VP}
1	3.510×10^{-6}	1.685	5.867×10^{-8}	2.318
2	9.246×10^{-6}	1.505	9.074×10^{-8}	2.236
11	7.880×10^{-7}	2.427	1.218×10^{-9}	3.576
12	6.298×10^{-7}	2.469	8.841×10^{-10}	3.643
13	3.136×10^{-5}	1.202	4.719×10^{-7}	1.746
18	8.682×10^{-5}	0.965	4.193×10^{-7}	1.944

Table 3.4: Adjusted parameters C and γ from a linear fit of the loglog plot in eq. (3.39).

The SE and VP contributions for the Group 13 and 18 elements of the periodic table are also listed for comparison. However, one needs to include QED effects self-consistently to properly account for second-order effects originating from SE/VP core-relaxation of the *s*-electrons at the nucleus, which leads to shielding/de-shielding of the nuclear charge. For a detailed discussion see Flambaum and Ginges [24] as well as Derevianko et al. [118]. Nevertheless, the results clearly show that even for the superheavy elements, SE and VP contributions for the *p*-shell rarely exceed 0.01 eV and one can expect even smaller effects for *d*-and *f*-shells.

Table 3.3 shows that, as expected, the frequency independent (instantaneous) Gaunt term is the dominant contribution to the total Breit interaction for all elements considered, as discussed earlier in great detail by Lindroth et al. [119]. It was confirmed that the frequency dependent contribution to the BI is negligible for the lighter elements, but can become rather large for high nuclear charges. For high Z such contributions cannot be neglected anymore in the valence space, even in lowest order.

There has been intensive discussion in the past if the two-electron Breit term should be used perturbatively or variationally [120–122]. Grant pointed out that a variational procedure is clearly preferred in a subsequent treatment of electron correlation [123]. Moreover, it has been argued that a variational treatment of the Breit interaction is most important for valence properties in many-electron systems [119]. In order to analyze this in more detail, the difference of a self-consistent with a perturbative treatment for the Breit interaction is compared for a series of elements in the periodic table. The results in Table 3.3 clearly show that the self-consistent total energy contribution to the ionization potential does not differ significantly from the perturbative treatment even for high Z atoms.

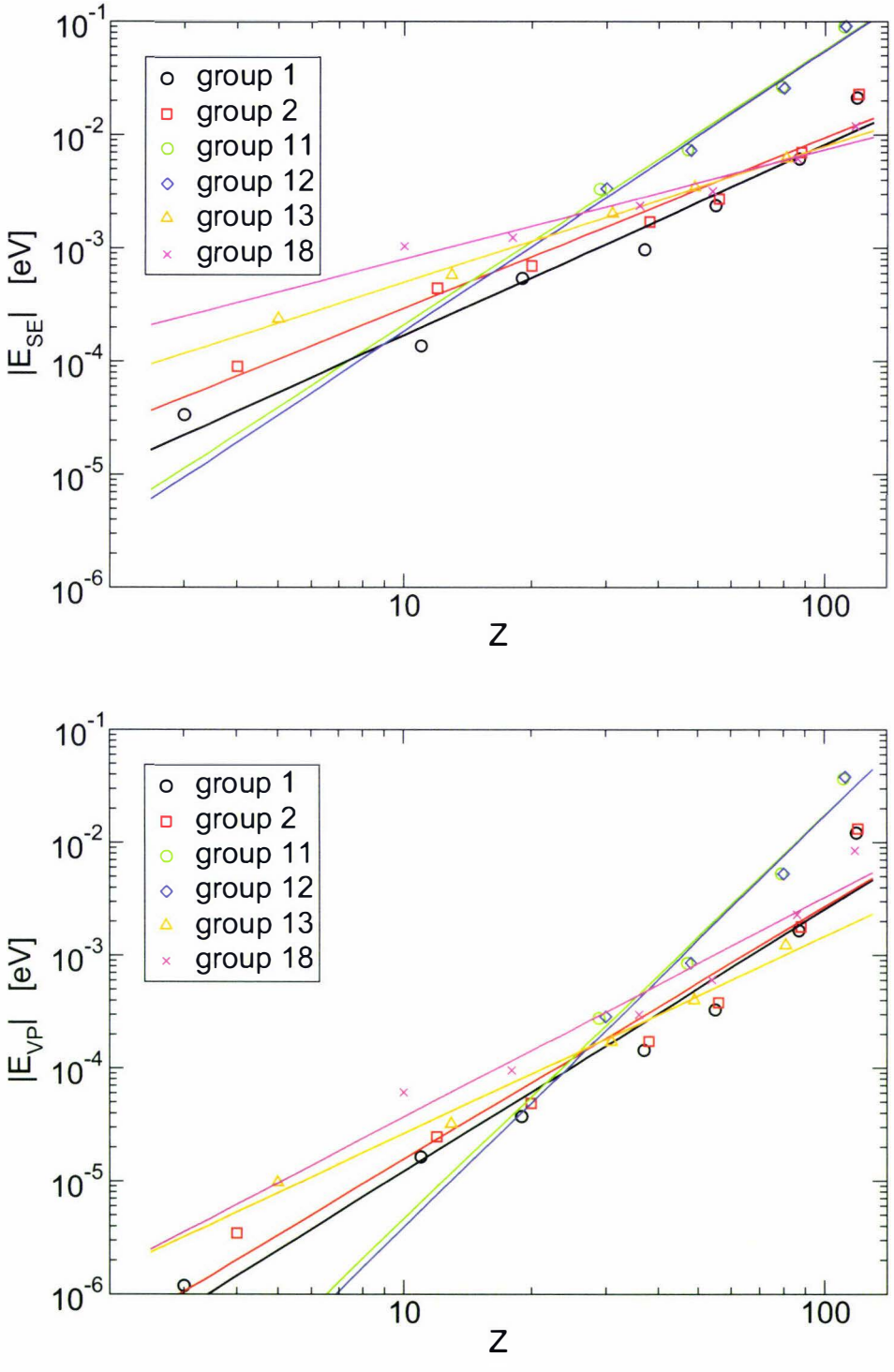

Figure 3.6: Self-energy and vacuum polarization contribution to the ionization potential of different atoms.

This is in agreement with the results of Ishikawa et al. who found similar small changes for Ne, Ar and Xe [124].

system	our work	Ref. [114]
Li	-3.366×10^{-5}	-3.84×10^{-5}
Na	-1.366×10^{-4}	-2.83×10^{-4}
K	-5.414×10^{-4}	-4.93×10^{-4}
Rb	-9.720×10^{-4}	-1.23×10^{-3}
Cs	-2.376×10^{-3}	-2.15×10^{-3}
Fr	-6.150×10^{-3}	-6.03×10^{-3}
E119	-2.120×10^{-2}	-2.74×10^{-2}
Cu	-3.328×10^{-3}	-2.66×10^{-3}
Ag	-7.377×10^{-3}	-6.14×10^{-3}
Au	-2.643×10^{-2}	-2.21×10^{-2}
Rg	-8.958×10^{-2}	-8.66×10^{-2}

Table 3.5: A comparison between our calculated SE contributions with those of Labzowsky et al. [114] for the ionization energies ($^2S_{1/2} \rightarrow {}^1S_0$) of the alkali and coinage metal atoms (in eV).

Furthermore a detailed study of the Breit contributions to the orbital energies for the neutral mercury atom, similar to the work by Lindroth et al. [119], was performed. (Table 3.6). For the self-consistent treatment, the results of Lindroth and co-workers [119] were reproduced. The perturbative treatment gives qualitatively the same values for the orbital energy contributions. Here, the orbitals from a Dirac-Hartree-Fock calculation (without Breit or any other QED contributions) were used to calculate the change in orbital energies due to the frequency independent Breit term. It is evident that the largest contributions come from the inner shells. However, the difference in both treatments becomes rather large in the valence shell, as observed earlier by Lindroth et al. [119].

Naturally, one relates orbital energies to ionization potentials by Koopmans theorem [125]. The data in Table 3.7 proves that Koopmans' theorem is still valid for the Breit contributions, as both changes in orbital energies and direct calculations of energy differences between the neutral and charged atoms give very similar results for all ionizations out of specific nlj levels in the mercury atom. A full variational treatment includes changes in Coulomb- and exchange contributions of the Breit interaction due to orbital relaxation, which obviously cannot be neglected anymore for orbital energies. Moreover, the DHF orbitals are not eigenfunctions to the Fock-operator including the Breit term. One should therefore

Hg	DHF	PT-BI	PT-BI [119]	SC-BI	SC-BI [119]
1s	-83696.997	312.191	315.103	298.661	298.233
2s	-14979.173	41.981	41.714	33.486	33.470
3s	-3623.573	9.926	9.635	6.198	6.193
4s	-834.330	2.761	2.496	1.272	1.270
5s	-138.927	0.568	0.493	0.192	0.191
6s	-8.932	0.038	0.042	0.012	0.012
2p*	-14336.797	66.549	65.470	56.259	56.245
3p*	-3337.260	15.397	14.337	10.704	10.702
4p*	-710.891	4.153	3.491	2.269	2.269
5p*	-96.271	0.778	0.593	0.330	0.330
2p	-12385.198	45.457	43.918	35.505	35.510
3p	-2899.170	11.147	9.736	6.386	6.386
4p	-603.760	3.203	2.322	1.186	1.186
5p	-77.326	0.628	0.373	0.131	0.131
3d*	-2433.623	9.369	8.304	4.648	4.648
4d*	-402.618	2.405	1.349	0.625	0.625
5d*	-17.683	0.273	0.119	0.007	0.007
3d	-2340.654	7.619	8.304	2.989	2.988
4d	-382.369	1.972	1.349	0.260	0.260
5d	-15.631	0.219	0.119	-0.030	-0.030
4f*	-121.699	1.218	0.759	-0.158	-0.158
4f	-117.313	1.032	0.597	-0.313	-0.313

Table 3.6: Dirac-Hartree-Fock (DHF) orbital energies and self-consistent (SC) as well as perturbative (PT) Breit (BI) contributions (eV) to the corresponding orbital energies of the mercury atom in comparison with Lindroth et al. [119]. In the usual angular momentum notation asterisk denotes $j = l - 1/2$ and no asterisk denotes $j = l + 1/2$.

not conclude from the original perturbative analysis for orbital energies [119] that the Breit interaction for valence energies cannot be treated perturbatively anymore for the valence shell. On the contrary, the results clearly demonstrate that, if high precision is not required, a perturbative treatment of the Breit interaction for the valence space is sufficient. However, to incorporate changes in atomic (or molecular) properties due to the Breit term (see for example refs. [126, 127] for recent molecular work), a variational treatment is preferred.

Finally, recent accurate Fock-space coupled-cluster calculations for the gold atom by Eliav et al. [128] should be mentioned. The calculated ionization potential of 9.197 eV changes to 9.176 eV when VP and SE is included, which now is in

nl	ΔE	$\Delta\varepsilon$
1s	302.439	298.661
2s	33.693	33.486
3s	6.186	6.198
4s	1.250	1.272
5s	0.184	0.192
6s	0.012	0.012
2p*	56.452	56.259
3p*	10.661	10.704
4p*	2.232	2.269
5p*	0.316	0.330
2p	35.741	35.505
3p	6.374	6.386
4p	1.165	1.186
5p	0.125	0.131
3d*	4.651	4.648
4d*	0.608	0.625
5d*	0.004	0.007
3d	3.010	2.989
4d	0.251	0.260
5d	-0.029	-0.030
4f*	-0.161	-0.158
4f	-0.308	-0.313

Table 3.7: Comparison of the Breit contribution (eV) to the ionization energy ΔE of the mercury atom compared to the Breit contribution to the orbital energy $\Delta\varepsilon$ obtained from a variational treatment of the Breit interaction for the mercury neutral atom. The removal of an electron is calculated for each shell with quantum number nlj. In the usual angular momentum notation the Asterix denotes $j = l - 1/2$ and no Asterix denotes $j = l + 1/2$.

less good agreement with the experimental value of 9.225 eV [129]. Hence, the total correlation error is estimated to be 0.049 eV in Eliav's calculation, that is 96.8 % of the total electron correlation has been accounted for. This clearly demonstrates that the bottleneck in such calculations still remains in the electron correlation treatment.

Chapter 4

Dirac-Hartree-Fock studies of X-ray transitions in Meitnerium

4.1 Superheavy elements

Transuranium elements are usually man-made. By neutron capture, for example in supernovae explosions or in high flux reactors, and subsequent β^- decay, it is possible to produce elements up to fermium. While from neptunium to californium some isotopes can be produced in amounts of grams, the two heaviest species, ^{254}Es and ^{257}Fm, are only available in quantities of micro- and picograms, respectively [130]. Due to the lack of β^- decay and too short α and fission half-lives of the heavier elements this method ends at fermium.

Hence, one faces huge problems for the production of superheavy elements. The best possibility to access elements beyond fermium is by utilizing heavy-ion fusion reactions. This can be done by shooting heavy, neutron-rich ions from accelerators on heavy-element targets. Unfortunately, the cross-section for such a process is very small. Nevertheless, a wide range of projectiles and targets are available. Possible combinations are actinide targets irradiated by relatively light projectiles ranging from neon to calcium, or bismuth targets with projectiles ranging from calcium to krypton for example. Since the ratio of neutrons to protons increases with the nucleon number A, one cannot easily combine nuclei from the known region to reach the so-called island of stability, because the produced nuclei would be severely neutron-deficient. The heaviest elements have so far been produced by

using very neutron-rich radioactive projectiles and targets. Generic accelerators are cyclotrons with diameters of a few meters and high-beam currents in order to compensate for the decreasing cross-section for the nuclear synthesis.

The first transuranium elements were identified by using their α-decay and chemical properties. Later, physical techniques were developed which made it possible to detect nuclei with lifetimes of less than a second. Further improvements of these methods culminated in the velocity Filter SHIP at the GSI in Darmstadt. It is an electromagnetic separator, designed for in-flight separation of unretarded complete fusion reaction products. The main subjects for investigation are α-, proton-emitting and spontaneously fissioning nuclei far from stability with half-lives as short as microseconds or below and formation cross-sections down to the picobarn region [12].

The study of the reaction $^{64}\mathrm{Ni} + ^{209}\mathrm{Bi} \rightarrow {}^{273}\mathrm{Rg}^*$ with beam energies ranging from 300 to 400 MeV revealed a complex decay chain (Fig. 4.1). In the first two measurements in 1994 and 2000 a total of six atoms were observed at the GSI in Darmstadt [131, 132]. The half-lives of the products are in the range of

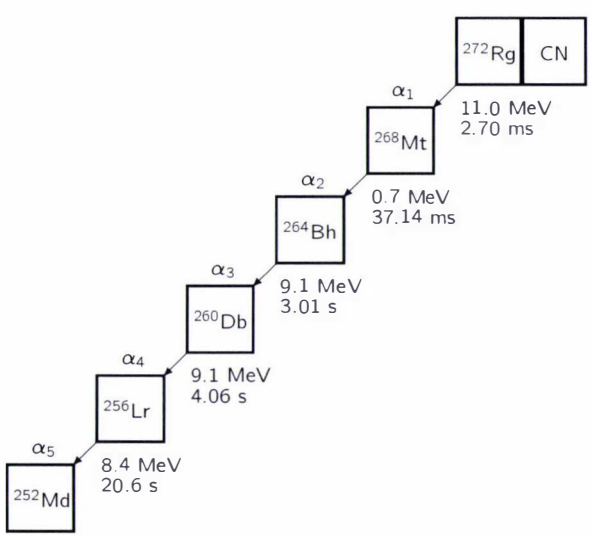

Figure 4.1: Possible decay chain of $^{272}\mathrm{Rg}$ which is produced by $^{64}\mathrm{Ni} + ^{209}\mathrm{Bi} \rightarrow {}^{273}\mathrm{Rg}^*$ and a subsequent neutron emission [132]

milliseconds to seconds and are very common for such superheavy elements. The nuclei were identified by position and time correlation analysis which allows to

establish genetic relations of the nuclei within the decay chain. The data were measured by using position sensitive Si detectors [133].

The stability of superheavy elements can be determined from calculations of the nuclear ground-state binding energy. In macroscopic-microscopic models the binding energy is given by a sum of the macroscopic part, derived from the liquid drop model of the nucleus, and the microscopic part, which is deduced from the nuclear shell model. The advantage of this hybrid model is that more exact values for the binding energy can be obtained as parameters are used from measurements of known nuclei [134, 135].

The knowledge of the ground-state binding energy, however, is not sufficient for the calculation of partial spontaneous fission half-lives. Here, it is also necessary to determine the size of the fission barrier over a wide range of deformation. These calculations of spontaneous fission and α-decay rates predict especially stable nuclei with closed shells near $Z = 114$, 120 or 126 and possibly for $Z = 164$.

4.2 Meitnerium Experiments

In heavy ion separators like the velocity filter SHIP at the GSI in Darmstadt, the produced superheavy nuclei come to rest in less than a μs before they are investigated by their nuclear decay properties [12]. Such studies include precise mass measurements in ion traps [136], or by atom-at-a-time chemistry [137]. Being at rest, the atoms fill their electron shells within much less than a microsecond, probably in the picosecond or femtosecond time scale. Exceptions may arise for some of the outer shell electrons or for some exotic atomic or nuclear isomeric states. Hence, the history of the fusion process is completely forgotten as far as the electrons are concerned.

During and after radioactive decay, the electron shells have to reorganize. In the case of $^{272}_{111}$Rg an α-particle of about 11 MeV is emitted from a neutral 111 atom sitting on a Si lattice. The electrons have to rearrange from $Z = 111$ to $Z = 109$. The α-particle populates a nuclear level at 207 keV, so the recoil nucleus is excited, but comes again to rest quickly ($< 10^{-12}$ s), as the recoil velocity is small, and the atom is again or still charge neutral. The 207 keV state decays by γ-emission or K-conversion with a lifetime of $< 1\,\mu$s. In the

latter case the kinetic energy of the emitted electron is 207 keV minus K-shell binding energy of the neutral atom [132]. This electron leaves the atom within approximate 10^{-19} s. The hole in the K-shell is filled within approximately 10^{-16} s by an L-electron under emission of a K-X-ray followed by L-X-ray emission and/or a cascade of Auger electrons.

It is currently a non-trivial task to unambiguously identify new superheavy elements, as the isotopes of the decay products are not always known. In this context the coincidence of the $^{272}_{111}$Rg α-decay with a measured signal of (155.0 ± 0.8) keV energy in the Ge detector [132] is especially interesting as it is close to the predicted $K_{\alpha 1}$ X-ray energy of $_{109}$Mt of Carlson *et al.* [138]. Ionization potentials of K- and L-shell electrons for superheavy elements can now accurately be obtained from relativistic quantum theoretical calculations [139] including quantum electrodynamic effects up to high orders for the most important inner shells, and up to the valence shell [24, 98, 99, 116, 140]. In the following the 155.0 keV signal is investigated as a possible K-inversion event of $^{268}_{109}$Mt.

4.3 Computational details

Dirac-Hartree-Fock (DHF) calculations were performed using the Dirac-Coulomb Hamiltonian The equations are solved numerically using a modified code of the program system GRASP [104]. The K_α transition energies are obtained by calculating the difference in the total electronic energy between the different electronic states. The 1s-shell radius of meitnerium is very small ($\langle r \rangle_{1s} = 546$ fm), and as a consequence the influence of the finite nuclear size cannot be neglected anymore. The electrostatic potential of the nucleus V_{nuc} was therefore modeled by an extended charge distribution. The nuclear charge distribution can be obtained from scattering experiments where high energy electrons are scattered on nuclei (Mott scattering) [141]. In scattering processes with large momentum transfer the resolution is increased due to the reduced wavelength of the virtual photon. Therefore the scattered electron is no longer sensible to the total charge of the nucleus, but only parts of it. The spatial extension of the spherically symmetric nucleus is described by the form factor $F(\vec{q}^2)$ which depends only on the momentum transfer $\vec{q}$. Experimentally, the magnitude of the form factor is determined

by the ratio of the measured cross section to the Mott cross section

$$\left(\frac{d\sigma}{d\Omega}\right)_{exp} = \left(\frac{d\sigma}{d\Omega}\right)_{Mott} \cdot |F(\vec{q}^2)|^2. \tag{4.1}$$

In principle, the normalized radial charge distribution $f(r)$ can be determined from the inverse Fourier transform of the $\vec{q}^2$-dependence of the experimental form factor

$$f(r) = \frac{1}{2\pi^3} \int F(\vec{q}^2) \exp(-i\vec{q} \cdot \vec{x}/\hbar) d^3\vec{q}. \tag{4.2}$$

Some examples are given in Fig. 4.2. It can be seen that the interior charge density is nearly constant and that it falls off over a relatively large range at the surface. These charge distributions can be approximately described by the

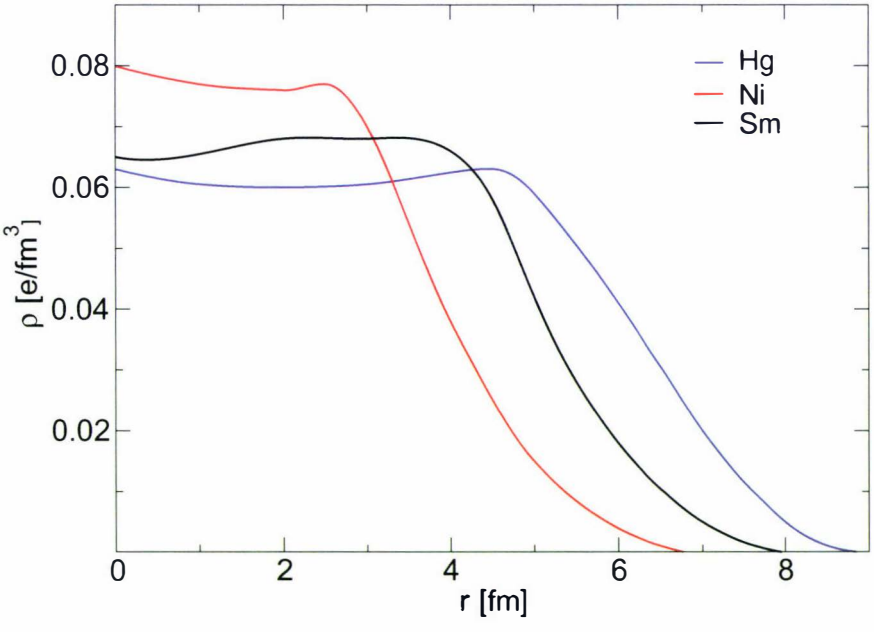

Figure 4.2: Radial charge distribution of various nuclei.

two-parameter Fermi distribution

$$\varrho(r) = \frac{\varrho_0}{1 + \exp\left[(r-a)/b\right]} \tag{4.3}$$

where a and b were taken from ref. [105]. For superheavy atoms, QED effects have to be taken into account [24, 98, 99, 116, 139, 140, 142], which is done perturbatively (as discussed in chapter 2). This approximation leads to deviations of no more than a few eV for all known K- and L-shell ionization potentials up to the heaviest elements [139]. All other (minor) corrections (*e.g.* electron correlation or mass polarization effects) are neglected.

4.4 Results and Discussion

In order to assess the accuracy of the various approximations used, the K_α transition energies for all Group 9 transition-metals are calculated. The results are shown in Table 4.1. For cobalt, rhodium and iridium they are accurate to 15 eV as compared to experiment, which implies that the code produces reliable results. However, for meitnerium this is not the case. The difference between the

element	$K_{\alpha_1}^{\text{exp}}$	$K_{\alpha_1}^{\text{calc}}$	$K_{\alpha_2}^{\text{exp}}$	$K_{\alpha_2}^{\text{calc}}$
$^{59}_{27}$Co	6.930	6.929	6.915	6.913
$^{103}_{45}$Rh	20.216	20.215	20.074	20.072
$^{193}_{77}$Ir	64.895	64.883	63.286	63.271
$^{268}_{109}$Mt	155.000	151.780	–	141.610

Table 4.1: Calculated and measured K_α transition energies (in keV) of the Group 9 transition-metals. Experimental values are from refs. [132, 143].

calculated and the experimental value is (3.2 ± 0.8) keV. The deviation cannot be explained by missing terms like electron correlation (which is less than 1 eV per electron [144]). Size-consistent effects neglected by the perturbative QED treatment are also in the eV region.

To further evaluate the accuracy of the method applied, some recently measured K_α and K_β transitions for few selected heavy actinide and transactinide elements (Table 4.2) are listed. These values were obtained in various spectroscopy studies at SHIP, see ref. [145], and the calculated values fit very well with the experimental findings. There are a number of possibilities for the rather large difference in the case of meitnerium. The first possibility is that the meitnerium atom could be in an ionized electronic state which implies that some of the outer valence electrons could be missing. Hence, the K-$(1s)$, L-$(2s)$, L-$(2s_{1/2})$ and L-$(2p_{3/2})$ electron

element	$K_{\alpha_2}^{exp}$	$K_{\alpha_2}^{calc}$	$K_{\alpha_1}^{exp}$	$K_{\alpha_1}^{calc}$	$K_{\beta_1}^{exp}$	$K_{\beta_1}^{calc}$	$K_{\beta_2}^{exp}$	$K_{\beta_2}^{II\,calc}$	$K_{\beta_2}^{I\,calc}$
$^{243}_{98}$Cf	110.1±0.1	109.837	115.2±0.1	115.040	129.6±0.1	129.821	134.6±0.4	133.317	133.651
$^{243}_{99}$Es	113.3±0.3	112.539	117.8±0.2	118.021	132.7±0.2	133.136	138.0±0.2	136.712	137.066
$^{251}_{100}$Fm	115.2±0.1	115.287	121.0±0.1	121.062	135.8±0.2	136.515	140.9±0.2	140.171	140.547
$^{253}_{100}$Fm	114.9±0.1	115.286	120.5±0.1	121.061	135.8±0.2	136.514	140.1±0.2	140.170	140.546
$^{253}_{101}$Md	117.7±0.1	118.090	123.9±0.1	124.173	138.7±0.2	139.968	144.1±0.4	143.704	144.103
$^{253}_{102}$No	121.0±0.1	120.952	127.2±0.1	127.359	142.6±0.2	143.498	147.4±3.1	147.316	147.738
$^{255}_{103}$Lr	123.9±0.2	123.867	130.5±0.1	130.613	–	147.101	–	151.000	151.446
$^{257}_{104}$Rf	126.7±0.4	126.839	133.5±0.4	133.941	150.3±0.3	150.782	–	154.762	155.235

Table 4.2: Calculated and measured K_α and K_β ($K_{\beta_2}^{I} = N_3 \rightarrow K, K_{\beta_2}^{II} = N_2 \rightarrow K$) transition energies (in keV) for various actinide and transactinide isotopes. Experimental values were obtained in various spectroscopy studies at SHIP, see for example ref. [145].

ionization potentials were calculated for various states of ionization, by varying the number of electrons between $N_E = 1$ and $N_E = Z$, that is successively filling the inner shells, with all atoms kept in the electronic ground state. For simplicity only closed shell states were selected. For future experimental and theoretical use all data are listed in table 4.3.

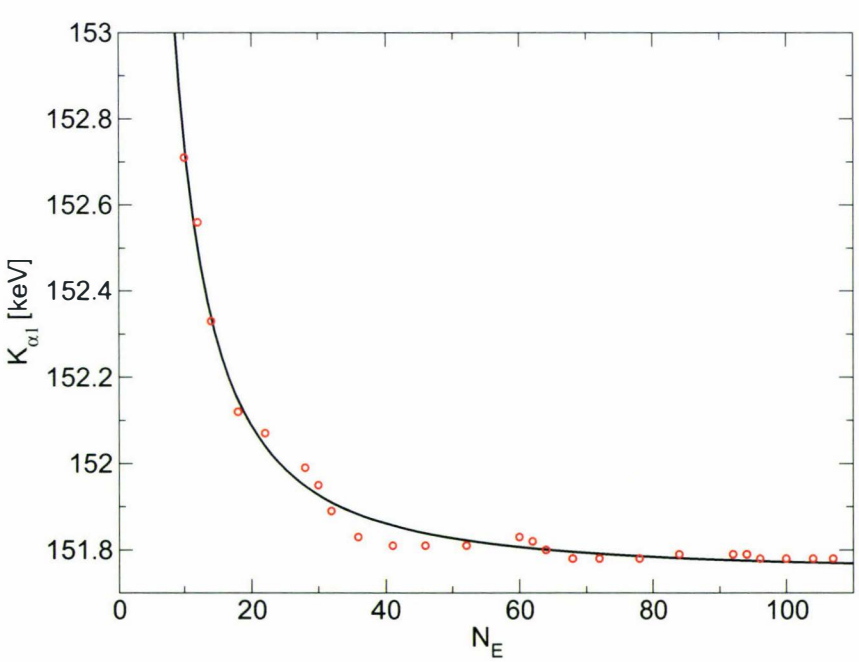

Figure 4.3: K_{α_1} transition energy of meitnerium depending on the number of remaining electrons N_E.

N_E	E^{ion}_{1s}	E^{ion}_{2s}	$E^{ion}_{2p_{1/2}}$	$E^{ion}_{2p_{3/2}}$
109	-177.322	-35.786	-34.724	-25.543
107	-177.344	-35.801	-34.737	-25.562
104	-177.387	-35.844	-34.780	-25.605
100	-177.459	-35.916	-34.852	-25.677
96	-177.552	-36.007	-34.944	-25.768
94	-177.610	-36.062	-35.999	-25.823
92	-177.671	-36.120	-35.058	-25.881
84	-177.975	-36.427	-35.364	-26.189
78	-178.243	-36.700	-35.636	-26.462
72	-178.570	-37.026	-35.964	-26.787
68	-178.811	-37.266	-36.204	-27.026
64	-179.076	-37.519	-36.460	-27.277
62	-179.236	-37.663	-36.605	-27.420
60	-179.392	-37.806	-36.751	-27.564
52	-180.237	-38.667	-37.608	-28.426
46	-180.943	-39.387	-38.325	-29.147
41	-181.727	-40.162	-39.109	-29.915
36	-182.302	-40.724	-39.673	-30.476
32	-182.904	-41.275	-40.241	-31.019
30	-183.283	-41.593	-40.560	-31.332
28	-183.630	-41.895	-40.875	-31.636
22	-185.283	-43.503	-42.517	-33.215
18	-186.514	-44.685	-43.709	-34.393
14	-187.781	-45.774	-44.855	-35.451
12	-188.640	-46.424	-45.504	-36.083
10	-189.377	-47.003	-46.132	-36.672
6	-192.329	-49.059	-48.547	-
4	-194.649	-50.299	-	-
2	-196.414	-	-	-
1	-199.599	-	-	-

Table 4.3: K- and L-shell ionization potentials (in keV) of meitnerium dependent on the number of electrons (N_E).

N_E	K_{α_2}	K_{α_1}
107	142.608	151.782
104	142.607	151.782
100	142.607	151.782
96	142.607	151.782
94	142.611	151.794
92	142.613	151.798
84	142.611	151.788
78	142.607	151.781
72	142.606	151.783
68	142.607	151.785
64	142.616	151.799
62	142.632	151.817
60	142.641	151.828
52	142.629	151.811
46	142.618	151.796
41	142.618	151.812
36	142.628	151.825
32	142.663	151.885
30	142.723	151.951
28	142.756	151.995
22	142.766	152.067
18	142.805	152.121
14	142.926	152.330
12	143.136	152.556
10	143.245	152.706
6	143.781	-

Table 4.4: K_{α_1} and K_{α_2} transition energies (in keV) of meitnerium dependent on the number of electrons (N_E).

Furthermore, the calculated K_{α_1} and K_{α_2} transition energies are listed in table 4.4.

A plot of the K_{α_1} transition energies (Fig. 4.3) reveals that the value increases exponentially with the number of missing electrons as discussed before for the superheavy elements [139]. This is attributed to the tail of one-particle functions that contribute to the screening of the nuclear charge.

Unfortunately, the transition energies are too small to explain the 155 keV transition even for the highest ionized closed shell state. Of course, some more exotic ionized states give more promising K_{α_1} values as shown in table 4.5, even though

these are most improbable. Another possibility is the influence of the finite nu-

element	K_{α_1}
$(1s^1 2p^1_{3/2}) \rightarrow (1s^2)$	155.026
$(1s^1 2s^1 2p^1_{3/2}) \rightarrow (1s^2 2s^1)$	155.671
$(1s^1 2s^2 2p^1_{3/2}) \rightarrow (1s^2 2s^2)$	154.327
$(1s^1 2p^1_{1/2} 2p^1_{3/2}) \rightarrow (1s^2 2p^1_{1/2})$	154.469

Table 4.5: K_{α_1} transition energies of meitnerium for some exotic highly ionized states.

element	K_{α_1}	K_{α_2}
$_{106}$Sg	140.832	132.961
$_{107}$Bh	144.403	136.114
$_{108}$Hs	148.061	139.336
$_{109}$Mt	151.782	142.606
$_{110}$Ds	155.625	145.965
$_{111}$Rg	159.554	149.389
$_{112}$Cp	163.563	152.867

Table 4.6: K_α transition energies (in keV) for elements with nuclear charge 106-112.

cleus size effect to the electronic structure. The effect of varying the radius a and the skin thickness b in the Fermi charge distribution, eq. (4.3), to the $K_{\alpha 1}$ energy is shown in Fig. 4.4. The total electronic energy is more sensitive to the size of the nucleus then to the skin thickness. Within the allowed variation (uncertainty) of nuclear size effects, this cannot explain the difference to the measured value either. Hence, one can conclude that the 155 keV event is not due to an X-ray, but is a γ-ray which is emitted from a 207 keV level in ^{268}Mt being populated by the α-decay of ^{272}Rg. For future reference the K_α transition energies for a number of superheavy elements are listed in table 4.6.

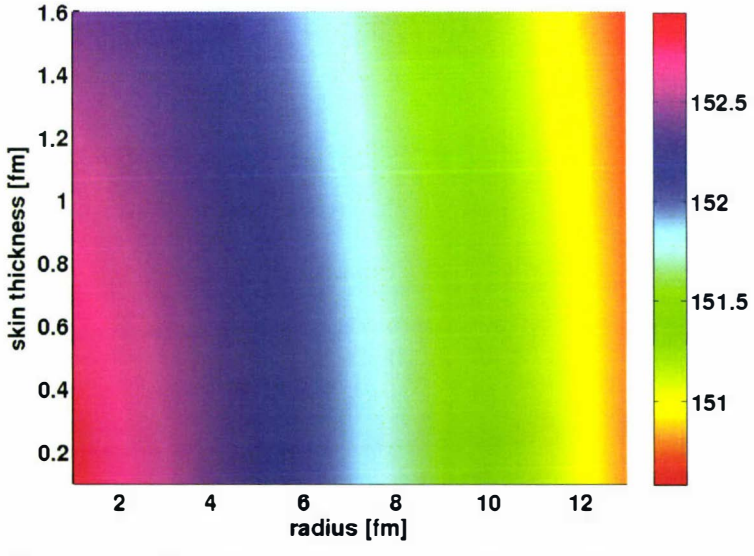

Figure 4.4: K_{α_1} transition energy (in keV) depending on the nuclear geometry.

Chapter 5

Static electric polarizabilities of group 14 atoms

The electric dipole polarizability is the tendency of a charge distribution, like the electron cloud of an atom or molecule, to be distorted from its normal shape by an external electric field. The static electric dipole polarizability α is defined as the ratio of the induced dipole moment $\vec{\mu}$ of an atom to the electric field $\vec{E}$ that produces this dipole moment,

$$\vec{\mu} = \alpha \vec{E}. \tag{5.1}$$

The polarizability is not a scalar quantity. In general, an homogeneous external electric field can induce a dipole moment in all three directions. Therefore, the polarizability is correctly described by an symmetric tensor of rank two

$$\mu_i = \alpha_{ij} E^j \tag{5.2}$$

and can be represented by a 3×3 matrix.

The accurate determination of these polarizabilities for isolated atoms or molecules currently constitutes a challenge for both experimental and theoretical research groups [146]. Recent advances on the experimental side include time-of-flight measurements of laser cooled atoms in an electric field, which, for example, have led to a considerable improvement in the accuracy for the dipole polarizability of cesium [147]. Also classical molecular beam electric field deflections meth-

ods [148–150] and interferometric techniques [151] offer valuable information. On the theoretical side one faces the difficulty of accurately describing electron correlation and relativistic effects, the latter increase substantially with increasing nuclear charge Z [152–154]. While closed-shell atoms and ions have been studied extensively in the past and accurate polarizabilities are available for most of these elements, open-shell species are far more difficult to treat as often a multi-reference procedure is required to resolve all the $|M_L|(|M_J|)$ components of the $LS(jj)$ coupled states [146]. It is therefore not surprising that accurate polarizabilities are not easily available for open p- [155] and especially for open d- and f-shell atoms or ions [154]. For the open d- and f-shell elements one has to rely on early relativistic local density functional calculations of Doolen, who lists averaged (isotropic) dipole polarizabilities [154, 156]. Laudable exceptions are the recent paper by Fleig [157], who calculated spin-orbit resolved static polarizabilities of the group 13 atoms using four-component relativistic configuration interaction and coupled-cluster methods, and the recent study of Kaldor and coworkers [158], who used Dirac-Coulomb coupled-cluster theory for the elements Hg, E112, Pb and E114.

Usually, electron correlation effects to dipole polarizabilities dominate over relativistic effects for the lighter elements, as electron correlation effects can be very large [159]. In 1981 both Desclaux et al. [160] and Sin Fai Lam [161] demonstrated however that relativistic effects cannot be neglected anymore for dipole polarizabilities in heavy atoms. An example is the Hg atom where relativistic effects almost halve the non-relativistic Hartree-Fock (NRHF) value from 80 to 43 au at the Dirac-Hartree-Fock (DHF) level of theory [162]. This is due to a large direct relativistic 6s-shell contraction. For closed p-shells, relativistic effects are much less pronounced, i.e. for Rn one obtains 47.6 au at the NRHF level of theory compared to 46.4 au at the DHF level of theory [161]. As the spin-orbit splitting becomes very large for the heaviest p-block elements in the periodic table, one expects that such effects will considerably influence the dipole polarizabilities. In order to fill the gap for open-shell polarizabilities, accurate non-relativistic and relativistic coupled-cluster calculations for all group 14 atoms in their $^3P_0$ ground state were performed. Here, one has the advantage that the $p_{1/2}$ shell is complete in the jj coupled scheme. Furthermore, there seems to be no experimental data available [163, 164]. As density functional theory came under scrutiny for properties which are dependent on the long-range behavior of the

density, the coupled-cluster results are compared to a number of well known density functional approximations. In addition, a comparison with new experimental measurements for the dipole polarizability of both Sn and Pb using a molecular beam electric field deflection technique [165] is performed.

5.1 Theoretical Methods

For the dipole polarizability calculations of the group 14 atoms non-relativistic (NR), scalar-relativistic Douglas-Kroll (DK) [166–169] and Dirac-Coulomb (four-component) [70] theory within both wavefunction based methods (Hartree-Fock, HF, second-order many-body perturbation theory for the electron correlation, MP2, and coupled-cluster singles-doubles including perturbative triples, CCSD(T)), and density functional theory (the local density functional approximation, LDA [170], the generalized gradient approximations PBE [171] and BLYP [172], and the hybrid functional B3LYP [173, 174]) were used. In the Dirac picture, Kramers (time-reversal) symmetry was applied in the coupled cluster procedure (KR-CCSD(T)) to save computer time [76]. If analytical procedures were not available for the calculation of the polarizability tensor, a finite field method was used instead. In this case, fields of 0.0, 0.001, 0.002 and 0.005 au were applied. In the non-relativistic and scalar relativistic cases the two tensor components of M_L=0 and $M_L = \pm 1$ were obtained in the finite field method by fixing the occupation of the p-orbitals lying parallel or perpendicular to the homogeneous electric field applied. For the open-shell case spin unrestricted Hartree-Fock and Kohn-Sham theory was used. Extensive, uncontracted Gaussian type basis sets were applied, which were thoroughly tested to yield converged polarizabilities with respect to basis set extension towards softer and harder functions at the coupled-cluster level. In detail: Starting from uncontracted, augmented correlation consistent quadruple-zeta basis sets (aug-cc-pVQZ) [175–177], $(13s/7p/4d/3f/2g)$ basis sets for C, $(17s/12p/4d/3f/2g)$ for Si and $(23s/19p/15d/4f/2g)$ for Ge were chosen. For these elements the full active orbital space was used in the electron correlation procedure. For Sn an extended dual-type Dyall-QZ basis set [178] was applied, and a soft $(3s/2p/3d/6f/2g)$ set of functions was added to end up with a $(36s/29p/21d/6f/2g)$ basis set. All orbitals between -12 au and +100 au (22 electrons) were correlated. Similarly, for Pb starting with the original Dyall-qz

set [178] a $(37s/33p/25d/19f/2g)$ basis set was finally chosen by adding a soft $(3s/2p/4d/5f/2g)$ set. Here, all orbitals between -10 au and +100 au (36 electrons) were correlated. For element 114 (E114) the Faegri basis set [179] was used as a starting point which lead to a decontracted $(32s/31p/24d/18f/3g)$ set of Gaussian functions. The correlated orbitals were between -7 au and +100 au (36 electrons). Finally, the Gaunt term was considered. In the Feynman gauge, the interaction between two electrons i and j becomes [180],

$$V_G\left(r_{ij}, \omega_{ij}\right) = r_{ij}^{-1}\left(1 - \vec{\alpha}_i \cdot \vec{\alpha}_j\right) e^{ic^{-1}|\omega_{ij}|r_{ij}}. \tag{5.3}$$

Since the frequency of the virtual exchange photon ω_{ij} is small compared to c/r_{ij} (c is the velocity of light), the frequency dependent exponential is neglected in the calculation (low frequency limit). Perdew and Cole implemented the Breit term within a local density approximation, but pointed out that accurate ionization potentials can only be achieved by including the self-interaction term in DFT [181]. Therefore the Gaunt interaction to the polarizability was evaluated at the Dirac-Hartree-Fock level of theory only.

At the non-relativistic and scalar-relativistic level of theory the (state) average polarizability $\bar{\alpha}$ and anisotropy $\Delta\alpha$ of the polarizability tensor for the $L = 1$ state is defined as

$$\bar{\alpha} = (\alpha_0 + 2\alpha_1)/3 \tag{5.4}$$

$$\Delta\alpha = \alpha_1 - \alpha_0, \tag{5.5}$$

where α_0 and α_1 are the polarizability components for M_L=0 and $M_L = \pm 1$ respectively.

5.2 Results and Discussion

The experimental setup that was used by the collaborating group at the University of Darmstadt will be explained briefly. Polarizabilities α of tin and lead atoms were experimentally determined by Schäfer and co-workers utilizing a molecular beam electric field deflection apparatus [150]. Short, pulsed molecular beams of tin and lead atoms were generated with a laser ablation source using tin and lead targets. The laser ablation source was equipped with a temperature-controlled,

cryogenic vacuum expansion nozzle, that offers the possibility to produce atomic ground state species, with a low kinetic energy, in the molecular beam. In the experiments on tin atoms the nozzle was held at 100 K, in the case of lead atoms at 40 K. After the expansion the molecular beam is tightly collimated and passes through an inhomogeneous electric field, where it gets deflected. The deflection d is measured by scanning a moveable slit across the molecular beam profile and detecting transmitted atoms with a time-of-flight mass-spectrometer. For this purpose the atoms are ionized with a F_2-excimer laser. The deflection d of the molecular beam is related to the polarizabilty α by

$$d = \frac{A}{mv^2}\alpha, \tag{5.6}$$

with an apparatus constant A, the mean velocity v of the particles, which is measured with a molecular beam shutter, and the mass m of the atoms. By comparing the deflection of e.g. lead d_{Pb} to the beam deflection of a species with known polarizability, as barium [182], the absolute value of the polarizability α_{Pb} is given by

$$\alpha_{\mathrm{Pb}} = \alpha_{\mathrm{Ba}} \frac{d_{\mathrm{Pb}}\, m_{\mathrm{Pb}}\, v_{\mathrm{Pb}}^2}{d_{\mathrm{Ba}}\, m_{\mathrm{Ba}}\, v_{\mathrm{Ba}}^2} \tag{5.7}$$

The current apparatus does not allow to measure the polarizablity of the lighter homologues of tin and lead, since the ionization potentials of carbon (11.26 eV), silicon (8.15 eV) and germanium (7.90 eV) [156] exceed the energy per photon of the ionization laser (7.87 eV).

The molecular beam profiles with and without electric deflection field of tin and lead atoms are shown in Figure 5.1 in comparison to the beam deflection of barium atoms, which was used as a calibrant [150]. The mean velocity of tin, lead and barium atoms was determined to be 1020, 650 and 1410 m/s, respectively, with an uncertainty of 2%. Using Eq. (5.7) and the experimental polarizability of the atomic barium $\alpha_{\mathrm{Ba}} = (268 \pm 21)$ au [182], the polarizabilities of tin $\alpha_{\mathrm{Sn}} = (42.4 \pm 11)$ au and lead $\alpha_{\mathrm{Pb}} = (47.1 \pm 7)$ au are obtained. The error margins in the case of tin are significantly enlarged compared to lead, since it was not possible to generate a sufficiently intense molecular beam of tin atoms at expansion nozzle temperatures below 100 K. This leads to the higher velocities of the tin atoms and thereby reduced deflections in the electric field.

The results of all calculations are summarized in Table 5.1. The most accurate

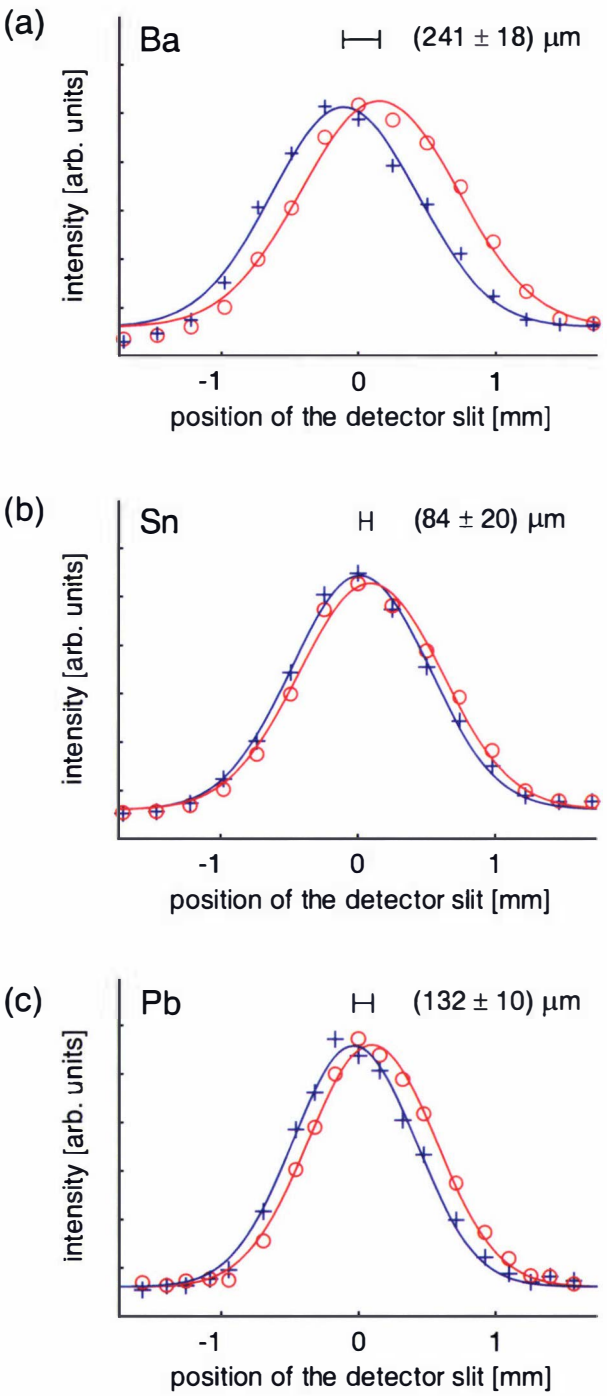

Figure 5.1: Molecular beam profiles of Ba (a) [150], Sn (b) and Pb (c) atoms with (circles) and without (crosses) applied electric deflection field. As a guide to the eye the experimental beam profiles are fitted with Gaussian functions. The field induced beam deflections d are indicated above the profiles.

coupled-cluster results including the Gaunt term at the DHF level are compared to other theoretical data in Table 5.2. There is excellent agreement of the presented results with the non-relativistic CCSD(T) value of carbon and silicon obtained by Thakkar and co-workers [183, 184]. These authors also provide a more complete overview of previous results. The anisotropy $\Delta\alpha$ for carbon and silicon of Thakkar and co-workers are 2.10 and 8.41 au, respectively, which are also in excellent agreement with the non-relativistic results (2.13 and 8.57 au). Further, very recent calculations at the Dirac-Coulomb level of theory for the heaviest elements Pb and E114 from Pershina and co-workers [158] also agree with the presented results.

Fig. 5.2 compares the calculated polarizabilities at the HF and CCSD(T) level of theory. Relativistic and electron correlation effects are shown in Fig. 5.4 and in Table 5.2. The following observations are made: (i) At the non-relativistic and scalar-relativistic level, both the polarizability α and the anisotropy $\Delta\alpha$ increase with increasing nuclear charge of the group 14 element. (ii) From a comparison between non-relativistic and scalar relativistic polarizabilities, one obtains a roughly Z^2 increase in relativistic effects for the M_L=0 component, while there is little change for the $M_L = \pm 1$ component of the polarizability tensor. (iii) The anisotropies are larger at the scalar relativistic level compared to the non-relativistic results. In fact, the relativistic change in the anisotropies roughly increase with Z^2. (iv) Electron correlation reduces the dipole polarizability (with the exception of the J=0 state for E114) by about 1 (C) to 6 (114) atomic units, but is much less pronounced than for the dipole polarizabilities of the s-block elements [152, 153, 158]. (v) For the lighter elements, LS-coupling (spin-orbit coupling small) gives a much better description than jj-coupling. Hence, it is of no surprise that the relativistic Hartree-Fock wavefunction, with the $p_{1/2}$ doubly occupied, is not the best zero-order wavefunction for the electron correlation procedure as the lowest energy field perturbation in the LS-coupled $M_L = \pm 1$ state. To compensate for this, the coupled-cluster procedure leads to a larger correlation effect in the jj-coupled compared to the LS-coupled case for elements where spin-orbit interactions can be neglected. In contrast to the HF case, the polarizabilities for the Dirac $J = 0$ and Douglas-Kroll $M_L = \pm 1$ state agree nicely at the coupled-cluster level for carbon. (vi) Fig. 5.4 clearly shows that spin-orbit

	NR (^3P)			DK (^3P)			Dirac J=0
	M_L=0	$M_L = \pm 1$	av.	M_L=0	$M_L = \pm 1$	av.	$M_J = 0$
Carbon							
HF	10.91	12.51	11.97	10.89	12.50	11.96	11.76
LDA	11.39	14.18	13.25	11.38	14.18	13.25	14.28
PBE	11.42	14.50	13.48	11.42	14.51	13.48	14.30
BLYP	11.44	14.42	13.42	11.43	14.42	13.42	14.44
B3LYP	11.05	13.55	12.72	11.04	13.55	12.71	13.52
MP2	9.64	12.31	11.42	9.64	12.31	11.42	12.06
CCSD	10.21	12.33	11.63	10.20	12.33	11.62	11.34
CCSD(T)	10.28	12.41	11.70	10.27	12.41	11.70	11.26
Silicon							
HF	32.56	41.39	38.45	32.48	41.46	38.46	41.66
LDA	33.71	45.48	41.56	33.67	45.63	41.64	44.95
PBE	34.00	45.53	41.68	33.95	45.66	41.76	44.93
B3LYP	33.44	44.33	40.70	33.39	44.45	40.76	44.09
MP2	32.02	40.68	37.79	31.97	40.76	37.83	40.73
CCSD	31.76	40.31	37.46	31.70	40.39	37.49	37.69
CCSD(T)	31.83	40.40	37.54	31.77	40.58	37.58	37.28
Germanium							
HF	34.02	45.26	41.51	33.24	45.30	41.28	43.86
LDA	34.14	49.18	44.17	33.59	49.63	44.29	46.23
PBE	35.29	50.60	45.49	34.73	51.09	45.64	47.92
B3LYP	34.39	48.60	43.86	33.78	48.96	43.91	45.94
MP2	32.66	43.43	39.84	31.93	43.47	39.63	41.70
CCSD	32.82	43.78	40.13	32.11	43.84	39.93	39.94
CCSD(T)	32.83	43.83	40.16	32.11	43.90	39.97	39.33
Tin							
HF	50.69	63.09	58.96	47.17	62.34	57.28	57.35
LDA	48.60	65.12	59.61	46.21	65.74	59.23	57.45
PBE	50.87	68.06	62.33	48.41	68.90	62.07	60.44
BLYP	51.06	69.44	63.31	48.76	70.29	63.11	60.80
B3LYP	49.67	65.51	60.23	47.05	65.90	59.62	58.01
MP2	45.88	59.53	54.98	43.58	59.79	54.39	54.25
CCSD	47.74	60.68	56.37	44.81	60.53	55.29	53.32
CCSD(T)	47.63	60.70	56.34	44.74	60.60	55.31	52.70
Lead							
HF	58.42	72.04	67.52	46.87	70.10	62.36	49.71
LDA	55.01	73.17	67.00	47.24	74.59	65.47	49.86
PBE	57.83	76.85	70.53	49.77	79.25	69.42	52.81
BLYP	58.01	77.89	71.46	50.45	80.34	70.37	53.05
B3LYP	56.46	73.88	68.09	48.02	74.82	65.89	50.48
MP2	51.75	66.77	61.76	43.65	67.30	59.42	47.63
CCSD	54.56	68.71	63.99	44.69	67.97	60.21	47.36
CCSD(T)	54.36	68.66	63.90	44.67	68.04	60.25	47.34
E114							
HF	76.75	91.18	86.39	49.69	101.40	84.16	30.13
LDA	70.27	88.92	82.70	52.31	98.37	83.02	33.34
PBE	75.18	96.83	89.61	56.17	109.14	91.48	34.17
BLYP	74.59	96.37	89.11	57.07	107.08	90.42	35.35
B3LYP	72.84	91.54	85.31	53.36	101.10	85.19	33.08
MP2	65.05	92.09	78.64	47.26	93.64	78.18	32.02
CCSD	70.92	88.25	82.47	47.88	94.97	79.28	31.05
CCSD(T)	70.29	88.04	82.12	47.90	94.66	79.07	31.49

Table 5.1: The static dipole polarizabilities (in au) of the group 14 elements at different levels of theory. Non-relativistic (NR) and scalar relativistic Douglas-Kroll (DK) calculations are for the $M_L = 0$ and $M_L = \pm 1$ components of the ^3P state, and Dirac values for the $J = 0$ state. av. is the average polarizability according to eq. (5.4)

Method	C	Si	Ge	Sn	Pb	E114
Δ_R	-1.15	-3.12	-4.50	-8.27	-21.33	-56.55
Δ_{Gaunt}	0.005	0.032	0.097	0.21	0.37	0.38
Δ_{corr}	-0.50	-4.38	-4.53	-4.65	-2.37	1.18
KR-CCSD(T)+Δ_{Gaunt}	11.26	37.31	39.43	52.91	47.70	31.87
others	11.67[a]	37.17[b]	41.0[c]	52.0[d]	46.96[e]	30.59[e]
recommended	11.3	37.3	39.4	52.9	47.3	31.0
experimental	–	–	–	42.4±11	47.1±7	–

Table 5.2: Total relativistic, Δ_R, including spin-orbit corrections for the $^3P_0$ state (relative to the $M_L = \pm 1$ component). Gaunt, Δ_{Gaunt}, at the DHF level of theory and electron correlation contributions, Δ_{corr}, for the $J = 0$ state, and final Gaunt corrected KR-CCSD(T) for the dipole polarizabilities of the group 14 elements compared to previous theoretical results. All values are in au. The recommended values are from the CCSD(T) results and from Pershina et al. [158], and corrected for Gaunt interactions. [a] $\bar{\alpha}$ NR-CCSD(T) from ref. [183]. [b] $\bar{\alpha}$ NR-CCSD(T) from ref. [184]. [c] $\bar{\alpha}$ NR-PNO-CEPA from ref. [185]. [d] R-LDA from ref. [156]. [e] Dirac-Coulomb CCSD(T) results for $J = 0$ from ref. [158].

contributions are as important as scalar relativistic effects for these *p*-block elements, and that they are not even negligible for carbon. (vii) Already for Ge, relativistic effects (including spin-orbit) are as important as electron correlation. For E114 a huge reduction in the dipole polarizability (64 %) from 88.0 to 31.5 au due to relativistic effects is observed. As a result, E114 has a smaller dipole polarizability compared to Si (37.3 au), as discussed in detail by Pershina et al. [158]. Pershina and co-workers also pointed out that the polarizability nicely correlates with the mean radius of the $p_{1/2}$ orbital. (viii) The Gaunt contribution increases with nuclear charge and, for the three heaviest elements, cannot be neglected anymore in precise calculations. (ix) Correlating the next shell below the *nsnp*-valence shell is also important. For example, a change from 37.47 to 37.28 au for Si and from 47.68 to 47.34 au for Pb due to core correlation is seen. (x) Triple contributions to the CCSD procedure are rather small, indicating that higher (quadruple) contributions are probably negligible. (xi) Finally, the results clearly show that relativistic and electron correlation effects are non-additive.

An important question is if some of the popular density functionals are able to accurately reproduce dipole polarizabilities for these *p*-block elements. There are some notable failures in the past. For example, Stott and Zaremba [186] reported a LDA value of 1.89 au for He, far too high compared to the experimental value of 1.3832 au [187]. More recent calculations with larger basis sets give a

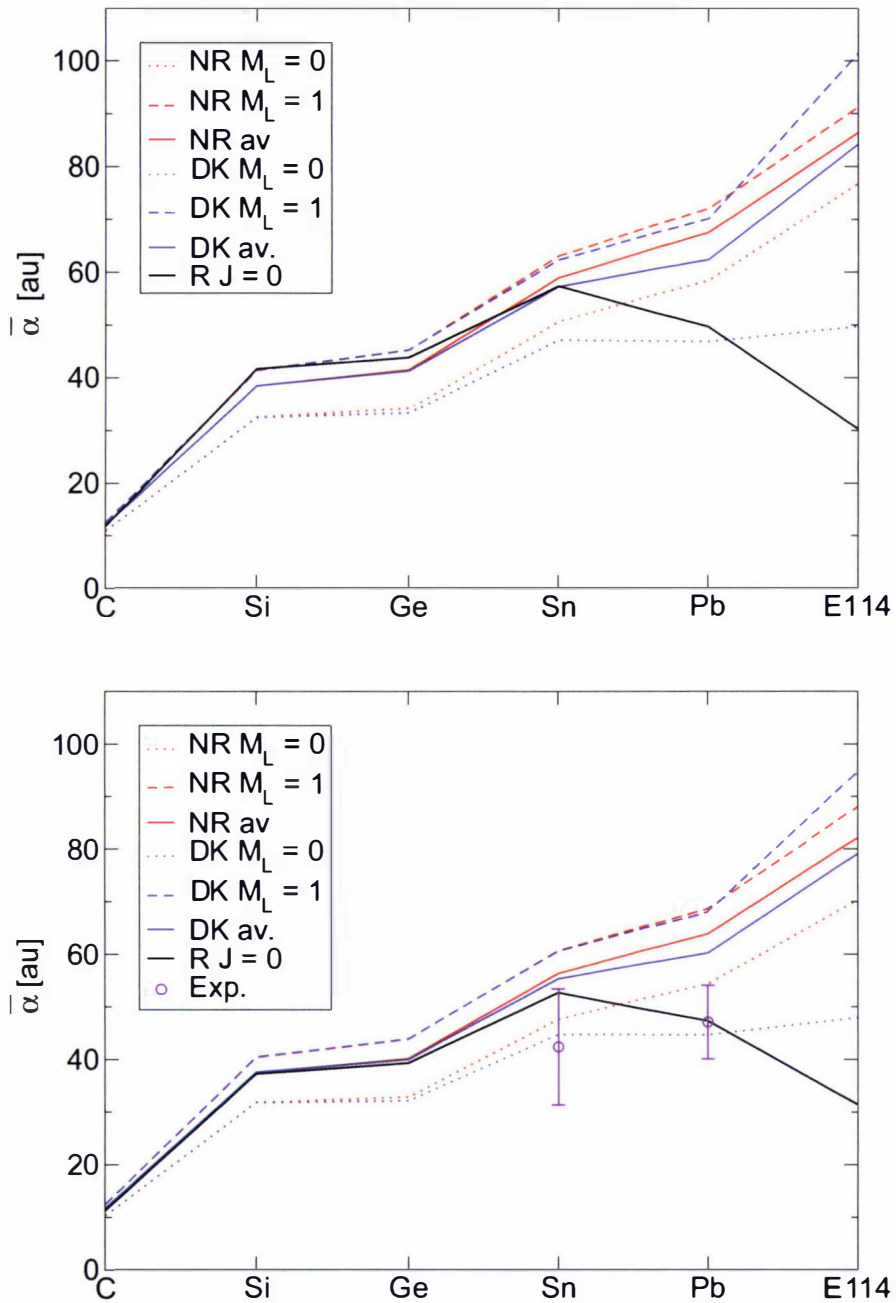

Figure 5.2: The static dipole polarizabilities of the group 14 elements at the HF (upper picture) and CCSD(T) (lower picture) level of theory. Non-relativistic (NR) and scalar-relativistic Douglas-Kroll (DK) calculations are for the $M_L = 0$ and $M_L = \pm 1$ components of the ^3P state, and Dirac values for the $J = 0$ state.

a) LDA

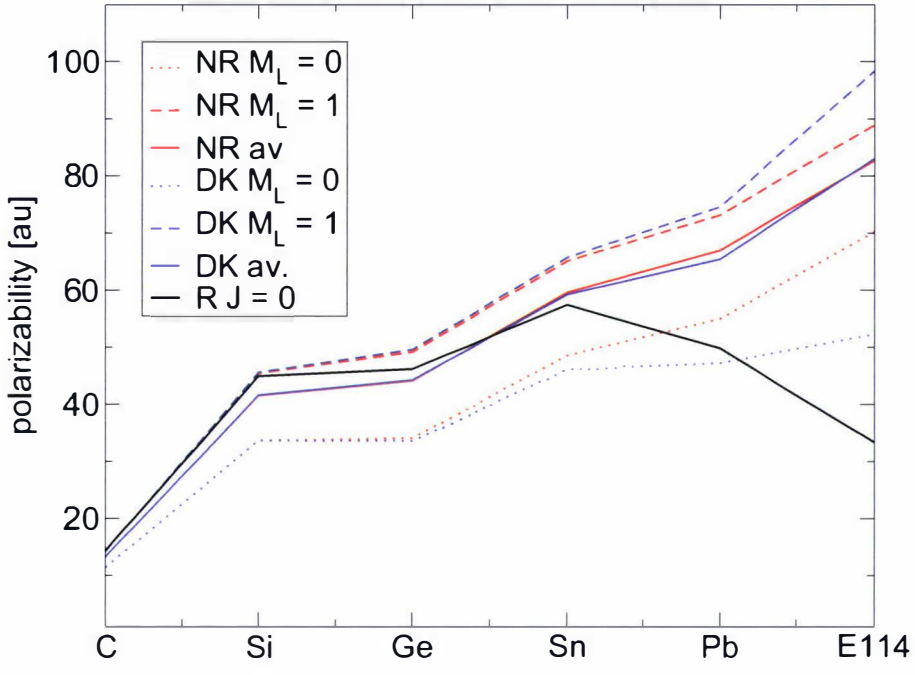
NR M_L = 0
NR M_L = 1
NR av
DK M_L = 0
DK M_L = 1
DK av.
R J = 0
polarizability [au]
100
80
60
40
20
C
Si
Ge
Sn
Pb
E114

b) PBE

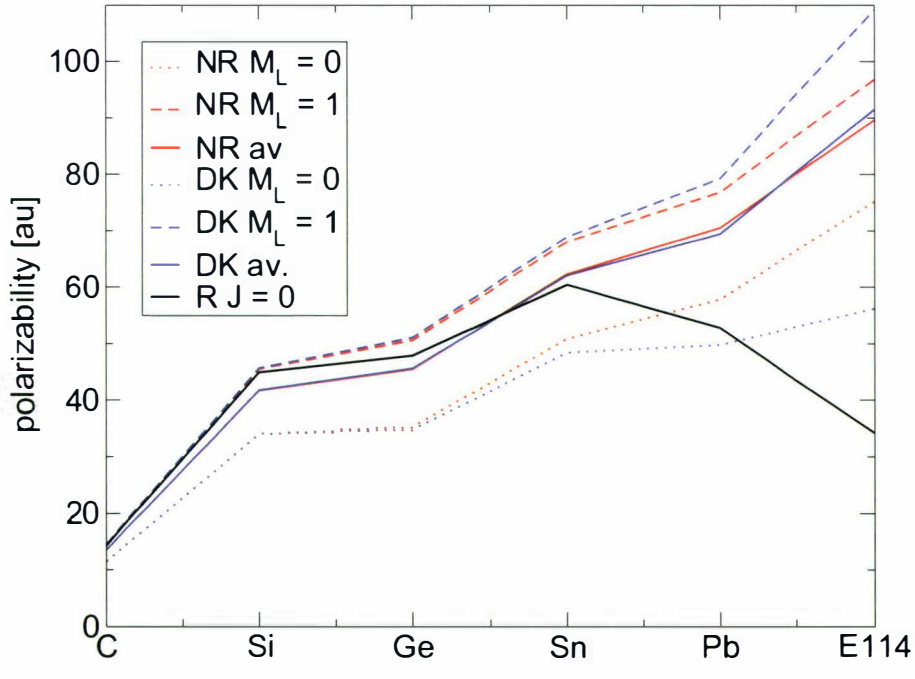
NR M_L = 0
NR M_L = 1
NR av
DK M_L = 0
DK M_L = 1
DK av.
R J = 0
polarizability [au]
100
80
60
40
20
0
C
Si
Ge
Sn
Pb
E114

c) BLYP

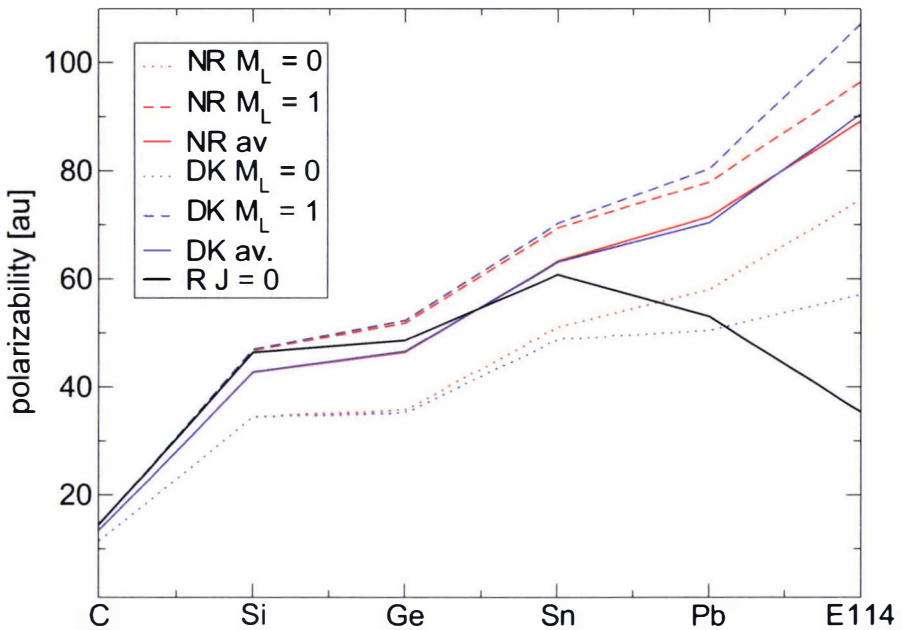

d) B3LYP

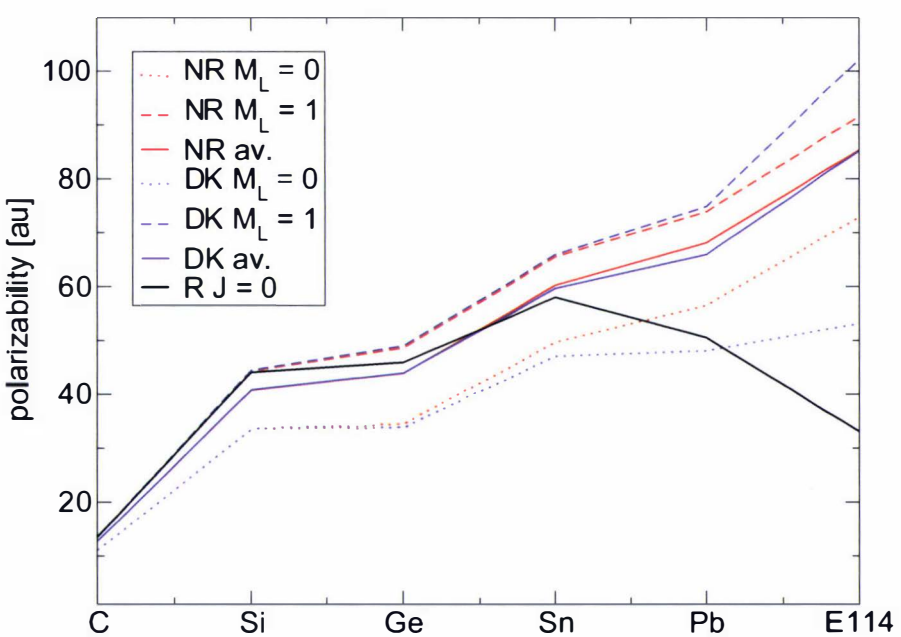

Figure 5.3: The static dipole polarizabilities of the group 14 elements for different DFT functionals. Non-relativistic (NR) and scalar-relativistic Douglas-Kroll (DK) calculations are for the $M_L = 0$ and $M_L = \pm 1$ components of the ^3P state, and Dirac values for the $J = 0$ state.

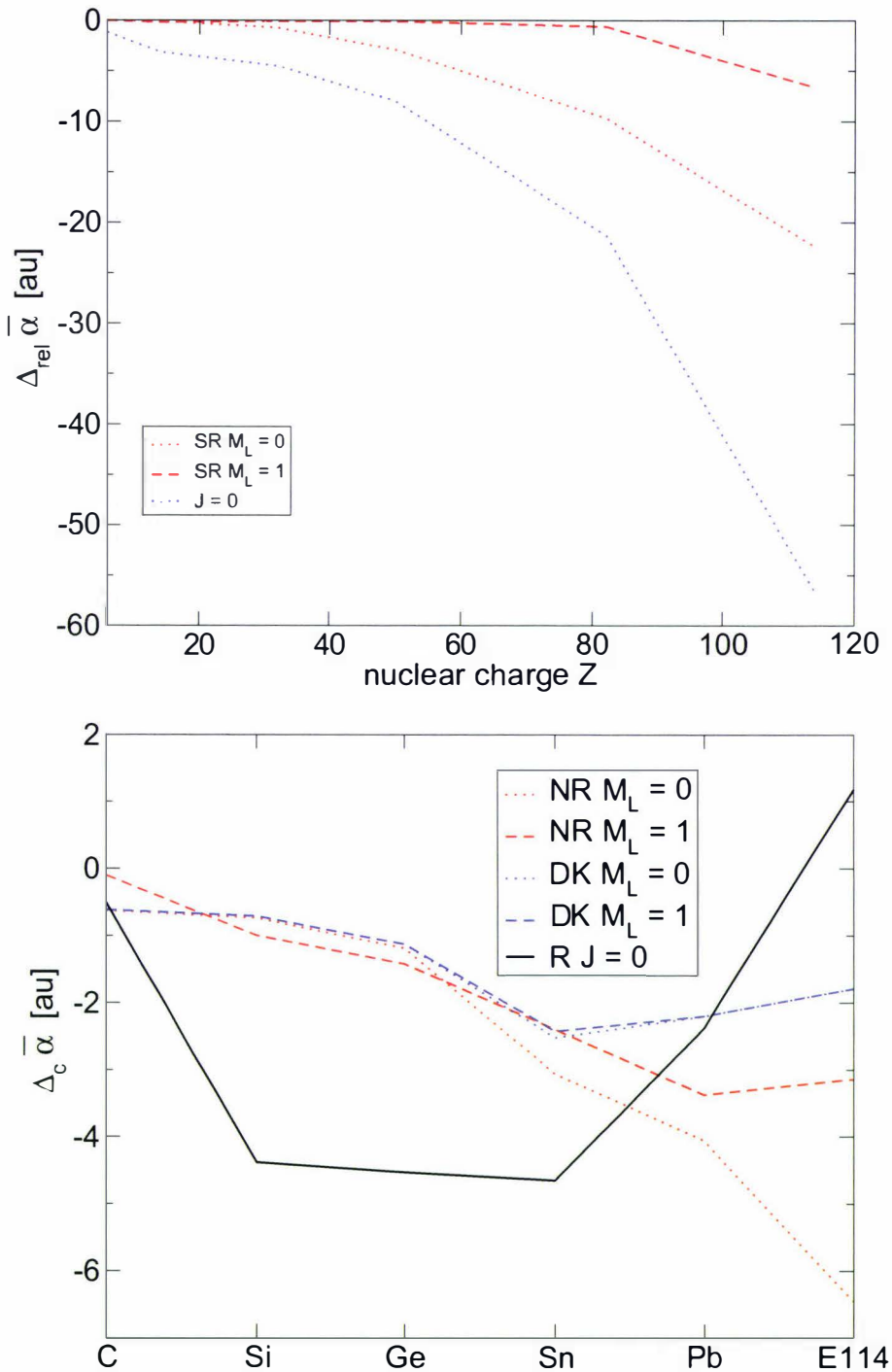

Figure 5.4: Relativistic (upper picture) and electron correlation (lower picture) effects for the $M_L = 0$ and $M_L = \pm 1$ components of the ^3P state, and for the Dirac $J = 0$ state compared to the non-relativistic $M_L = \pm 1$ state.

better comparison, i.e. one obtains 1.322 (HF), 1.362 (MP2), 1.686 (Xα), 1.644 (LDA), 1.558 (BPW91), and 1.505 (B3LYP) au [154]. In this case, all functionals overestimate the dipole polarizability by a few atomic units. Increasing the exact exchange will not help as the HF value is larger than the coupled-cluster value. Instead one needs to correct for the wrong long-range behavior in common density functionals. The overestimation is proportional to the polarizability, that is the worst DFT results are obtained for the Sn atom, which exhibits the highest polarizability of all group 14 elements.

The recommended polarizabilities for all Group 14 elements for the lowest $^3P_0$ state are listed in Table 5.2. For Pb and 114 Pershina et al. [158] chose slightly different basis sets including *h*-functions. As their values are slightly smaller compared to the presented ones here, they are listed including the here calculated Gaunt contribution.

Comparing the experimentally determined polarizabilities of Sn and Pb with the theoretical predictions in Table 5.1, it is obvious, especially in the case of Pb, that not only the scalar-relativistic but also the spin-orbit correction has to be taken into account in order to reproduce the experimental data. However, the large error margins of the experimental polarizabilities express the need for future high-precision experiments to actually check the accuracy of the theoretically predicted polarizabilities for the open-shell atoms discussed here. More work has to be done on other open *p*- as well as the open *d*- and *f*-shell elements. In addition for the energetically higher lying J=1 and 2 states, a multi-reference treatment is also required.

Chapter 6

Scalar relativistic and spin-orbit effects in superheavy hydrides

Investigations of the existence of new chemical elements resulted in the recent discovery of the elements with nuclear charge 111 (Rg) and 112 (Cp) by the GSI in Darmstadt [12, 131, 132, 188], and most recently the elements with nuclear charge 113, 114, 115, 116 and 118 by the JINR group in Dubna [189–193]. Isotopes of these elements are extremely short-lived, undergoing α-decay within a second or less [194]. It is hoped that in near future more long-lived neutron-rich isotopes can be synthesized [195] making these elements better accessible to atom-at-a-time chemical experiments [6, 196, 197]. The latest super-heavy elements for which atom-at-a-time chemistry has been carried out are the ones with nuclear charge 112 [198–200] (α-decay half-life $t^{\alpha}_{1/2}$=3.8 s for ^{283}112 and 29 s for ^{285}112) [201] and 114 ($t^{\alpha}_{1/2}$=0.6 s for ^{287}114 and 2.7 s for ^{289}114).

Once these rare isotopes have been successfully prepared, one naturally is interested in their physical and chemical properties, and how these elements compare with their lighter group members (in the periodic table) [6, 196]. Recent advances in atomic spectroscopy made it possible to observe the atomic level structure of the element with nuclear charge Z =100 (^{255}Fm with a half-life of 20.1 h) in an optical cell filled with argon buffer gas [202]. However, 2.7×10^{10} atoms of ^{255}Fm were used in these experiments, and such a large number of isotopes is not available for experiments on the newly discovered superheavy elements. Therefore one relies on chemistry on a one-atom-at-a-time scale [203]. Even if great progress has been made in trapping single atoms or molecules [204–208] and fu-

ture experimental studies might well be able to explore spectroscopic properties of short-lived superheavy elements by such techniques, the current situation is that only few chemical studies are available for the trans-actinides [6, 196]. Thus, one should mention the recent atom-at-a-time experiments on Bh (Z=107) [209], Hs (Z=108) [197], element 112 [198–200], and very recently on element 114.

In the meantime one can study the chemistry and physics of superheavy elements by using theoretical methods [210–213]. However, the treatment of superheavy elements is non-trivial as a large number of electrons is involved and both relativistic and electron correlation effects need to be taken into account [210, 214–220]. Considering the main-group superheavy elements there are already a number of theoretical studies available on atoms and molecules, mostly using the relativistic pseudopotential approximation [221] or relativistic density functional theory [222, 223]. It is however important to have benchmark calculations to test the various relativistic methods in use [224, 225]. Therefore one can study the closed-shell superheavy element monohydrides from Rg to element 120 at both the Dirac-Hartree-Fock and Dirac-Kohn-Sham level of theory, and include electron correlation effects by a coupled-cluster procedure. Further, to discuss the importance of spin-orbit and scalar relativistic effects in electronic properties corresponding scalar relativistic (spin-free) as well as non-relativistic calculations were carried out. Some of the monohydrides have been studied before using various relativistic approximations, i.e. RgH [222, 223, 226–230], CpH^+ [162, 231–233], 113H [234–237], $114H^+$ [232], 117H [235, 237, 238] and $118H^+$ [232]. For example, spin-orbit effects in the series of neutral element hydrides from 113H to 118H have been investigated by Lee and co-workers using a relativistic pseudopotential approximation [235]. Finally, there are only few atomic studies on electronic properties of element 119 [152, 211, 239–242] and 120 [211, 242], and molecular calculations containing these two elements have not been carried out so far.

6.1 Computational Details

In order to investigate the molecular properties of superheavy element hydrides non-relativistic (NR), scalar-relativistic spin-free (SF) [167, 168, 243] and relativistic Dirac-Coulomb (four component) [70] theory (R) were applied. On the method side, wave-function based theory applying the Hartree-Fock (HF) approx-

imation, second-order many body perturbation theory (MP2) and coupled-cluster theory including single and double substitutions (CCSD) and including the perturbative triples (CCSD(T)) to account for electron correlation [244], as well as density functional theory using the local density approximation (LDA) [170], the generalized gradient approximations (GGA) with the Perdew-Burke-Ernzerhof functional (PBE) [171], and the hybrid three-parameter Becke-Lee-Yang-Parr functional (B3LYP) [172–174] were used. In the Dirac picture, Kramers (time-reversal) symmetry was applied in the coupled cluster procedure to save computer time [76]. The active orbital space included the 6s, 6p, 7s, 6d, 7p, and 8s orbitals with the virtual space being truncated above 100 a.u., i.e. we correlated 20 electrons for RgH and CpH^+, 22 electrons for 113H and $114H^+$, 26 electrons for 117H and $118H^+$, and 28 electrons for 119H and $120H^+$. The (SS|SS) two-electron integrals over the small components were neglected and Visscher's correction was used instead [245]. A finite-size Gaussian nuclear model was chosen [246].

All all-electron calculations were performed using extensive, uncontracted Gaussian-type basis sets tested to yield converged molecular properties with respect to the basis set extension towards softer functions. For the superheavy elements with nuclear charges 111-118 we started from Faegri's four component basis sets [179] and arrived at $(28s/24p/20d/12f/3g)$ by adding a number soft s, p and d-functions as well as three g-functions. Basis sets were not available for the elements 119 and 120. Therefore new basis sets were adjusted by starting from the exponents for element 118 extended by three s-functions and subsequently reoptimized the Gaussian exponents at the Dirac-Hartree-Fock (DHF) level using the program package GRASP [104], until the energy difference compared to the Dirac-Hartree-Fock basis set limit was smaller than 20mH (Appendix A). For hydrogen an uncontracted $(9s/5p/4d/1f)$ set of Gaussian functions was used obtained from refs. [247, 248]. The variational stability in all four-component calculations was ensured by using dual basis sets with the appropriate kinetic balance condition [249]. The basis sets are large enough to suppress the basis set superposition error, i.e. using the Boys-Bernardi counterpoise method [250] the bond distance at the scalar relativistic CCSD(T) level of theory increases only by 0.0009 Å for RgH and 0.00012 Å for 117H.

The equilibrium bond lengths r_e and force constants k_e were obtained from polynomial fits of the potential curve around the minimum. The calculation of the

dissociation energy D_e for the molecules was only carried out at the DHF, DHF-MP2 and DHF-CCSD(T) levels of theory and required more attention. First DHF, MP2 and CCSD(T) calculations were performed for the intermediate dissociation of the hydrides into a proton (H^+) and the corresponding closed-shell superheavy element or ion, whose total electronic energy could be calculated accurately with the program system DIRAC [70]. To obtain the correct dissociation energies, the ionization potential (IP) of hydrogen and the electron affinities (EA) or ionization potentials for the charged and neutral superheavy elements are required at different levels of theory, which were obtained from DHF and Fock-space coupled-cluster (FSCC) calculations [251,252] using the same basis sets. The considered dissociation paths for the investigated superheavy hydrides are as follows

$$
\begin{array}{llllll}
\mathrm{RgH} & \rightarrow & \mathrm{H^+ + Rg^-} & (^1S_0) & \rightarrow & \mathrm{H + Rg} \quad (^2D_{5/2}/^2S_{1/2}) \\
\mathrm{CpH^+} & \rightarrow & \mathrm{H^+ + Cp} & (^1S_0) & \rightarrow & \mathrm{H + Cp^+} \quad (^2D_{5/2}/^2S_{1/2}) \\
\mathrm{113H} & \rightarrow & \mathrm{H^+ + 113^-} & (^1S_0) & \rightarrow & \mathrm{H + 113} \quad (^2P_{1/2}) \\
\mathrm{114H^+} & \rightarrow & \mathrm{H^+ + 114} & (^3P_0) & \rightarrow & \mathrm{H + 114^+} \quad (^2P_{1/2}) \\
\mathrm{117H} & \rightarrow & \mathrm{H^+ + 117^-} & (^1S_0) & \rightarrow & \mathrm{H + 117} \quad (^2P_{3/2}) \\
\mathrm{118H^+} & \rightarrow & \mathrm{H^+ + 118} & (^1S_0) & \rightarrow & \mathrm{H + 118^+} \quad (^2P_{3/2}) \\
\mathrm{119H} & \rightarrow & \mathrm{H^+ + 119^-} & (^1S_0) & \rightarrow & \mathrm{H + 119} \quad (^2S_{1/2}) \\
\mathrm{120H^+} & \rightarrow & \mathrm{H^+ + 120} & (^1S_0) & \rightarrow & \mathrm{H + 120^+} \quad (^2S_{1/2})
\end{array}
$$

The results of our atomic FSCC calculations are shown in Table 6.1. The non-relativistic ground state for Rg and Cp^+ is of $^2S_{1/2}$ symmetry with a $6d^{10}7s^1$ configuration, while the correct relativistic ground state is of $^2D_{5/2}$ symmetry ($6d^97s^2$) [211,253]. Further, positive electron affinities indicate that the electron in the negatively charged species is not bound, and in the complete basis set limit it should be zero. Nevertheless, these small positive electron affinities were used for correcting our dissociation energies. Small errors, which stem from the different coupled-cluster treatment for the molecules and dissociated atoms, are within the basis set and correlation error. For example, for RgH and 113H a dissociation energy of 2.052 and 3.435 eV were calculated at the non-relativistic level of theory respectively, whereas from unrestricted coupled CCSD(T) calculations [166] one obtains 2.139 and 3.511 eV respectively. The Gaunt term of the Breit interaction [180, 254] was considered as well as a small correction to the usual Coulomb interaction between two electrons. However, the changes in bond lengths and other properties are much smaller compared to the errors introduced by the use of

Transition	Method	R	SF	NR
Rg→Rg^-	HF	-0.210	-1.436	-0.071
	FSCC	-1.645	-2.533	-1.103
Cp→Cp^+	HF	10.441	11.482	6.246
	FSCC	11.668	12.813	7.721
113→113^-	HF	-0.090	0.633	0.514
	FSCC	-0.484	-0.087	-0.486
114→114^+	HF	8.029	5.592	5.882
	FSCC	8.390	6.558	6.684
117→117^-	HF	-0.602	-1.968	-2.475
	FSCC	-1.369	-2.765	-3.070
118→118^+	HF	7.805	10.076	10.209
	FSCC	8.668	10.795	10.777
119→119^-	HF	-0.092	0.064	0.053
	FSCC	-0.164	-0.162	0.157
120→120^+	HF	5.011	4.903	3.647
	FSCC	5.470	5.407	3.998

Table 6.1: Electron affinities (EA) and ionizations energies (IP) of the superheavy elements (in eV) from four-component (R), scalar relativistic spin-free (SF) and non-relativistic (NR) Hartree-Fock (HF) and Fock-space coupled-cluster (FSCC) calculations.

finite basis sets, restricted orbital space in the correlation procedure or corrections from non-iterative triples or higher substitutions in the coupled cluster procedure, and were therefore neglected. For example, for RgH and 117H the bond lengths increased by 6.2×10^{-4} Å and 9.3×10^{-4} Å respectively at the DHF level of theory upon inclusion of the Gaunt term.

6.2 Results and Discussion

The results of our molecular calculations are summarized in Tables 6.2, 6.3, 6.4 and 6.5. Before discussing the properties of the superheavy element hydrides with respect to their lighter congeners, the presented results will be compared with previously published calculations using various models of approximations.

There are a number of papers concerning RgH [222, 223, 226–230]. Here one should mention Dolg et al. who obtained from benchmark spin-orbit coupled pseudopotential calculations including electron correlation at the CCSD(T) level

of theory r_e=1.529 Å, k_e= 409.8 Nm^{-1} and D_e= 2.83 eV [229]. This is in excellent agreement with the here applied all-electron DHF-CCSD(T) treatment. Earlier all-electron DHF-CCSD(T) results by Seth and Schwerdtfeger (r_e=1.523 Å, k_e= 419.7 Nm^{-1} and D_e= 2.83 eV [227]) are in similar good agreement. Concerning CpH^+ Mosyagin et al. obtained r_e= 1.537 Å, k_e= 387.4 Nm^{-1} and D_e= 3.96 eV using Fock-space coupled-cluster calculations within a generalized relativistic effective core potential scheme [233], again in very good agreement with the presented results. For comparison Seth et al. obtained r_e= 1.517 Å, k_e= 419.4 Nm^{-1} and D_e= 4.09 eV [162], and Nash obtained r_e= 1.583 Å and D_e= 3.50 eV [232], both using CCSD(T) calculations but differently adjusted relativistic pseudopotentials (RPP). 113H has been investigated before by Seth et al. (r_e= 1.789 Å, k_e= 109 Nm^{-1} and D_e= 1.44 eV) using four-component CCSD(T) [234] but applying much smaller basis sets. Lee et al. (r_e= 1.759 Å and D_e= 1.46 eV) performed two component CCSD(T) using RPPs [235], and Choi and co-workers (r_e= 1.755 Å, k_e= 132.5 Nm^{-1} and D_e= 1.53 eV) used spin-orbit DFT (SO-DFT) in connection with RPPs [236, 237]. For $114H^+$ there is only one paper published by Nash (r_e= 1.73 Å and D_e= 1.01 eV) using a RPP in a CCSD(T) scheme [232]. For 117H one can mention three different calculations by Lee et al. (r_e= 1.949 Å and D_e= 1.79 eV) obtained by using a two component RPP within a CCSD(T) procedure [235], by Choi et al. (r_e= 1.957 Å, k_e= 143.2 Nm^{-1} and D_e= 1.58 eV) using SO-DFT [237], and by Peng et al. (r_e= 1.988 Å, k_e= 128.3 Nm^{-1} and D_e= 2.04 eV) using a Dirac (four component) Kohn-Sham scheme [238]. Lastly, one should cite results for $118H^+$ by Nash (r_e= 1.992 Å and D_e= 1.60 eV) obtained by CCSD(T) calculations using a RPP [232], which deviate substantially from our values indicating problems in the pseudopotential approximation used. The Tables 6.2 and 6.3 also show that density functional theory performs reasonably well for these superheavy elements, with the B3LYP functional apparently performing best.

The calculated relativistic and electron correlation effects for various properties are shown in Table 6.6. One can observe clear trends within the series of superheavy element hydrides. For the bond distances, relativistic effects are much larger than electron correlation effects with the largest bond contractions calculated for RgH and CpH^+ due to scalar relativistic contributions. For these two compounds spin-orbit contributions to the bond distance are very small. Moreover, scalar relativistic effects to the bond distance are much larger for RgH and

	RgH		CpH^+		113H		$114H^+$	
Method	r_e	k_e	r_e	k_e	r_e	k_e	r_e	k_e
Dirac-Coulomb								
DHF	1.520	454.0	1.526	390.9	1.698	136.6	1.716	194.6
MP2	1.505	427.4	1.525	397.7	1.701	134.1	1.728	165.8
CCSD	1.519	438.1	1.530	373.2	1.721	130.5	1.747	158.5
CCSD(T)	1.522	438.4	1.534	371.2	1.728	129.0	1.762	144.5
LDA	1.540	409.6	1.559	344.0	1.759	134.3	1.789	143.8
PBE	1.558	344.9	1.560	344.9	1.798	114.1	1.811	131.3
B3LYP	1.540	411.8	1.552	369.7	1.777	126.0	1.789	146.0
scalar relativistic								
HF	1.513	488.9	1.531	403.2	2.013	93.4	1.911	171.3
MP2	1.501	504.4	1.527	414.1	1.939	110.5	1.881	178.8
CCSD	1.512	470.2	1.530	389.2	1.973	101.2	1.901	161.1
CCSD(T)	1.515	467.1	1.533	387.7	1.967	99.6	1.902	159.3
LDA	1.528	418.4	1.555	345.2	1.982	99.7	1.921	154.8
PBE	1.532	419.3	1.555	346.4	2.021	89.4	1.939	144.6
B3LYP	1.528	420.7	1.550	370.5	2.020	90.3	1.932	152.9
non-relativistic								
HF	2.019	109.0	1.952	157.2	2.079	121.4	1.980	182.2
MP2	1.876	133.9	1.888	166.6	2.032	123.0	1.955	193.1
CCSD	1.931	115.2	1.926	144.8	2.051	118.3	1.966	182.7
CCSD(T)	1.923	116.8	1.930	138.6	2.048	116.8	1.968	180.6
LDA	1.871	128.2	1.907	147.0	2.069	110.5	1.993	154.3
PBE	1.911	118.7	1.931	130.0	2.094	103.7	2.004	157.8
B3LYP	1.928	112.6	1.930	143.4	2.089	106.0	1.991	160.6

Table 6.2: Bond distances r_e (in Å) and force constants k_e (in Nm^{-1}) for the superheavy element hydrides at various levels of theory.

CpH^+ compared to the other two *s*-block element hydrides 119H and $120H^+$, which stems from the relativistic maximum at the group 11 or 12 elements along a period in the periodic table (see refs. [255–259] for a detailed discussion). The situation changes completely for the *p*-block element hydrides. Here spin-orbit coupling becomes the dominant relativistic contribution for bond distances, with scalar relativistic effects being much smaller but still large in comparison to electron correlation. This is expected from the pronounced spin-orbit splitting in the 7*p*-shell [256], i.e. FSCC calculations by Kaldor and co-workers give a $^2P_{1/2}/^2P_{3/2}$ splitting for element 113 of 2.79 eV [260], and Dirac-Fock-Breit calculations give

	117H		$118H^+$		119H		$120H^+$	
Method	r_e	k_e	r_e	k_e	r_e	k_e	r_e	k_e
Dirac-Coulomb								
DHF	1.970	150.5	1.904	191.9	2.529	53.1	2.291	118.8
MP2	1.902	166.6	1.868	201.2	2.402	61.6	2.226	112.5
CCSD	1.939	143.8	1.895	181.5	2.443	55.7	2.254	100.6
CCSD(T)	1.941	144.5	1.902	168.6	2.434	56.1	2.255	98.2
LDA	1.961	140.8	1.929	160.9	2.452	56.1	2.284	93.9
PBE	1.982	130.2	2.937	163.5	2.480	52.9	2.292	95.1
B3LYP	1.979	131.9	1.930	165.2	2.489	52.9	2.289	97.6
scalar relativistic								
HF	1.793	267.8	1.774	277.1	2.601	46.7	2.328	99.6
MP2	1.767	268.7	1.757	275.6	2.450	56.0	2.254	102.8
CCSD	1.781	250.7	1.765	261.6	2.501	49.8	2.289	93.4
CCSD(T)	1.782	247.5	1.768	258.4	2.491	51.4	2.290	91.9
LDA	1.811	231.6	1.805	226.3	2.494	50.3	2.310	88.0
PBE	1.821	221.9	1.807	228.8	2.528	47.6	2.319	89.2
B3LYP	1.814	234.4	1.800	242.4	2.540	49.9	2.319	91.9
non-relativistic								
HF	1.847	269.3	1.823	284.9	2.761	35.8	2.231	90.3
MP2	1.817	294.3	1.797	296.6	2.633	39.7	2.156	97.1
CCSD	1.826	277.1	1.801	295.8	2.655	37.4	2.161	96.5
CCSD(T)	1.827	274.0	1.803	292.7	2.643	38.9	2.154	95.0
LDA	1.858	234.5	1.846	250.6	2.603	41.2	2.170	99.7
PBE	1.864	236.6	1.844	252.0	2.625	39.5	2.177	96.2
B3LYP	1.857	251.8	1.836	252.7	2.667	37.1	2.192	93.9

Table 6.3: Bond distances r_e (in Å) and force constants k_e (in Nm^{-1}) for the superheavy element hydrides at various levels of theory.

a $^2P_{3/2}/^2P_{1/2}$ splitting of 9.91 eV (!) for element 117. Hence, a spin-orbit bond contraction for 113H and $114H^+$ can be observed due to the spin-orbit contraction of the $7p_{1/2}$-shell, and a spin-orbit bond lengthening for 117H and $118H^+$ due to the spin-orbit expansion of the $7p_{3/2}$-shell. These spin-orbit effects are greatly diminished when moving from the neutral to the isoelectronic positively charged molecule, i.e. from 113H to $114H^+$ and from 117H to $118H^+$, as depletion of electron density of either the $7p_{1/2}$- or $7p_{3/2}$-shell reduces these relativistic effects.

An exception to the whole trend is found for $120H^+$ where a *relativistic bond*

Method	RgH	CpH^+	113H	$114H^+$	117H	$118H^+$	119H	$120H^+$
Dirac-Coulomb								
DHF	1.675	2.583	0.546	0.192	0.892	0.698	0.583	0.580
CCSD(T)	2.989	3.776	1.774	1.402	2.170	2.181	1.793	1.804
scalar relativistic								
HF	2.658	3.462	2.077	2.261	1.833	2.144	0.474	0.464
CCSD(T)	3.721	4.812	3.264	3.635	3.246	3.551	1.656	1.676
non-relativistic								
HF	0.906	0.688	2.032	2.648	2.180	2.505	1.101	2.408
CCSD(T)	2.052	1.786	3.435	3.755	3.616	3.914	2.242	3.514

Table 6.4: Dissociation energies D_e (in eV) for the superheavy element hydrides at the DHF and CCSD(T) level of theory using the atomic values listed in Table 6.1.

Method	RgH	113H	117H	119H
Dirac-Coulomb				
DHF	-0.309	0.507	-2.544	-6.847
CCSD(T)	-0.013	0.067	-1.943	-5.605
scalar relativistic				
HF	-0.544	-2.797	-0.700	-7.698
CCSD(T)	-0.139	-2.467	-0.617	-5.488
non-relativistic				
HF	-5.792	-0.499	0.261	-9.902
CCSD(T)	-4.213	-0.819	0.070	-9.233

Table 6.5: Dipole moments μ_e (in Debye) for the neutral superheavy element hydrides at the DHF and CCSD(T) level of theory.

expansion, rather than a contraction is seen as one might expect. As a consequence no change in the trend of bond lengths is observed due to relativistic effects for the positively charged group 2 hydrides in contrast to the group 1 series of hydrides, cf. Figure 6.1. In order to verify this rather intriguing result FrH, RaH^+ and BaH^+ were investigated as well, but only at the B3LYP level of theory using a Dyall triple-zeta basis set with three *g*-functions. For FrH similar results compared to 119H are obtained showing a relativistic bond contraction, i.e. r_e= 2.537 Å (Dirac), 2.547 Å (SF), and 2.563 Å (NR). However, for RaH^+ one obtains r_e= 2.234 Å (Dirac), 2.241 Å (SF), and 2.167 Å (NR). In comparison for BaH^+ one gets r_e= 2.137 Å (Dirac), 2.135 Å(SF), and 2.111 Å (NR). Hence

	RgH	CpH^+	113H	$114H^+$	117H	$118H^+$	119H	$120H^+$
Δr_e^{Corr}	0.001	0.008	0.030	0.047	-0.029	-0.002	-0.095	-0.036
Δr_e^{SR}	-0.408	-0.397	-0.081	-0.066	-0.044	-0.035	-0.152	0.135
Δr_e^{SO}	0.007	0.000	-0.240	-0.140	0.158	0.134	-0.057	-0.034
Δr_e^{SR+SO}	-0.401	-0.396	-0.321	-0.206	0.114	0.099	-0.209	0.101
Δk_e^{Corr}	-15.6	-19.7	-7.6	-50.1	-6.1	-23.3	3.1	-20.6
Δk_e^{SR}	350.4	249.1	-17.1	-21.3	-26.5	-34.3	12.5	-3.6
Δk_e^{SO}	-28.8	-16.5	29.4	-14.8	-103.1	-89.8	4.8	6.4
Δk_e^{SR+SO}	321.6	232.6	12.2	-36.2	-129.6	-124.1	17.2	3.3
ΔD_e^{Corr}	1.314	1.193	1.228	1.210	1.278	1.483	1.209	1.224
ΔD_e^{SR}	1.669	3.027	-0.172	-0.120	-0.370	-0.363	-0.589	-1.838
ΔD_e^{SO}	-0.733	-1.063	-1.489	-2.233	-1.076	-1.370	0.137	0.128
ΔD_e^{SR+SO}	0.937	1.990	-1.661	-2.353	-1.446	-1.733	-0.449	-1.710
$\Delta \mu_e^{Corr}$	0.322		-0.440		-0.601		-1.242	
$\Delta \mu_e^{SR}$	4.074		-1.648		-0.687		3.745	
$\Delta \mu_e^{SO}$	0.126		2.534		-1.326		-0.117	
$\Delta \mu_e^{SR+SO}$	4.200		0.886		-2.013		3.628	

Table 6.6: Relativistic effects at the CCSD(T) level of theory and electron correlation effects at the DHF level of theory for bond distances r_e (in Å), force constants k_e (in Nm^{-1}), and dissociation energies D_e (in eV) for the superheavy element hydrides. SR: scalar relativistic effects, SO: spin-obit effects, Corr: Correlation effects.

RaH^+ shows exactly the same trend in relativistic effects compared to $120H^+$. What is the origin of this relativistic bond expansion in view of the relativistic valence *s*-contraction?

The answer lies perhaps in a previous study on BaH^+ and RaH^+ by Pyykkö and co-workers [261, 262], who emphasized the importance of the vacant *d*-orbitals in the bonding, which is analyzed in more detail here for $120H^+$. Table 6.7 shows the gross atomic charges obtained from a Mulliken population analysis. What is interesting here is not only the large charge flow from the neutral hydrogen atom to the metal atom due to relativistic effects for the compounds RgH (Rg becomes negatively charged), 113H and to a lesser extent 119H, but also the rather large positive charge at element 120 indicating that $120H^+$ is best described as $120^{2+}H^-$. The first and second ionization potentials for element 120, which are 5.47 eV (see Table 6.1) and 11.58 eV (from the first ionization poten-

tial in Table 6.1 and the double ionization potential calculated recently by Dinh et al. [242]) respectively. One observes that the second ionization potential is relatively small. In fact smaller than the ionization potential of the hydrogen atom (13.595 eV [263]). Depleting almost completely the valence *s*-shell will significantly reduce relativistic effects [264] as this is the case for $120H^+$. However, similar small ionization potentials are found for all the group 2 elements, and one should therefore expect similar small relativistic effects for the lighter elements. This is indeed the case for RaH^+ and BaH^+ as discussed above, and has been demonstrated earlier for these two molecules in calculations by Pyykkö and co-workers [261, 262]. The scalar relativistic valence populations for the vacant *d*-orbital at the heavy atom at the HF level of theory for $120H^+$, RaH^+ and BaH^+ are -0.02, -0.10 and -0.15 respectively. In contrast, at the non-relativistic level we have -0.14, -0.19 and -0.19 respectively. Hence, going down the group 2 elements, the relativistic valence-*s* contraction and the relativistic expansion of the vacant *d*-orbitals opens up the *s*-*d* gap and diminishes the valence *d*-participation in the bond, thus rationalizing the relativistic increase in the bond length observed for $120H^+$. Indeed, in removing the most diffuse *d*-functions reduces substantially the relativistic bond expansion in $120H^+$. It is worthwhile to mention that for $120H^+$ the vacant *f*- and *g*-orbitals show negligible populations. The bond distances along the 7th period main group hydrides RgH, CpH^+, 113H, $114H^+$, 117H and $118H^+$, as well as 119H and $120H^+$ are compared in Figure 6.2 at different levels of theory, which nicely shows the interplay between scalar relativistic and spin-orbit effects as discussed above. Note that the close proximity of the HF and coupled cluster curves which shows that relativistic effects are more important than electron correlation. Figure 6.3 shows the trend in bond distances down the periodic table for the neutral element hydrides. One clearly sees changes in trends between the elements Fr/119 and Ag/Au due to a scalar relativistic valence *s*-contraction causing bond contractions, between the elements Tl/113 due to a spin-orbit $7p_{1/2}$-contraction causing a large bond contraction for 113H, and a large increase in bond length for 117H due to a spin-orbit $7p_{3/2}$-expansion (see also ref. [218] for a detailed discussion on relativistic effects in bond distances). The trend in bond distances down a specific group of elements in the periodic table depicted in Figure 6.3, closely resembles the trends in atomic radii published by Fricke [211], and the more recently published trends in covalent radii published by Pyykkö and Atsumi [230]. The force constants show similar relativistic effects

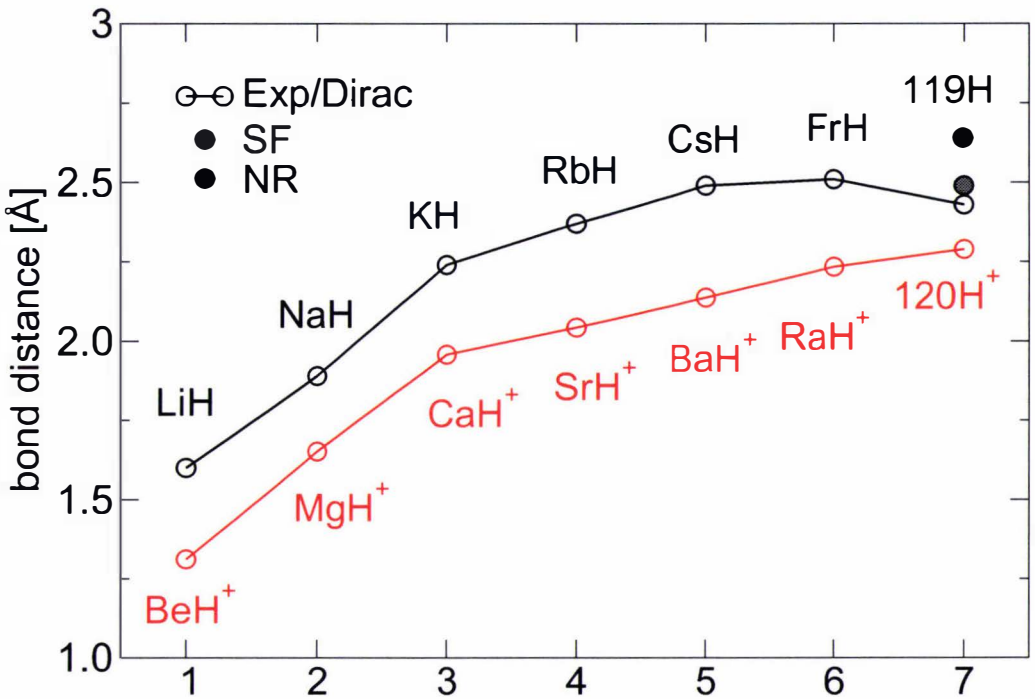

Figure 6.1: Bond distances for the Group 1 (MH) and 2 (MH^+) metal hydrides. Experimental values are extracted from ref. [265]. All other values are obtained from our calculations or from ref. [266].

as shown in Table 6.6. The corresponding trends across and down the periodic table are illustrated in Figures 6.4 and 6.5. Here, one sees rather large relativistic effects for the group 11 and 12 element hydrides leading to a strong increase in force constants causing large changes in periodic trends already at gold, which has been discussed in detail before [4, 264]. For 117H and $118H^+$ a very large relativistic decrease in the force constants was obtained, leading to a monotonic decrease in the force constants down the group 17 series of elements as shown in Figure 6.5. The rather small force constant calculated for 117H is in agreement with the rather small dissociation energy calculated at the four-component CCSD(T) level of theory. The dissociation energies are more difficult to discuss, as relativistic effects for the separated atoms have to be considered and electron correlation effects are significant as one expects. For both RgH and CpH^+ the large scalar relativistic effect is partly cancelled by spin-orbit coupling due to a change in the electronic configuration from $^2S_{1/2}(6d^{10}7s^1)$ to $^2D_{5/2}(6d^97s^2)$ for the elements Rg and Cp^+ [211, 253]. Nevertheless, there is a large relativistic increase in the dissociation energy for RgH and CpH^+ as shown in Figure 6.6,

Transition	Method	R	SF	NR
RgH	HF	-0.25	-0.25	0.66
	B3LYP	-0.43	-0.44	0.48
CpH^+	HF	0.49	0.51	1.47
	B3LYP	0.37	0.37	1.29
113H	HF	0.16	0.60	0.62
	B3LYP	0.16	0.55	0.52
$114H^+$	HF	0.89	1.53	1.52
	B3LYP	0.90	1.47	1.45
117H	HF	0.52	0.43	0.39
	B3LYP	0.42	0.39	0.34
$118H^+$	HF	1.36	1.29	1.25
	B3LYP	1.28	1.26	1.20
119H	HF	0.77	0.77	0.89
	B3LYP	0.61	0.59	0.83
$120H^+$	HF	1.75	1.76	1.92
	B3LYP	1.60	1.58	1.94

Table 6.7: Mulliken charges at the superheavy element at the HF and B3LYP level of theory at he relativistic Dirac (R), scalar relativistic spin-free (SF) and non-relativistic (NR) level of theory.

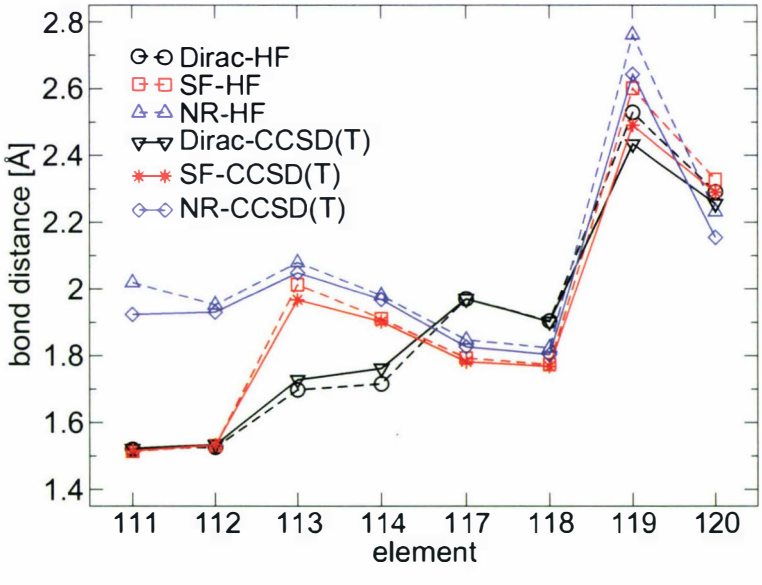

Figure 6.2: Comparison of calculated relativistic (Dirac), spinfree scalar relativistic (SF) and non-relativistic (NR) HF and CCSD(T) bond distances across the 7th period main group hydrides RgH, CpH^+, 113H, $114H^+$, 117H and $118H^+$, as well as 119H and $120H^+$.

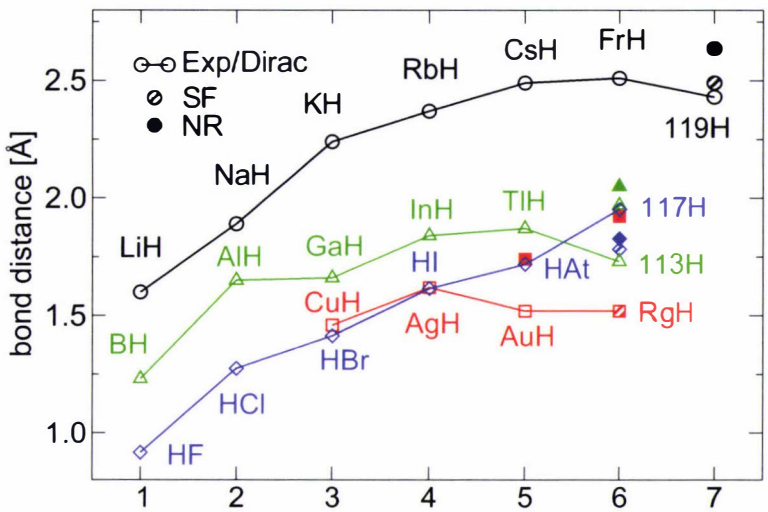

Figure 6.3: Comparison of the calculated relativistic (not filled), spinfree (partly filled) and non-relativistic (filled) CCSD(T) bond distances for RgH, 117H, 113H and 119H with experimental values for the lighter homologes. Experimental values (circle) are taken from [265], the non-relativistic value of AuH from ref. [225] and the relativistic value for AtH from ref. [267] respectively.

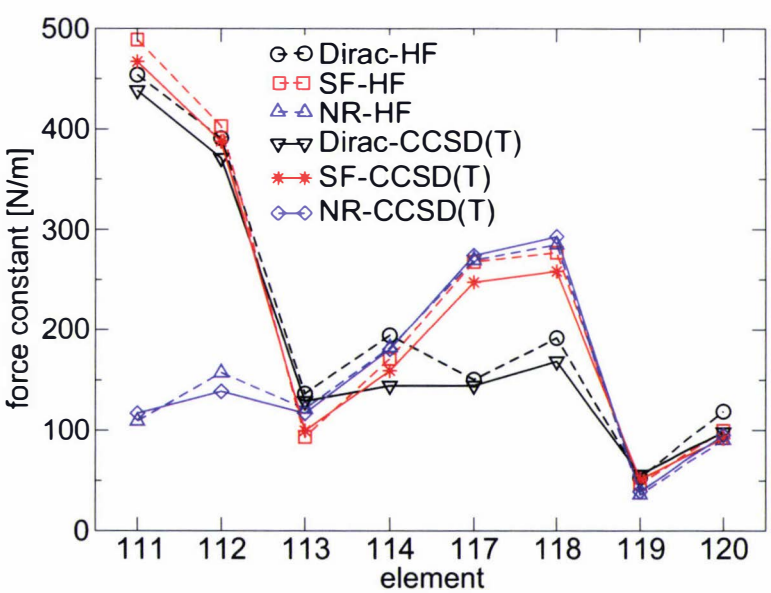

Figure 6.4: Comparison of calculated relativistic (Dirac), spinfree scalar relativistic (SF) and non-relativistic (NR) HF and CCSD(T) force constants across the 7th period main group hydrides RgH, CpH^+, 113H, $114H^+$, 117H and $118H^+$, as well as 119H and $120H^+$.

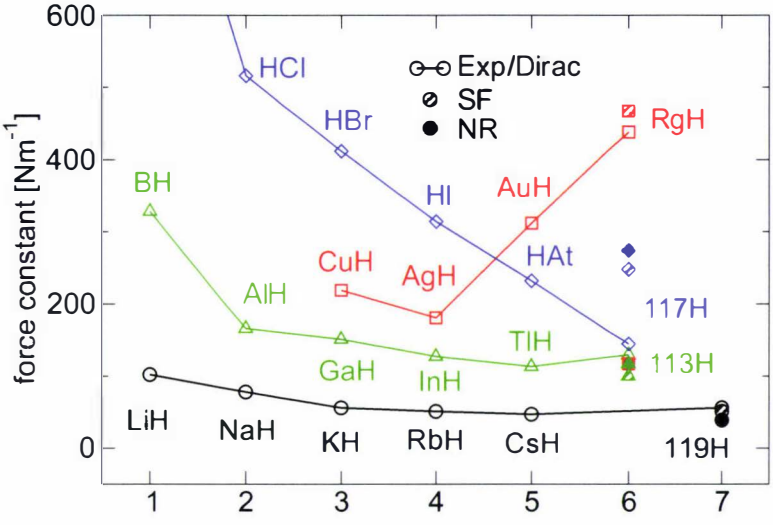

Figure 6.5: Comparison of the calculated relativistic (not filled), spinfree (partly filled) and non-relativistic (filled) CCSD(T) force constants for RgH, 113H, 117H and 119H with experimental values for the lighter homologes. Experimental values (circle) are taken from ref. [265] and the relativistic value for AtH from ref. [267] respectively.

leading for example to a dissociation energy of RgH larger than that of AgH (but smaller than that of AuH due to the spin-orbit effects as just discussed). The *p*-block element hydrides all undergo relativistic destabilization effects mainly due to spin-orbit stabilization at the atomic level. One should mention the very large scalar relativistic destabilization of $120H^+$, (and to a lesser extent for 119H), which again is rather unexpected and contrary to the dissociation energies for the group 11 or 12 element hydrides.

Finally it is worth mentioning that the large changes in the Mulliken charges and corresponding charge flow from the hydrogen to the superheavy element (except for $118H^+$) results in rather large changes (especially for RgH) in the dipole moments as can be seen in Table 6.5.

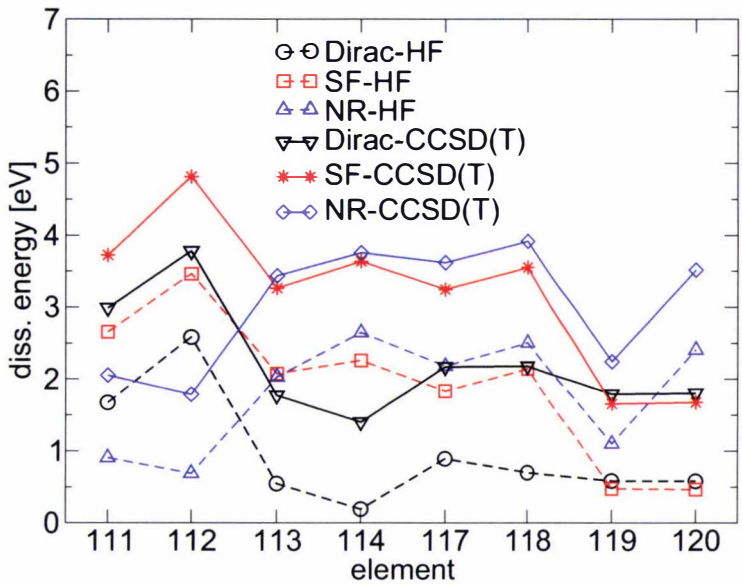

Figure 6.6: Comparison of calculated relativistic (Dirac), spinfree scalar relativistic (SF) and non-relativistic (NR) HF and CCSD(T) dissociation energies across the 7th period main group hydrides RgH, CpH^+, 113H, $114H^+$, 117H and $118H^+$, as well as 119H and $120H^+$.

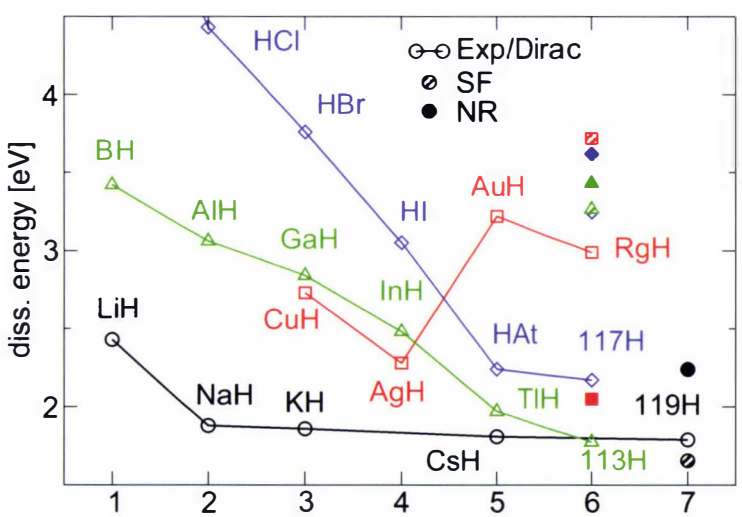

Figure 6.7: Comparison of the calculated relativistic (not filled), spinfree (partly filled) and non-relativistic (filled) CCSD(T) dissociation energies for RgH, 113H, 117H and 119H with experimental values for the lighter homologes. Experimental values (circle) are taken from ref. [265] and the relativistic value for AtH from ref. [267] respectively.

Chapter 7

Electric field gradients of transition-metal halides

With the development of generalized gradient approximations (GGA) into density functional theory (DFT), it has now become the preferred choice for the quantum theoretical treatment of large molecules and the solid state [268]. It is now well documented that density functionals perform well for most atomic and molecular electronic properties. There are, however, several shortcomings in the DFT methodology. The (rather long) list includes the incorrect description of highly non-local, long-range dispersive type of interactions [269–271], strongly correlated systems [272], magnetic materials [273], systems of high multi-reference character in the wavefunction [274] (for example in transition states of chemical reactions [275, 276]), charge-transfer processes [277], properties which delicately depend on the charge distribution, like dipole moments or electric field gradients [278–281] in transition metal compounds, or dipole and hyper-polarizabilities [154, 282, 283], and a few more.

One remaining notorious problem is the correct description of the quadrupolar charge distribution close to the nucleus in atoms, molecules and solids, which gives rise to the electric field gradient (EFG). In 1999 it was reported that currently applied density functionals perform poorly for the calculation of EFGs in transition metal containing compounds, especially in late transition metals where the polarization of the *d*-core has to be accurately described [278]. It was shown that the error in the electric field gradient (EFG) at the copper nucleus in CuCl correlates with the error in the valence charge distribution (dipole moment). Sim-

ilar defects were found for other transition metal compounds [284–286]. Thus, errors introduced in the long-range charge distribution of an atom leads to errors in the short range as the total charge has to be conserved.

In a recent paper [287] it was demonstrated that the charge distribution in Group 11 halides can be correctly described by coupling short-range gradient-corrected DFT with long-range exact exchange. Further improvement was achieved by combining the gradient-corrected short-range functionals with coupled-cluster theory [287]. The present study aims at calculating EFGs in copper and gold compounds by using the newly developed CAM-B3LYP functional of Yanai et al. [282]. This functional already gave notably improved dipole polarizabilities [288] and dipole moments [287] compared to the standard B3LYP functional. It will be shown here that this method will also lead to substantially improved electric field gradients at the metal center.

7.1 The CAM-B3LYP functional

The Ewald decomposition of the electron-electron Coulomb operator into a short-range density functional and a long-range wavefunction based part goes back to a work in 1985 by Savin and Stoll [289]. The CAM-B3LYP approximation starts from a generalization of this decomposition [282]

$$V_{ee} = \sum_{i<j} \frac{1 - [\alpha + \beta \operatorname{erf}(\mu r_{ij})]}{r_{ij}} + \sum_{i<j} \frac{\alpha + \beta \operatorname{erf}(\mu r_{ij})}{r_{ij}} \tag{7.1}$$

by introducing two new parameters α and β with the constraints $0 \leq \alpha + \beta \leq 1$, $0 \leq \alpha \leq 1$ and $0 \leq \beta \leq 1$, erf is the well-known error function. The first term accounts for the short-range interaction described by DFT and the second term for the long-range part described with the Hartree-Fock (HF) exchange. The parameter α determines the weight of the HF exchange for all distances, while additional long-range HF exchange is mixed in with parameter β. The short-range DFT part the B3LYP functional is used, which already contains the exact exchange [172, 174]. The resulting Coulomb-attenuated form is called CAM-B3LYP, where the parameters were determined to be optimal for $\alpha = 0.19$, $\beta = 0.46$ and $\mu = 0.33$ [282]. The commonly used hybrid functional B3LYP is obtained by setting $\alpha = 0.2$ and $\beta = 0.0$ and adjusting the pre-factor of the B88

gradient correction to LDA exchange. The original routines have been written by Salek [288] and recently been implemented by Saue into the program package DIRAC [70].

7.2 Electric Field Gradients

The components of the electronic and nuclear field-gradient tensor $\hat{q}^{el}_{\alpha\beta}$ and $\hat{q}^{nuc}_{\alpha\beta}$ at nucleus X are the expectation values over the corresponding operators [290]

$$\hat{q}^{el}_{\alpha\beta}(\vec{R}_X) = -\sum_i^n \frac{3(r_{i\alpha} - R_{X\alpha})(r_{i\beta} - R_{X\beta}) - \delta_{\alpha\beta}|\vec{r}_i - \vec{R}_X|^2}{|\vec{r}_i - \vec{R}_X|^5} \tag{7.2}$$

and

$$\hat{q}^{nuc}_{\alpha\beta}(\vec{R}_X) = \sum_{Y\neq X} \frac{Z_X[3(R_{Y\alpha} - R_{X\alpha})(R_{Y\beta} - R_{X\beta}) - \delta_{\alpha\beta}|\vec{R}_X - \vec{R}_Y|^2]}{|\vec{R}_X - \vec{R}_Y|^5}. \tag{7.3}$$

In expressions (7.2) and (7.3) α, β stand for x, y or z, $(x, y, z) = \vec{r}_\alpha$ and $(X, Y, Z) = \vec{R}_\alpha$; the summation in (7.2) runs over all electrons i and the summation in eq. (7.3) runs over all nuclei X. The nuclear part (7.3) is easily determined as a constant addition to the electronic part of the field-gradient tensor. In the Kohn-Sham case the expectation value can be written as a sum of one-particle integrals of the form

$$q^{el}_{\alpha\beta}(\vec{R}_X, \phi_i^{KS}) = \sum_l^n \left\langle \phi_l(\vec{r}) \left| \frac{\partial^2}{\partial R_{X\alpha}\partial R_{X\beta}} \frac{1}{|\vec{r} - \vec{R}_X|} \right| \phi_l(\vec{r}) \right\rangle, \tag{7.4}$$

where ϕ_l represent the Kohn-Sham orbitals.

7.3 Calculations for ^{63}Cu and ^{197}Au

Diatomic compounds CuX and AuX (X=H,F,Cl,Br and I) with and without CO attached were chosen for the studies, i.e. OC-CuX and OC-AuX (X=F,Cl,Br and I). This provides nuclear quadrupole coupling constants (NQCCs) over a large range of values. All calculations were carried out applying relativistic basis sets in their fully uncontracted form to allow maximum flexibility of the one-

particle density close to the nucleus. Energy-optimized dual-type Gaussian basis sets (GTOs) for Cu $(20s/16p/11d/3f)$ and Au $(26s/24p/18d/12f)$ [284] were used. For the halides the following basis sets were applied: $(13s/7p/4d)$ for F, $(17s/12p/4d)$ for Cl, $(19s/17p/9d/2f)$ for Br and $(20s/19p/11d/2f)$ for I [247,291,292]. The basis set for hydrogen was a $(11s/6p/4d/3f)$. For C and O a $(11s/6p/3d/2f)$ and a $(11s/6p/3d/2f)$ basis-set was used respectively [247].

The equilibrium bond distances and nuclear quadrupole coupling constants for the diatomic compounds were taken from experiment [265], and from recent experimental measurements by Gerry and co-workers [293, 294] and Okabayashi [295]. The corresponding data for the four-atomic compounds are from OCAuX (X=F,Cl,Br) [296], OCAuI [297], OCCuX (X=F,Cl,Br) [298] and OCCuI [299].

The parameters published by Yanai et al. [282] were determined to accurately produce atomization energies and charge transfer excitations. Therefore, it seems to be necessary to re-optimize these parameters for EFG calculations. Thus, the parameters were adjusted to the experimental copper electric field gradient in CuCl (-0.31(2) au). Not surprisingly one finds a strong dependence of the copper field gradient on the value of α, see Fig. 7.1. For different values of α the EFG can even change sign. There is also a slight dependence on β. Finally, the parameter set $\alpha = 0.4$, $\beta = 0.179$ and $\mu = 0.99$ was obtained and the resulting functional will be called CAMB3LYP*. For this parameter region, the value for the Cl field gradient (1.63 au) is also quite close to the experimental one (1.68(2) au). A second indicator for the good performance is that the calculated dipole moment of CuCl (5.47 Debye) is also close to the DK-CCSD(T) value of (5.32 Debye) given in ref. [278].

According to

$$\nu_{\mathrm{NCQQ}}[\mathrm{MHz}] = 234.9647q\ [\mathrm{au}]\ Q\ [\mathrm{b}]\ , \tag{7.5}$$

where ν_{NCQQ} is the NQCC, the (spectroscopic) nuclear electric quadrupole moment Q of ^{63}Cu and ^{197}Au is determined by the slope of the experimental NQCC at the metal center to the theoretically determined electric field gradient. The slopes are obtained by a linear least-square fit. This method is by construction of the best fit of the slope, and more robust than the indirect method used in ref. [300]. The quality of the calculated EFGs and the linear fit is given by the

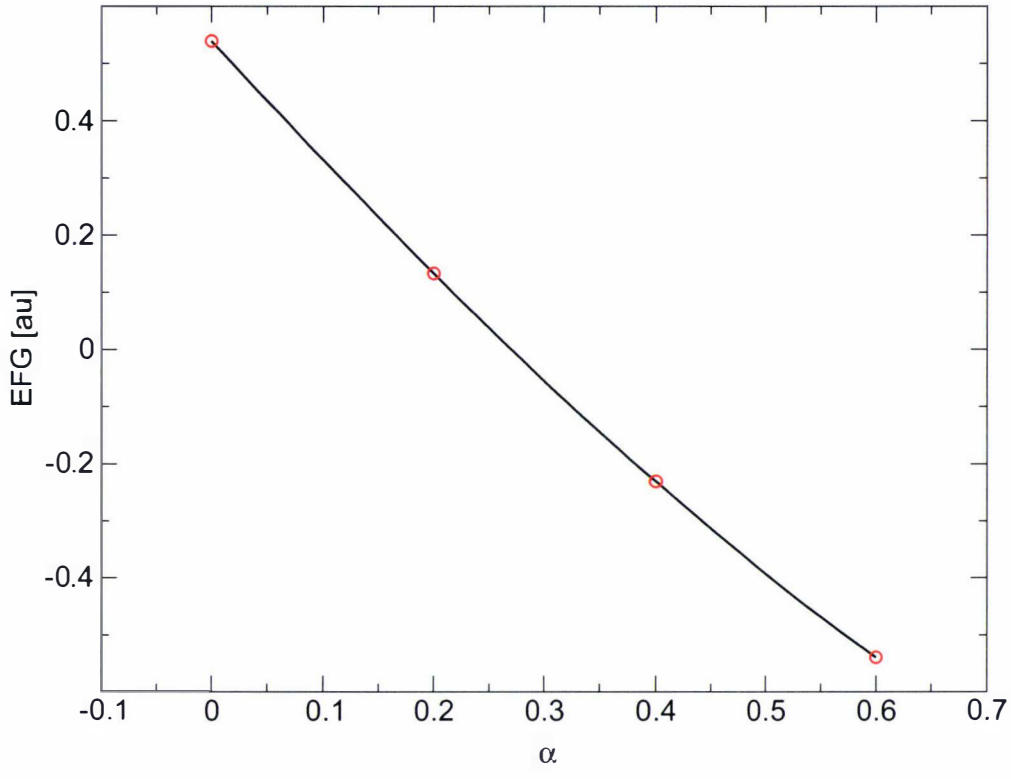

Figure 7.1: The calculated EFG (in atomic units) of CuCl for different values of α of the CAMB3LYP functional.

linear correlation coefficient of the linear regression and by the intercept which should be exactly zero [301]. Any deviation from the zero intercept points towards a systematic error in the method applied. The experimental field gradients are obtained from the nuclear quadrupole moments listed in ref. [302], which are -0.220(15) b for ^{63}Cu and +0.547(16) b for ^{197}Au (1 b = 10^{-28} m^2).

7.4 Results and Discussion

The electric field gradients at Cu and Au for a variety of diatomic compounds with and without CO attached are shown in Tables 7.1-7.4. First one should note that all pure density functionals (LDA and GGA) yield the wrong sign for the copper EFG in all diatomic compounds. In the case of the diatomic gold compounds the EFGs are similar in error, as pointed out before [286]. This is in contrast to other properties (structures, energies vibrational frequencies, etc.)

where density functionals (especially hybrid functionals) like B3LYP are found to perform extremely well. Also the CAM-B3LYP functional with the suggested parameters does not perform well for EFGs. For the molecules with CO attached, the EFGs are in somewhat better agreement, as the absolute values are rather large and less close to zero. Nevertheless, the variation in the EFGs between the different density functionals is still not acceptable.

Method	CuH	CuF	CuCl	CuBr	CuI
HF	-0.702	-1.335	-0.896	-0.742	-0.571
LDA	0.616	0.570	0.498	0.505	0.487
PBE	0.598	0.546	0.404	0.429	0.418
PW91	0.708	0.792	0.634	0.617	0.572
BLYP	0.776	0.879	0.718	0.696	0.640
B3LYP	0.338	0.112	0.149	0.181	0.208
CAMB3LYP	0.311	0.145	0.129	0.152	0.176
CAMB3LYP*	-0.085	-0.503	-0.315	-0.237	-0.141

Table 7.1: Calculated electric field gradients (in atomic units) at Cu for different diatomic copper compounds.

Method	OCCuF	OCCuCl	OCCuBr	OCCuI
HF	-2.178	-1.961	-1.876	-1.783
LDA	-0.686	-0.706	-0.668	-0.659
PBE	-0.739	-0.751	-0.711	-0.697
PW91	-0.736	-0.748	-0.708	-0.695
BLYP	-0.685	-0.699	-0.663	-0.654
B3LYP	-1.012	-0.976	-0.932	-0.907
CAMB3LYP	-1.148	-1.123	-1.082	-1.059
CAMB3LYP*	-1.558	-1.450	-1.391	-1.339

Table 7.2: Calculated electric field gradients (in atomic units) at Cu for different triatomic copper compounds.

The calculated nuclear quadrupole moments (NQM) are given in Tables 7.5 and 7.6. As pointed out before [286] for LDA, the GGAs and B3LYP erratic NQMs for each sub-set of molecules, the diatomics as well as the four-atomics, were derived. In fact the intercept is not even close to zero. Obviously the CAM-B3LYP with the original parameter set does not perform well either.

Considerable improvement for all subsets and molecules is achieved for the CAM-B3LYP* approximation with the newly adjusted parameters. For the first time a

Method	AuH	AuF	AuCl	AuBr	AuI
HF	-2.015	-4.610	-3.428	-2.903	-2.240
LDA	4.013	4.074	3.746	3.700	3.514
PBE	3.693	3.718	3.375	3.348	3.204
PW91	3.746	3.783	3.441	3.411	3.259
BLYP	3.886	4.005	3.659	3.625	3.445
B3LYP	2.899	2.190	2.206	2.280	2.310
CAMB3LYP	2.142	1.285	1.384	1.502	1.625
CAMB3LYP*	0.780	-0.858	-0.290	-0.010	0.332

Table 7.3: Calculated electric field gradients (in atomic units) at Au for different diatomic gold compounds.

Method	OCAuF	OCAuCl	OCAuBr	OCAuI
HF	-1.186	-1.169	-1.143	-1.119
LDA	-4.059	-4.653	-4.583	-4.676
PBE	-4.405	-4.950	-4.881	-4.957
PW91	-4.339	-4.883	-4.815	-4.896
BLYP	-4.125	-4.663	-4.661	-4.702
B3LYP	-5.784	-6.161	-6.059	-6.091
CAMB3LYP	-6.677	-7.094	-7.002	-7.039
CAMB3LYP*	-8.544	-8.708	-8.542	-8.470

Table 7.4: Calculated electric field gradients (in atomic units) at Au for different triatomic gold compounds.

	diatomics CuX			four-atomics OCCuX			all CuX + OCCuX		
Method	ic.	Q	corr.	ic.	Q	corr.	ic.	Q	corr.
HF	-6.2	-91	0.808	16.2	-117	0.989	-26.9	-205	0.970
LDA	35.8	-189	0.308	15.7	-345	0.389	37.9	-206	0.980
PBE	24.3	-108	0.278	41.9	-655	0.817	34.9	-203	0.980
PW91	-9.6	139	0.351	-42.8	-663	0.816	39.5	-175	0.971
BLYP	-15.8	160	0.425	-49.0	-747	0.738	42.3	-172	0.965
B3LYP	29.7	-382	0.968	-25.8	-424	0.994	21.7	-214	0.994
CAMB3LYP	29.0	-397	0.860	-57.6	-490	0.987	20.2	-192	0.990
CAMB3LYP*	0.1	-200	0.955	-1.5	-210	0.997	-0.3	-208	0.998
Exp							0.0	-220(15)	1.000

Table 7.5: The nuclear quadrupole moment Q (in 10^{-3} b) of ^{63}Cu. Intercept (ic. in MHz) and correlation factor (corr.) from the linear fit of the NQCC vs. EFG.

reasonable accuracy in the NQMs of ^{63}Cu and ^{197}Au is achieved, despite somewhat large deviations for the OCAuX compounds with an intercept which differs substantially from zero. Nevertheless, the correlation factor is close to one and CAM-B3LYP* performs significantly better than any other density functional used here.

	diatomics AuX			four-atomics OCAuX			all AuX + OCAuX		
Method	ic.	Q	corr.	ic.	Q	corr.	ic.	Q	corr.
HF	290.1	333	0.911	-438.1	208	0.771	419.8	522	0.996
LDA	119.2	-75	0.046	-1040.3	-35	0.129	-432.1	539	0.991
PBE	3.4	59	0.035	-1039.9	-33	0.108	-390.8	542	0.992
PW91	35.3	20	0.012	-1041.6	-34	0.115	-398.8	542	0.991
BLYP	255.9	-230	0.136	-1054.3	-48	0.167	-423.7	541	0.991
B3LYP	-606.8	1184	0.917	-948.6	39	0.080	-246.3	536	0.996
CAMB3LYP	-363.9	1119	0.981	-987.9	9	0.002	-143.6	527	0.997
CAMB3LYP*	53.1	598	0.977	516.3	755	0.960	53.6	526	0.999
Exp							0.0	547(16)	1.000

Table 7.6: The nuclear quadrupole moment Q (in 10^{-3} b) of ^{197}Au obtained from a linear fit. Intercept (ic. in MHz) and correlation factor (corr.) from the linear fit of NQCC vs. EFG.

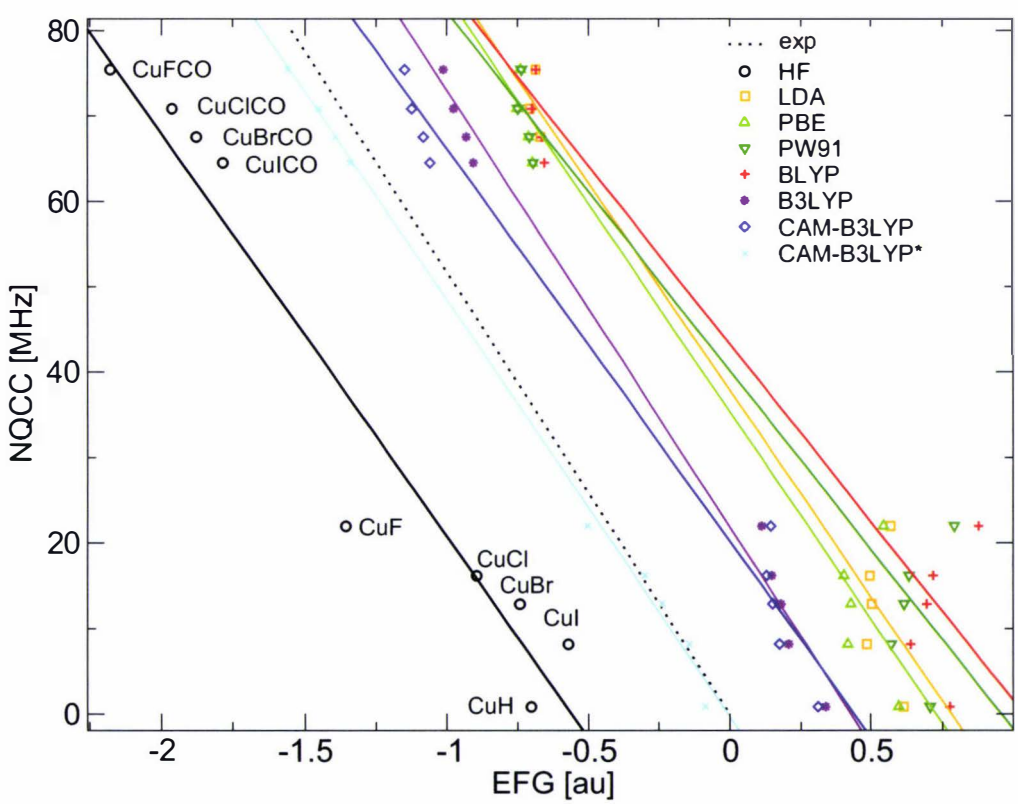

Figure 7.2: The experimental NQCC (in MHz) as a function of the calculated EFG (in atomic units) for different copper compounds.

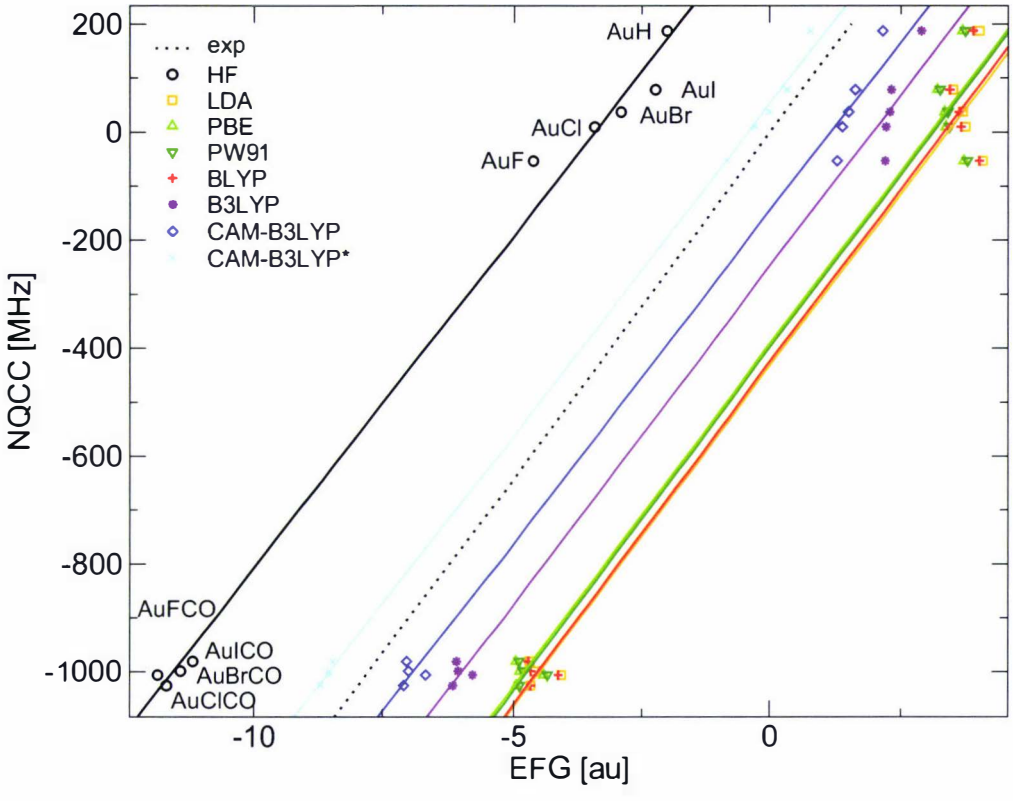

Figure 7.3: The experimental NQCC (in MHz) as a function of the calculated EFG (in atomic units) for different gold compounds.

By correlating all compounds, as shown in Fig. 7.2 and 7.3, one obtains an excellent performance for the CAM-B3LYP* method with NQMs now in good agreement with the experimentally predicted ones. For instance, for ^{63}Cu one gets -0.208 b, which lies within the experimental uncertainty [302].

For ^{197}Au the muonic value of 0.547 b [303] has been debated very recently. Schwerdtfeger et al. [284] obtained 0.64 b using the (CO)AuF molecule and 0.61 b using several solids. It was pointed out that it is currently very difficult to obtain an accurate NQM for ^{197}Au, and consequently the muonic value remained unchallenged. More recently Belpassi et al. [300] obtained 0.510 b, Itano [304] 0.587(29) b using the Au atom $5d^96s^2\ ^2D_{3/2,5/2}$ states in multi-configuration Dirac-Hartree-Fock and relativistic configuration-interaction calculations, and Palade et al. [305] give 0.560(30) b for Au-Al alloys obtained from ^{197}Au Mössbauer spectroscopy measurements and relativistic linearized augmented plane wave (LAPW) calculations. Pyykkö et al. obtained 0.509 b for AuH

from relativistic coupled-cluster calculations including both Gaunt and quantum electrodynamic contributions [306]. The most accurate value comes perhaps from the Tel-Aviv group with 0.521(7) b obtained from relativistic Fock-space coupled-cluster calculations with single and double excitations including the Gaunt term for $^2D_{3/2,5/2}$ states of atomic gold [307]. The calculated result reported here with 0.526 b is in excellent agreement with this value.

Finally one should mention that whilst the EFG is not reproduced accurately by most density functionals, in spanning the whole range of all possible EFGs using a variety of compounds, one clearly observes an error cancellation when the NQM is determined. Hence, all density functionals perform reasonably well, i.e. from -0.206 b (LDA) to -0.172 b (BLYP) for ^{63}Cu, and 0.526 b (CAM-B3LYP*) to 0.542 b (PW91) for ^{197}Au. However, the intercept can deviate substantially from the correct value of zero which is disappointing. Therefore one can conclude that the readjusted CAM-B3LYP* hybrid functional is currently the best density functional to be used in electric field gradient calculations of transition element containing compounds.

Chapter 8

Parity Violation in CHFClBr

Despite the well accepted fact that the weak neutral currents between electrons and nucleons predicted by the electroweak theory create an energy difference between the two enantiomers of a chiral molecule, this kind of parity violation (PV) has never been observed in experiments. Unfortunately this energy difference can not be measured directly. One promising method is to measure PV-shifts in vibrational transitions of chiral molecules. Currently Chardonnet and co-workers are setting up an experiment using highly frequency-stable tunable lasers [43] for high-resolution measurements, which can reach resolutions below 1 Hz, coming close to the order of magnitude for the PV effect predicted for example for a molecule like CHFClBr.

Because of the very small size of the PV effect, it is essential for experimentalists to have an accurate theoretical value for comparison. However, it is well known that electron correlation is very important in electronic structure calculations especially for PV energy shifts [57]. State-of-the-art methods to predict this energy shift are Dirac-Kohn-Sham (DKS) calculations using various functionals due to the advantage of low computational costs and wave-function based methods like Kramers-restricted coupled-cluster theory.

In this investigation one of the most promising molecules, bromochlorofluoromethane (CHFClBr) was chosen to test a number of different methods. The atoms form a tetrahedron with the hydrogen, fluorine, chlorine and bromine at the corners and the chiral carbon atom in the center (Fig. 8.1).

In this study it is shown that none of the density-functionals work very well in

Figure 8.1: Two enantiomers of the CHFClBr molecule. The molecule on the left is the S-enantiomer, the one on the right is the R-enantiomer.

PV calculations and therefore cannot be used without further investigations. A consistent wave-function based correlation treatment might give the only accurate solution at present. Coupled-cluster [CCSD(T)] calculations were therefore performed, using a finite field approach for the PV operator as suggested previously by Thyssen et al. [308]. The CCSD(T) results were subsequently used to evaluate the quality of various density functional approximations. Furthermore the three parameters of the Coulomb attenuated functional CAM-B3LYP [282] were adjusted to reproduce the PV energy shifts of each atom in CHFClBr as obtained by the CCSD(T) calculations. It was found in previous studies that this procedure works quite well for dipole moments and electric field gradients in transition-metal halides (see previous chapter) [287, 309].

8.1 Theory of Electroweak Interaction

The route to the effective 4-component relativistic parity-violating (PV) electronic neutral weak Hamiltonian for molecular calculations is a long journey "through the beautiful field of particle physics, gauge theories, and quantum field theory" [310] which is beyond the scope of this thesis. The Lagrangian density of the neutral weak electron-nucleon (e-nuc) contact interaction in the low-energy (zero momentum transfer) limit [310], serves as a starting point here

$$\mathcal{L}_{\text{int}}^{\text{e-nuc}} = \frac{G_F}{\sqrt{2}} j_\mu^e J^{\text{nuc},\mu} \tag{8.1}$$

with the Fermi coupling constant $G_F = 2.22255 \times 10^{-14}$ au and an implicit sum over all nucleons (nuc), that is, all protons (p) and neutrons (n). Being a contact

interaction, the attention can be restricted to one atomic center, say nucleus K, with Z_K protons and N_K neutrons. At this stage, the generalized 4-currents j_μ can be regarded as linear combinations of the generalized densities $\psi^\dagger M\psi$ with M denoting the Dirac matrices. The Dirac matrices and the associated currents can be classified according to the transformation under parity reversal as polar vectors (V) and pseudoscalars (P) which change sign, and as axial vectors (A) and scalars (S) which do not.

It can be shown [310] that only V-A (polar vector minus axial vector) Fermi coupling is of relevance, and the corresponding electron and nucleon 4-currents that appear in eq. 8.1 are given by

$$\begin{aligned} j^{\mathrm{e}}_\mu &= j^{\mathrm{e}}_{\mu\mathrm{V}} - j^{\mathrm{e}}_{\mu\mathrm{A}} \\ &= C^{\mathrm{e}}_{\mathrm{V}}\psi^\dagger_{\mathrm{e}}(\vec{\alpha}, 1_{4\times4})\psi_{\mathrm{e}} - C^{\mathrm{e}}_{\mathrm{A}}\psi^\dagger_{\mathrm{e}}(\vec{\Sigma}, \gamma^5)\psi_{\mathrm{e}} \qquad (8.2) \\ j^{\mathrm{nuc}}_\mu &= j^{\mathrm{nuc}}_{\mu\mathrm{V}} - j^{\mathrm{nuc}}_{\mu\mathrm{A}} \\ &= C^{\mathrm{nuc}}_{\mathrm{V}}\psi^\dagger_{\mathrm{nuc}}(\vec{0}, 1_{2\times2})\psi_{\mathrm{nuc}} - C^{\mathrm{nuc}}_{\mathrm{A}}\psi^\dagger_{\mathrm{nuc}}(\vec{\sigma}, 0)\psi_{\mathrm{nuc}}, \qquad (8.3) \end{aligned}$$

where $\gamma^5 = \alpha_x\alpha_y\alpha_z$ and $\vec{\Sigma} = \gamma^5\vec{\alpha}$. In eq. (8.3) the so-called non-relativistic approximation has been invoked which means to neglect of the nucleon small component bispinors.

Before giving the explicit coupling coefficients C of eqs. (8.2) and (8.3), and actually coupling the electron and nucleon 4-currents, it is worthwhile to study first the transformation under the parity operation of the space-like components $(\vec{\alpha}, \vec{\Sigma}, \vec{\sigma})$ and time-like components $(1_{4\times4}, \gamma^5, 1_{2\times2})$ and their combinations: $\vec{\alpha}$ transforms as the coordinates which change sign (V), matrices $\vec{\Sigma}$ and $\vec{\sigma}$ transform as rotations (A), $1_{4\times4}$ and $1_{2\times2}$ as S, and finally γ^5 is the pseudoscalar chirality matrix (P). The four possible electron-nucleon combinations are

$j^{\mathrm{e}}_{\mu,\mathrm{V}}\, j^{\mathrm{nuc},\mu}_{\mathrm{V}}$	which transforms as	S
$j^{\mathrm{e}}_{\mu,\mathrm{V}}\, j^{\mathrm{nuc},\mu}_{\mathrm{A}}$		V
$j^{\mathrm{e}}_{\mu,\mathrm{A}}\, j^{\mathrm{nuc},\mu}_{\mathrm{V}}$		P
$j^{\mathrm{e}}_{\mu,\mathrm{A}}\, j^{\mathrm{nuc},\mu}_{\mathrm{A}}$		A

The parity-even S and A combinations can be dropped being practically unobservable due to the minute size of the Fermi coupling constant G_F. Only the

parity-odd V and P combinations shall be considered in the following. They are tiny, too. However, they distinguish themselves from all other fundamental interactions by symmetry breaking which makes them observable in a suitable experiment.

Returning to eqs. (8.2) and (8.3), the electron (e), up quark (u), and down quark (d) coupling coefficients read as [310]

$$C_V^e = 1 - 4\sin^2\theta_W \tag{8.4}$$

$$C_V^u = 1 - \frac{8}{3}\sin^2\theta_W \tag{8.5}$$

$$C_V^d = 1 - \frac{4}{3}\sin^2\theta_W \tag{8.6}$$

$$C_A^e = -\frac{1}{2} \tag{8.7}$$

$$C_A^u = \frac{1}{2} \tag{8.8}$$

$$C_A^d = -\frac{1}{2} \tag{8.9}$$

with the Weinberg parameter $\sin^2\theta_W = 0.2397(13)$ [310]. The p and n coupling coefficients are approximately given by

$$C_V^p = 2C_V^u + C_V^d \tag{8.10}$$

$$C_V^n = 2C_V^d + C_V^u, \tag{8.11}$$

with corresponding relations for C_V^p and C_V^n since protons consist of two u and one d and neutrons of two d and one u quark.

The nucleon V-currents can be combined (added up) to the weak charge Q_w^K which allows us to express the V current for nucleus K by

$$j_{\mu V}^K = (\vec{0}, Q_w^k \rho_K), \tag{8.12}$$

where ρ_K is the nuclear charge distribution (typically modeled by a Gaussian distribution), and the weak charge Q_w^K is given by

$$\begin{aligned} Q_w^K &= (2Z_K + N_K)C_V^u - (2N_K + Z_K)C_V^d \\ &= Z_K(1 - 4\sin^2\theta_W) - N_K. \end{aligned} \tag{8.13}$$

Z_K and N_K are the proton and the neutron number of nucleus K. In contrast to $j^K_{\mu,V}$ the combination of nucleon A-currents to form $j^K_{\mu,A}$ is less evident. Typically, $j^K_{\mu,A}$ is approximately given by

$$\begin{aligned} j^K_{\mu,\mathrm{A}} &= (\lambda_K \vec{I}_K \rho_K, 0) \\ &= \left(\frac{\lambda_K}{\gamma_K} \vec{M}_K \rho_K, 0 \right) \end{aligned} \tag{8.14}$$

with the nucleus-dependent form factor λ_K on the order of unity and chosen as $\lambda_K = 1$ in actual calculations. The nuclear spin distribution is approximated by the nuclear Gaussian charge distribution scaled with the nuclear spin $\vec{I}_K$, or equivalently, scaled with the nuclear magnetic moment $\vec{M}_K$ and divided by the gyromagnetic ratio γ_K.

We have now gathered all ingredients to form the parity-odd combinations of electron and nucleon 4-currents and obtain the effective one-electron Hamiltonians

$$H_{i,\mathrm{A}} = -\frac{G_F C^{\mathrm{e}}_{\mathrm{A}}}{\sqrt{2}} \gamma^5 \sum_K Q^K_w \rho_K(\vec{r}_i) \tag{8.15}$$

and

$$H_{i,\mathrm{V}} = -\frac{G_F C^{\mathrm{e}}_{\mathrm{V}}}{\sqrt{2}} \vec{\alpha} \sum_K \frac{\lambda_K}{\gamma_K} \vec{M}_K \rho_K(\vec{r}_i), \tag{8.16}$$

respectively, with $C^{\mathrm{e}}_{\mathrm{A}}$ and $C^{\mathrm{e}}_{\mathrm{V}}$ given in eqs. (8.4) and (8.7). The first Hamiltonian $H_{i,\mathrm{A}}$ is employed in calculations of PV energy differences between enantiomers. The second Hamiltonian $H_{i,\mathrm{V}}$ is employed in calculations of PV effects on nuclear spin dependent effects like nuclear magnetic resonance.

8.2 Computational Method

At the Dirac-Hartree-Fock (DHF) and DKS level the contribution of atom K in a molecule to the parity violation energy shift E_{PV} can be calculated as the expectation value

$$E^K_{\mathrm{PV}} = \langle \Psi | H^K_{\mathrm{PV}} | \Psi \rangle \tag{8.17}$$

over the nuclear spin-independent P-odd operator (8.15)

$$H_{\mathrm{PV}}^{K} = \frac{G_F}{2\sqrt{2}} \sum_i Q_w^K \gamma_i^5 \rho_n(\vec{r}_i). \tag{8.18}$$

The summation is over all electrons. For the number of nucleons $A_K = N_K + Z_K$, values of 1, 12, 19, 35 and 79 have been used for H, C, F, Cl and Br respectively. All calculations were performed by using the program package DIRAC [70], which calculates the expectation value at the DHF and DKS level of theory. Because it is currently not possible to obtain a CCSD(T) wave function to calculate the expectation value, the finite field method [308] was applied instead to obtain the parity violation energy for CHFClBr at various correlated levels. The parity-violation energy shift can be written as

$$E_{\mathrm{PV}} = \frac{G_F}{2\sqrt{2}} \sum_i Q_w^K M_{\mathrm{PV}}^K. \tag{8.19}$$

where M_{PV}^K is given by

$$\begin{aligned} M_{\mathrm{PV}}^K &= \left\langle \Psi \left| \sum_i \gamma_i^5 \rho_K(\vec{r}_i) \right| \Psi \right\rangle \\ &= \langle \Psi | \hat{M}_{\mathrm{PV}}^K | \Psi \rangle \end{aligned} \tag{8.20}$$

The basic idea is to deploy the parity violation operator as an perturbation for the DHF operator with perturbation strength λ

$$\hat{H}(\lambda) = \hat{H}_{\mathrm{DHF}} + \lambda \hat{M}_{PV}^K. \tag{8.21}$$

M_{PV}^K is found as the first derivative of the total energy of the molecule with respect to λ, which has to be sufficiently small to obtain converged values for M_{PV}^K.

8.3 Results and Discussion

Density functional calculations using the functionals (LDA, BLYP, B3LYP, PBE and CAM-B3LYP) were performed for the molecule CHFClBr at the CCSD(T) optimized geometry using completely uncontracted cc-pVDZ basis sets [176,247,

291]. The results are summarized in Tab. 8.1 and depicted in Fig. 8.2. Each functional gives different atomic PV contributions. Some LDA and PBE even yield the opposite sign for the bromine value compared to the Dirac-Hartree-Fock calculation. As a result of this varying performance for different func-

	Br	Cl	F	C	H
HF	1.683E-05	-1.845E-05	6.803E-06	5.761E-07	-0.829E-08
LDA	-0.483E-05	-0.529E-05	7.802E-06	6.874E-07	-3.274E-08
BLYP	0.029E-05	-0.868E-05	7.645E-06	5.548E-07	-3.099E-08
B3LYP	0.623E-05	-1.279E-05	7.752E-06	6.127E-07	-2.555E-08
PBE	-0.057E-05	-0.749E-05	7.581E-06	5.545E-07	-3.083E-08
CAM-B3LYP	1.208E-05	-1.712E-05	8.318E-06	6.532E-07	-1.911E-08
CAMB3LYP*	1.393E-05	-1.772E-05	7.741E-06	6.422E-07	-1.637E-08
MP2	0.959E-05	-1.413E-05	6.740E-06	6.820E-07	-1.522E-08

Table 8.1: M_{PV}^{K} values for CHFClBr calculated at different levels of theory using a cc-pVDZ basis set.

tionals, relativistic DHF, MP2 and CCSD(T) calculations were performed using completely decontracted cc-pVDZ and cc-pVTZ correlation consistent basis sets for all atoms by utilizing the finite field method. The perturbation strength λ was varied over a large range ($10^{-1} - 10^{-6}$ au). The first task was to reproduce the PV expectation value at DHF level for each atom. It was found that for $\lambda > 10^{-2}$ au the weak perturbation regime was left and the M_{PV}^{K} value drifted to larger values. For $\lambda < 10^{-4}$ au an oscillational behavior was observed which can be explained as to be due to numerical instabilities at such tiny perturbation strengths (Fig. 8.3). The MP2, CCSD and CCSD(T) values were also found to be converged in the same parameter region (Fig. 8.3). In-between, the M_{PV} values remained almost constant over a range of two orders of magnitude. For the DHF and MP2 calculations they differed less than 0.5% from the expectation value (Tab. 8.2). This indicates that the finite field method in numerically stable and provides reasonable accuracy. For the coupled-cluster calculations it was however necessary to determine which orbitals need to be correlated. Even by using state-of-the-art computers one is forced to restrict the correlation space to the valence shell. In this study we restricted our calculations to correlate only the valence electrons otherwise the calculations would not be feasible on the available computers. The multi-reference character of the system was tested, and

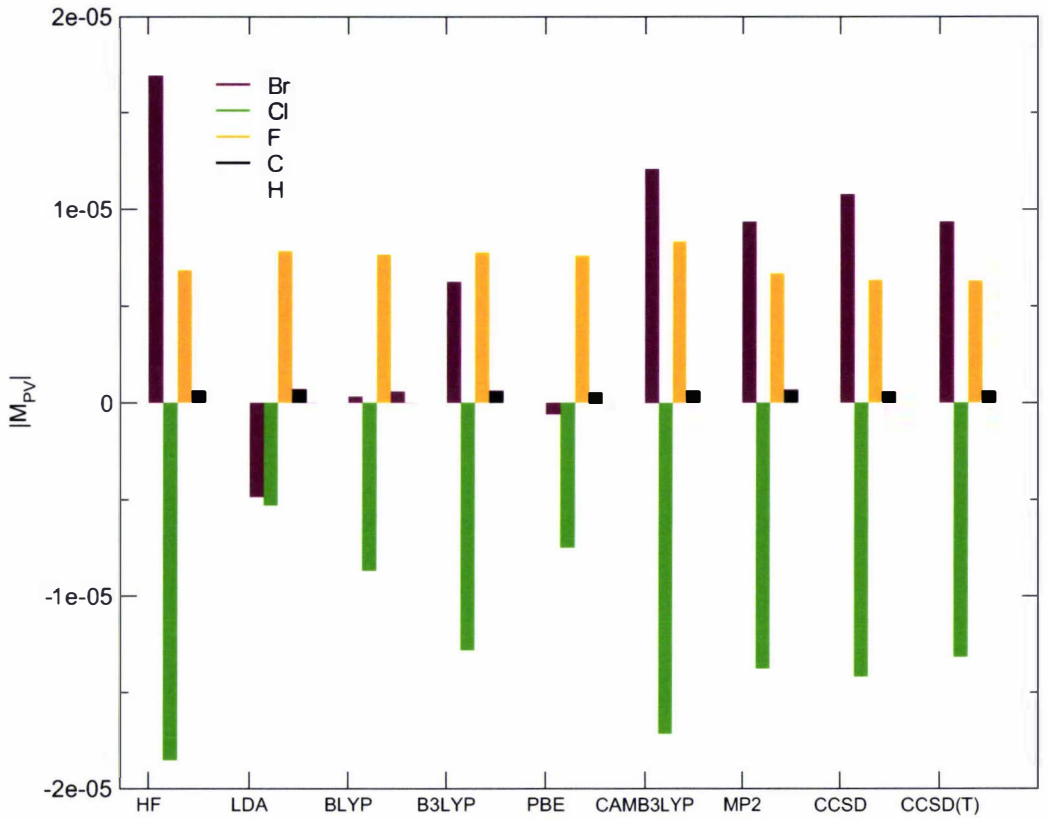

Figure 8.2: M_{PV}^{K} of CHFClBr calculated at different levels of theory using a cc-pVDZ basis set

atom	method	expectation value	finite field
Br	DHF	1.6832×10^{-5}	1.6830×10^{-5}
	MP2	0.9591×10^{-5}	0.9587×10^{-5}
Cl	DHF	-1.8454×10^{-5}	-1.8450×10^{-5}
	MP2	-1.4131×10^{-5}	-1.4180×10^{-5}
F	DHF	0.6803×10^{-5}	0.6826×10^{-5}
	MP2	0.6740×10^{-5}	0.6702×10^{-5}
C	DHF	0.0576×10^{-5}	0.0577×10^{-5}
	MP2	0.0682×10^{-5}	0.0677×10^{-5}
H	DHF	-0.0008×10^{-5}	-0.0008×10^{-5}
	MP2	-0.0014×10^{-5}	-0.0013×10^{-5}

Table 8.2: Parity violation (M_{PV}) at different levels of correlation, cc-pVDZ basis sets are used for all atoms of CHFClBr

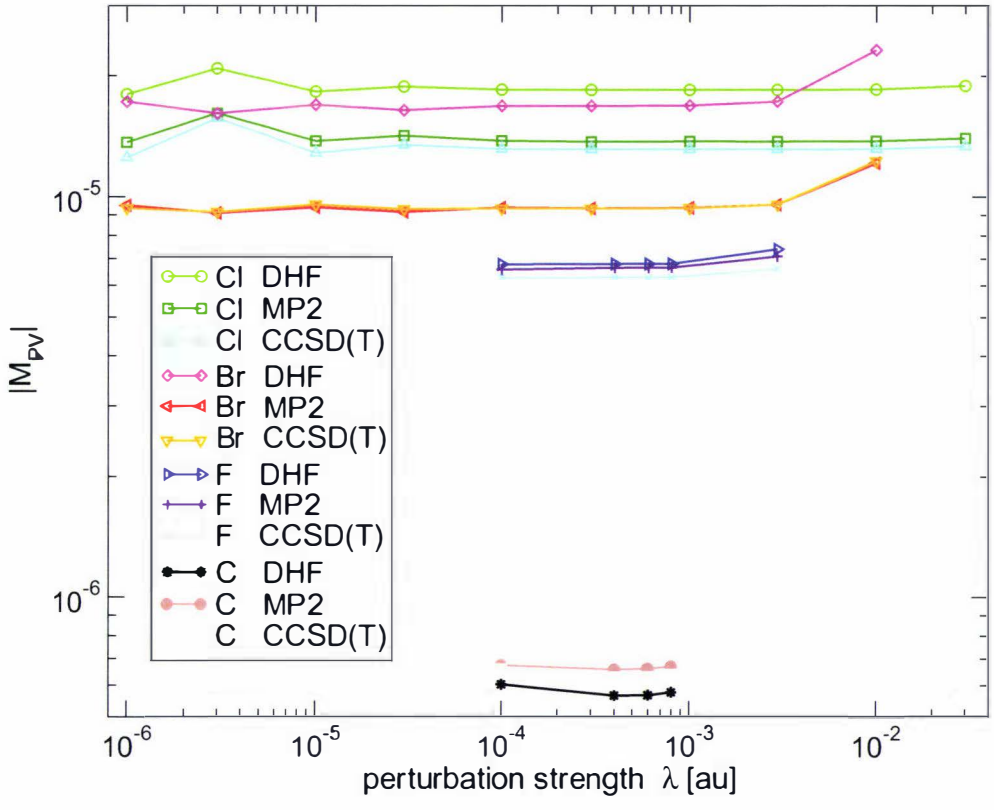

Figure 8.3: Correlation dependence of the PV contribution of the single atoms on the perturbation strength λ

the obtained value of 0.009 for the T1-diagnostic implies that it is reasonable to perform single reference CCSD(T) calculations.

With the knowledge of the perturbation strengths to be applied to each atom, it was possible to extend the basis sets to cc-pVTZ. The DHF value with that basis set increased by roughly 30% for each atom compared to the cc-pVDZ calculations. The MP2 results are summarized in table 8.3.

Nevertheless, it was impossible to perform a vast number of coupled-cluster calculations using this basis set to find a regime for the perturbation strength where a converged PV energy difference could be obtained. Therefore difference between the MP2 and CCSD(T) results at the cc-pvDZ level of theory was added to the MP2 value obtained by a cc-pVTZ calculation.

By using the same perturbation strength as in the cc-pVDZ calculations, single CCSD(T) calculations were performed and the PV energy difference calculated.

The PV energy differences at cc-pVTZ level obtained by both methods are listed in Tab. 8.4. One can see that both procedures give basically the same value close to the MP2 result.

method	M_{PV}^{Br}	M_{PV}^{Cl}	M_{PV}^{F}	M_{PV}^{C}	M_{PV}^{H}
DZ DHF	$1.683\,10^{-5}$	$-1.845\,10^{-5}$	$6.803\,10^{-6}$	$5.761\,10^{-7}$	$-8.291\,10^{-9}$
DZ MP2	$9.591\,10^{-6}$	$-1.413\,10^{-5}$	$6.740\,10^{-6}$	$6.820\,10^{-7}$	$-1.371\,10^{-8}$
DZ CCSD(T)	$9.340\,10^{-6}$	$-1.310\,10^{-5}$	$6.280\,10^{-6}$	$6.340\,10^{-7}$	-
TZ DHF	$2.230\,10^{-5}$	$-2.360\,10^{-5}$	$9.700\,10^{-6}$	$8.510\,10^{-7}$	$-1.880\,10^{-8}$
TZ MP2	$1.055\,10^{-5}$	$-1.710\,10^{-5}$	$9.610\,10^{-6}$	$1.090\,10^{-6}$	$-8.712\,10^{-9}$

Table 8.3: Parity violation M_{PV} values at different levels of correlation. cc-pVDZ and cc-pVTZ basis sets are used for all atoms of CHFClBr.

method	M_{PV}^{Br}	M_{PV}^{Cl}	M_{PV}^{F}	M_{PV}^{C}	E_{PV} [au]
extrap.	$1.030\,10^{-5}$	$-1.615\,10^{-5}$	$9.155\,10^{-6}$	$1.045\,10^{-6}$	-1.945×10^{-18}
single calc.	$1.054\,10^{-5}$	$-1.570\,10^{-5}$	$8.860\,10^{-6}$	$1.010\,10^{-6}$	-2.064×10^{-18}

Table 8.4: Parity violation (M_{PV}) at different levels of correlation. cc-pVTZ basis sets were used

The CAM-B3LYP functional performed reasonably well, but the parameters publish by Yanai *et al.* [282] were determined to accurately reproduce atomization energies and charge transfer excitations. Hence, it was necessary to reoptimize these parameters for calculations of the PV contributions of the single atoms. The adjusted parameters are $\alpha = 0.10$, $\beta = 0.25$ and $\mu = 0.50$ for which the coupled-cluster values for the Br as well as the Cl atoms were reproduced within an error of less than 5%. This functional should be used in future PV calculations.

Conclusion

Relativistic quantum chemistry is the relativistic formulation of quantum mechanics applied to many-electron systems, i.e., to atoms, molecules and solids. It combines the principles of special relativity, which are obeyed by any fundamental physical theory, with the basic rules of quantum mechanics (NB: So far no violation of the CPT theorem has been found which would imply violation of Lorentz invariance). By construction, it represents the most fundamental theory of all molecular sciences, which describes matter by the action, interaction and motion of the elementary particles. This science is of vital importance to physicists, chemists, material scientists, and biologists with a molecular view of the world. Nevertheless, a full relativistic treatment of atoms and molecules which includes the quantization of the electromagnetic field has been and will remain a challenging task for future investigations.

The goal of the presented thesis therefore was to study relativistic effects in atoms and molecules. A combination of wave function based and density functional methods within the four-component approach proved necessary to achieve accurate *ab-initio* results of atomic and molecular properties.

Quantum electrodynamic (QED) calculations were presented within the Furry picture of bound state QED for the frequency-dependent Breit interaction between electrons, the vacuum polarization and the electron self-energy correction. Starting from the Dirac-Coulomb Hamiltonian, QED effects in the ionization potentials of the group 1, 2, 11, 12, 13 and 18 elements of the periodic table, down to the superheavy elements up to nuclear charge Z=120, were investigated. The results for the *s*-block elements were found to be in excellent agreement with earlier studies by Labzowsky et al. using a different methodology.

The K-shell and L-shell ionizations potentials for $^{268}_{109}$Mt were calculated at the Dirac-Hartree- Fock level taking into account QED and finite nuclear-size effects.

The $K_{\alpha 1}$-transition energies for different ionization states are accurately predicted and compared with recent experiments for the α-decay of $^{272}_{111}$Rg. It was concluded that the observed γ-ray came from a nuclear and not from an electronic transition as originally postulated.

Static dipole polarizabilities for the $^3P_0$ ground state of the neutral group 14 elements C, Si, Ge, Sn, Pb and the element with nuclear charge $Z = 114$ were studied by utilizing all-electron relativistic coupled cluster theory. A comparison to molecular beam electric field deflection experiments for Sn and Pb shows good agreement with the theoretical values presented here. The isotropic and anisotropic components of the polarizability increase monotonically with the nuclear charge Z, except for the spin-orbit coupled $J = 0$ states, which start to decrease from Sn to Pb and even further to element $Z = 114$. Hence, spin-orbit coupling leads to a significant reduction of the polarizability of the superheavy element with $Z = 114$, i.e., from 47.9 au at the scalar-relativistic Douglas-Kroll level to 31.5 au at the Dirac-Coulomb level of theory, which is even below the value of Si (37.3 au). The calculations further demonstrated that relativistic and electron correlation effects are non-additive.

Relativistic and electron correlation effects were studied for the closed-shell superheavy element mono-hydrides RgH, $112H^+$, 113H, $114H^+$, 117H, $118H^+$, 119H, and $120H^+$. In particular, the chemical bonding of the elements 119 and 120 were discussed for the first time. Periodic trends were discussed by comparing the calculated properties to the ones for the lighter elements. The size of the relativistic effects varied considerably between the different molecules, with the *s*-block elements being dominated by scalar relativistic effects and the *p*-block elements by spin-orbit effects. In most cases, relativistic effects are more important than electron correlation effects, and both are non-additive as one expects. $120H^+$ behaves in a counterintuitive way as it shows a relativistic bond-length expansion together with a large relativistic decrease in the dissociation energy. The reason behind this anomalous behavior is due to the relativistically diminished valence-7*d* participation in the 120-H bond.

The electric field gradient in late transition metal compounds is incorrectly determined by most density functionals. It was shown that the coupling of short-range density-functional based with long-range wave-function based methods using a reparametrization of the Coulomb-attenuated Becke three-parameter Lee-Yang-

Parr approximation gives reliable results for the electric field gradients of copper and gold for a series of compounds. The obtained results for the nuclear quadrupole moment of -0.208 b for ^{63}Cu and +0.526 b for ^{197}Au are in good agreement with experimental values of -0.220(15) and +0.547(16) b, respectively.

Finally, the parity violation energy difference in the chiral molecule bromochlorofluoromethane (CHFClBr) was investigated by coupled-cluster theory to provide benchmark results for future investigations in this field. It was shown that several common density-functionals do not give reliable parity violation energy differences, and post-Hartree-Fock methods are necessary to determine reliable values.

Apart from the methodological developments presented in this thesis, further developments on the proper treatment of QED effects including the variational treatment of the frequency dependent Breit interaction for molecules are required in the future. It would also be desirable to obtain the first-order density matrix at the coupled-cluster level to obtain analytical values for parity violation effects. Concerning more fundamental physics, future directions could include CP-violation in molecules and the variation of fundamental constants in space-time. As a final note, a variation of the fine-structure constant α in time would make relativistic effects an observable although we are living in a relativistic world.

Publications

Peer-reviewed publications co-authored by Christian Thierfelder during his Ph.D. studies.

1. **C. Thierfelder**, A. Hermann, P. Schwerdtfeger, W.G. Schmidt.
   Strongly bonded water monomers on the ice Ih basal plane:
   Density-functional calculations.
   Phys. Rev. B, 74:045422, 2006.
   Selected for *Virtual Journal of Nanoscale Science & Technology* 14(6), 2006.

2. P. Schwerdtfeger, **C. Thierfelder**
   Relativistic Quantum Chemistry: A Historical Overview
   In: *Trends and Perspectives in Modern Computational Science,*
   Lecture Series on Computer and Computational Sciences,
   eds. G. Maroulis, T. Simos, Volume 6
   Brill Academic Publishers, Leiden, The Netherlands, 2006.

3. E. Goll, H. Stoll, **C. Thierfelder**, P. Schwerdtfeger
   Improved dipole moments by combining short-range gradient-corrected density-functional theory with long-range wave-function methods.
   Phys. Rev. A, 76:032507, 2007.

4. **C. Thierfelder**, P. Schwerdtfeger, T. Saue
   ^{63}Cu and ^{197}Ag nuclear quadrupole moments from four-component relativistic density-functional calculations.
   Phys. Rev. A, 76:034502, 2007.

5. **C. Thierfelder**, W.G. Schmidt
Ethanol adsorbed on ice: A first-principles study
Phys. Rev. B, 76:195426, 2007.
Selected for *Virtual Journal of Biological Physics Research* 14(11), 2007.

6. C.R. Jacob, L. Visscher, **C. Thierfelder**, P. Schwerdtfeger
Nuclear quadrupole moment of ^{139}La from relativistic electronic structure calculations of the electric field gradients in LaF, LaCl, LaBr and LaI.
J. Chem. Phys., 127:204303, 2007.

7. **C. Thierfelder**, P. Schwerdtfeger, F.P. Heßberger, S. Hofmann
Dirac-Hartree-Fock Studies of X-ray Transitions in Meitnerium
Eur. Phys. J. A, 35:227 2008.

8. **C. Thierfelder**, B. Assadollahzadeh, P. Schwerdtfeger, S. Schäfer, R. Schäfer
Relativistic and electron correlation effects in static polarizabilities for the group 14 elements from Carbon to Element 114
Phys. Rev. A, 78:052506, 2008.

9. B. Assadollahzadeh, **C. Thierfelder**, P. Schwerdtfeger
From clusters to the solid state: Global minimum structures for Cesium clusters Cs_n ($n = 2...20, \infty$) and their electronic properties
Phys. Rev. B, 78:245423, 2008.
Selected for *Virtual Journal of Nanoscale Science & Technology* 19(2), 2009.

10. B. Lange, R. Posner, K. Pohl, **C. Thierfelder**, G. Grundmeier, S. Blankenburg W.G. Schmidt
Water adsorption on hydrogenated Si(111) surfaces
Surf. Sci., 603:60, 2009.

11. **C. Thierfelder**, P. Schwerdtfeger
The effect of relativity and electron correlation in static dipole polarizabilities of Ytterbium and Nobelium
Phys. Rev. A, 79:032512, 2009.

12. **C. Thierfelder**, P. Schwerdtfeger, A. Koers, A. Borshchevski, B. Fricke
Scalar relativistic and spin-orbit effects in closed-shell superheavy element monohydrides
Phys. Rev. A, 80:022501, 2009.

13. B. Vest, K. Klinkhammer, **C. Thierfelder**, M. Lein, P. Schwerdtfeger
Kinetic and thermodynamic stability of group 13 trihydrides
Inorg. Chem. 48:7953, 2009.

14. **C. Thierfelder**, S. Sanna, A. Schindlmayr, W.G. Schmidt
Do we know the band gap of lithium niobate?
Phys. Stat. Sol. C 362:7, 2010

15. **C. Thierfelder**, G. Rauhut, P. Schwerdtfeger
A Relativistic Coupled Cluster Study of the Parity Violation Energy Shift of CHFClBr
accepted in *Phys. Rev. A*

16. E. Pahl, D. Figgen, **C. Thierfelder**, Kirk A. Peterson, Florent Calvo, P. Schwerdtfeger
A highly accurate potential energy curve for the mercury dimer
accepted in *J. Chem. Phys.*

17. M. Witte, **C. Thierfelder**, S. Blankenburg, E. Rauls, W. G. Schmidt
Methane adsorption on graphene: Influence of dispersion interaction
accepted in *Phys. Rev. A*

18. **C. Thierfelder**, P. Schwerdtfeger
Quantum electrodynamic corrections for the valence shell in heavy many-electron atoms
in preparation

Appendix A

Optimized all-electron basis set for E119:

s-function

5.091668956E+07	1.347831724E+07	4.530740933E+06	1.665507863E+06
6.607847134E+05	2.737019912E+05	1.176557660E+05	5.164287912E+04
2.301056890E+04	1.037559421E+04	4.747374580E+03	2.215375000E+03
1.042165304E+03	5.123914361E+02	2.620383859E+02	1.371848955E+02
7.648605902E+01	3.542020946E+01	2.038134279E+01	1.032790533E+01
5.694991331E+00	2.546113509E+00	1.350338309E+00	5.051671669E-01
2.321115096E-01	7.180576917E-02	3.321066380E-02	1.658290237E-02

p-functions

5.031897077E+07	1.523337693E+07	4.903828414E+06	1.669357228E+06
5.929368615E+05	2.183325340E+05	8.307012207E+04	3.262132975E+04
1.324032464E+04	5.575565265E+03	2.444836914E+03	1.116155971E+03
5.291243799E+02	2.588492993E+02	1.305792752E+02	6.743056066E+01
3.421889384E+01	1.829221006E+01	9.067189643E+00	4.654906999E+00
2.078539763E+00	9.508184813E-01	3.680182730E-01	1.272904516E-01
1.658290237E-02			

d-functions

1.542441377E+05	3.866202542E+04	1.217614717E+04	4.461979426E+03
1.891395079E+03	8.774341485E+02	4.333455716E+02	2.238953375E+02
1.204406179E+02	6.666032461E+01	3.716339889E+01	2.118231734E+01
1.207024238E+01	6.655835950E+00	3.664465519E+00	1.996186902E+00
1.056798873E+00	3.396845605E-01	6.076462852E-01	6.204466083E-03

f-functions

4.120309094E+03	1.316576971E+03	5.358876458E+02	2.497599114E+02
1.271125591E+02	6.792952691E+01	3.672053657E+01	2.011846380E+01
1.091116838E+01	5.816823986E+00	2.993907297E+00	1.387176783E+00

g-functions

4.289594660E+00	1.966077054E+00	8.317942084E-01

Optimized all-electron basis set for E120:

s-function

5.162618437E+07	1.370909772E+07	4.644059340E+06	1.731442084E+06
7.007021263E+05	2.951775330E+05	1.271902118E+05	5.479045503E+04
2.358607440E+04	1.022285093E+04	4.500247349E+03	2.030244380E+03
9.277500091E+02	4.446344710E+02	2.215381115E+02	1.138341954E+02
5.928136973E+01	3.106605433E+01	1.651074746E+01	8.526138493E+00
4.310842507E+00	2.000679334E+00	9.045727573E-01	3.601002333E-01
1.364072274E-01	5.508453754E-02	2.374576348E-02	1.035348933E-02

p-function

4.407272658E+07	1.230100536E+07	3.730589360E+06	1.207666545E+06
4.110495924E+05	1.459007846E+05	5.379213794E+04	2.059076555E+04
8.205427711E+03	3.418125913E+03	1.490376017E+03	6.787826028E+02
3.207412860E+02	1.556393871E+02	7.777038082E+01	3.935273324E+01
2.018757553E+01	1.016391211E+01	4.972996091E+00	2.320541515E+00
1.014299392E+00	3.289355306E-01	1.007678935E-01	5.023479845E-02

d-function

5.479045503E+04	2.358607440E+04	1.022285093E+04	4.500247349E+03
2.030244380E+03	9.277500091E+02	4.446344710E+02	2.215381115E+02
1.138341954E+02	5.928136973E+01	3.106605433E+01	1.651074746E+01
8.526138493E+00	4.310842507E+00	2.000679334E+00	9.045727573E-01
3.601002333E-01	1.364076777E-01	5.509376426E-02	2.372309746E-02

g-function

3.418125913E+03	1.490376017E+03	6.787826028E+02	3.207412860E+02
1.556393871E+02	7.777038082E+01	3.935273324E+01	2.018757553E+01
1.016391211E+01	4.972996091E+00	2.320541515E+00	1.014299392E+00

h-function

4.972993223E+00	2.320545345E+00	8.563543110E-01

Bibliography

[1] P.M.A. Dirac. Quantum mechanics of many-electron systems. *Proc. R. Soc. Lond.*, A123:714, 1929.

[2] P. Pyykkö. Relativistic quantum chemistry. *Adv. Quantum Chem.*, 11:353, 1978.

[3] P. Pyykkö and J.P. Desclaux. Relativity and the periodic system of elements. *Acc. Chem. Res.*, 12:276, 1979.

[4] P. Pyykkö. Relativistic effects in structural chemistry. *Chem. Rev.*, 88:563, 1988.

[5] C.F. Fischer. Correlation and relativistic effects on transitions in lighter atoms. *Physica Scripta*, T83:49, 1999.

[6] M. Schädel. *The Chemistry of Superheavy elements.* Kluwer, 2003.

[7] L. Meitner and O.R. Frisch. Disintegration of uranium by neutrons: a new type of nuclear reaction. *Nature*, 143:239, 1939.

[8] H.L. Anderson, E.T. Booth, J.R. Dunning, E. Fermi, G.N. Glasoe, and F.G. Slack. The fission of uranium. *Phys. Rev.*, 55:511, 1939.

[9] E. McMillan and P.H. Abelson. Radioactive element 93. *Phys. Rev.*, 57:1185, 1940.

[10] G.T. Seaborg, E.M. Mcmillan, J.W. Kennedy, and A.C. Wahl. Radioactive element 94 from deuterons on uranium. *Phys. Rev.*, 69:366, 1946.

[11] Yu.Ts. Oganessian, V.K. Utyonkov, Yu.V. Lobanov, F. Sh. Abdullin, A. N. Polyakov, I. V. Shirokovsky, Yu. S. Tsyganov, G. G. Gulbekian, S. L. Bogomolov, B. N. Gikal, A. N. Mezentsev, S. Iliev, V. G. Subbotin, A. M.

Sukhov, O. V. Ivanov, G. V. Buklanov, K. Subotic, M. G. Itkis, K. J. Moody, J. F. Wild, N. J. Stoyer, M. A. Stoyer, and R. W. Lougheed. Synthesis of superheavy nuclei in the $^{48}Ca + ^{244}Pu$ reaction: $^{288}114$. *Phys. Rev. C*, 62(4):041604, Sep 2000.

[12] S. Hofmann and G. Münzenberg. The discovery of the heaviest elements. *Rev. Mod. Phys.*, 72:733, 2000.

[13] B. Odoma, D. Hanneke, B. D'Urso, and G. Gabrielse. New measurement of the electron magnetic moment using a one-electron quantum cyclotron. *Phys. Rev. Lett.*, 97:030801, 2006.

[14] K. Hagiwara, A.D. Martin, Daisuke Nomura, and T. Teubner. Improved predictions for g−2 of the muon and $\alpha_{QED}(M_z^2)$. *Phys.Lett. B*, 649:173, 2007.

[15] Z.-C. Yan, W. Nörtershäuser, and G.W.F. Drake. High precision atomic theory for Li and Be^+: QED shifts and isotope shifts. *Phys. Rev. Lett.*, 100:243002, 2008.

[16] J. Schwinger. Quantum electrodynamics I. A covariant formulation. *Phys. Rev.*, 74:1439, 1948.

[17] J. Schwinger. Quantum electrodynamics II. Vacuum polarization and self energy. *Phys. Rev.*, 75:651, 1949.

[18] J. Schwinger. Quantum electrodynamics III. The electromagnetic properties of the electronradiative corrections to scattering. *Phys. Rev.*, 76:790, 1949.

[19] N.M. Kroll and W.E. Lamb Jr. On the self-energy of a bound electron. *Phys. Rev.*, 75:388, 1949.

[20] M. Gell-Mann and F. Low. Bound states in quantum field theory. *Phys. Rev.*, 84:350, 1951.

[21] E. Salpeter and H. Bethe. A relativistic equation for bound-state problems. *Phys. Rev.*, 84:1232, 1951.

[22] M. Baranger, H. A. Bethe, and R. P. Feynman. Relativistic correction to the Lamb shift. *Phys. Rev.*, 92:482, 1953.

[23] G. E. Brown, J. S. Langer, and G. W. Schaefer. Lamb shift of a tightly bound electron. I. Method. *Proc. Roy. Soc. A*, 251:92, 1959.

[24] V.V. Flambaum and J.S.M. Ginges. Radiative potential and calculations of QED radiative corrections to energy levels and electromagnetic amplitudes in many-electron atoms. *Phys. Rev. A*, 72:052115, 2005.

[25] E. Novais, E. Miranda, A.H. Castro Neto, and G.G. Cabrera. Phase diagram of the anisotropic Kondo chain. *Phys. Rev. Lett.*, 88:217201, 2002.

[26] I.P. Grant and H.M. Quiney. Application of relativistic theories and electrodynamics to chemical problems. *Int. J. Quant. Chem.*, 80:283, 2000.

[27] W.H. Furry. On bound states and scattering in positron theory. *Phys. Rev.*, 81:115, 1951.

[28] H.F. Beyer, G. Menzel, D. Liesen, A. Callus, F. Bosch, R. Deslattes, P. Indelicate, Th. Stöhlker, O. Klepper, R. Moshammer, F. Nolden, H. Eickhoff, B. Franzke, and M. Steck. Measurement of the ground-state Lamb-shift of hydrogenlike uranium at the electron cooler of the ESR. *Z. Phys. D*, 35:169, 1995.

[29] E.A. Uehling. Polarization effects in the positron theory. *Phys. Rev.*, 48:55, 1935.

[30] W.E. Lamb and R.C. Retherford. Fine structure of the hydrogen atom by a microwave method. *Phys. Rev.*, 72:241, 1947.

[31] J. Erler and M.J. Ramsey-Musolf. Low energy tests of the weak interaction. *Prog. Part. Nucl. Phys.*, 54:351, 2005.

[32] F. Wilczek. In search of symmetry lost. *Nature*, 433:239, 2005.

[33] C.S. Wu, E Ambler, R.W. Hayward, D.D. Hoppes, and R.P. Hudson. Experimental test of parity conservation in beta decay. *Phys. Rev.*, 105:1413, 1957.

[34] T.D. Lee and C.N. Yang. Question of parity conservation in weak interactions. *Phys. Rev.*, 104:254, 1956.

[35] J.K. Laedahl, R. Wesendrup, and P. Schwerdtfeger. D- or L-alanine: That is the question. *Chem. Phys. Chem.*, 1:50, 2000.

[36] R. Berger and M. Quack. Electroweak quantum chemistry of alanine: Parity violation in gas and condensed phases. *Chem. Phys. Chem.*, 1:57, 2000.

[37] P. Cintas. Elementary asymmetry and biochirality: No longer twinned. *Chem. Phys. Chem.*, 2:409, 2001.

[38] F. Faglioni, A. Passalacqua, and P. Lazzaretti. Parity violation energy of biomolecules - I: Polypeptides. *Origins Life Evol. B*, 35:461, 2005.

[39] G. Lente. Stochastic analysis of the parity violating energy differences between enantiomersand its implications for the origin of biological chirality. *J. Phys. Chem. A*, 110:12711, 2006.

[40] A.S. Lahamer, S.M. Mahurin, R.N. Compton, D. House, J.K. Laerdahl, M. Lein, and P. Schwerdtfeger. Search for a parity-violating energy difference between enantiomers of a chiral iron complex. *Phys. Rev. Lett.*, 85:4470, 2000.

[41] A. Szabo-Nagy and L. Keszthelyi. Demonstration of the parity-violating energy difference between enantiomers. *Proc. Natl. Acad. Sci.*, 96:4252, 1999.

[42] Ch. Daussy, T. Marrel, A. Amy-Klein, C. T. Nguyen, Ch. J. Bordé, and Ch. Chardonnet. Limit on the parity nonconserving energy difference between the enantiomers of a chiral molecule by laser spectroscopy. *Phys. Rev. Lett.*, 83:1554, 1999.

[43] J. Crassous, F. Monier, J.-P. Dutasta, M. Ziskind, C. Daussy, C. Grain, and C. Chardonnet. Search for resolution of chiral fluorohalogenomethanes and parity violation effects at the molecular level. *Chem. Phys. Chem.*, 4:541, 2003.

[44] M. Quack and M. Willeke. Stereomutation tunneling switching dynamics and parity violation in chlorineperoxide Cl-O-O-Cl. *J. Phys. Chem. A*, 110:3338, 2006.

[45] R. Berger, M. Gottselig, M. Quack, and M. Willeke. Parity violation dominates the dynamics of chirality in dichlorodisulfane. *Angew. Chem. Int. Ed.*, 40:4195, 2001.

[46] P. Schwerdtfeger, T. Saue, J.N.P. van Stralen, and L. Visscher. Relativistic second-order many-body and density-functional theory for the parity-violation contribution to the C?F stretching mode in CHFClBr. *Phys. Rev. A*, 71:012103, 2005.

[47] M. Quack and J. Stohner. Influence of parity violating weak nuclear potentials on vibrational and rotational frequencies in chiral molecules. *Phys. Rev. Lett.*, 84:3807, 2000.

[48] J.K. Laedahl, P. Schwerdtfeger, and H.M. Quiney. Theoretical analysis of parity-violating energy differences between the enantiomers of chiral molecules. *Phys. Rev. Lett.*, 84:3811, 2000.

[49] V.S. Letokhov. On difference of energy levels of left and right molecules due to weak interactions. *Phys. Lett. A*, 53:275, 1975.

[50] P. Schwerdtfeger, J.K. Laerdahl, and C. Charonnet. Calculation of parity-violation effects for the C-F stretching mode of chiral methyl fluorides. *Phys. Rev. A*, 65:042508, 2002.

[51] R.G. Viglione, R. Zanasi, P. Lazzeretti, and A. Ligabue. Theoretical determination of parity-violating vibrational frequency differences between the enantiomers of the CHFClBr molecule. *Phys. Rev. A*, 62:052516, 2000.

[52] M. Ziskind, T. Marrel, C. Daussy, and C. Chardonnet. Improved sensitivity in the search for a parity-violating energy difference in the vibrational spectrum of the enantiomers of CHFClBr. *Eur. Phys. J. D*, 20:219, 2002.

[53] A.A. Fokin, P.R. Schreiner, R. Berger, G.H. Robinson, P. Wei, and C.F. Campana. Pseudotetrahedral polyhalocubanes: Synthesis, structures, and parity violating energy differences. *J. Am. Chem. Soc.*, 128:5332, 2006.

[54] B.Y. Zeldovich, D.B. Saakyan, and I.I. Sobelman. . *JETP Lett.*, 25:94, 1977.

[55] R.A. Harris and L. Stodolsky. Quantum beats in optical activity and weak interactions. *Phys. Lett. B*, 78:313, 1978.

[56] D.W. Rein, R.A. Hegstrom, and P.G.H. Sandars. Parity non-conserving energy difference between mirror image molecules. *Phys. Lett. A*, 71:499, 1979.

[57] J.K. Laerdahl and P. Schwerdtfeger. Fully relativistic ab initio calculations of the energies of chiral molecules including parity-violating weak interactions. *Phys. Rev. A*, 60:4439, 1999.

[58] R. Bast and P. Schwerdtfeger. Parity-violation effects in the C-F stretching mode of heavy-atom methyl fluorides. *Phys. Rev. Lett.*, 91:023001, 2003.

[59] P. Schwerdtfeger, J. Gierlich, and T. Bollwein. Large parity-violation effects in heavy-metal-containing chiral compounds. *Angew. Chem. Int. Ed.*, 42:1293, 2003.

[60] P. Schwerdtfeger and R. Bast. Large parity violation effects in the vibrational spectrum of organometallic compounds. *J. Am. Chem. Soc.*, 126:1652, 2004.

[61] F. Faglioni and P. Lazzeretti. Parity-violation effect on vibrational spectra. *Phys. Rev. A*, 67:32101, 2003.

[62] A. Szabo and N.S. Ostlund. *Modern Quantum Chemistry*. McGraw-Hill, 1989.

[63] T. Helgaker, P. Jorgensen, and J. Olsen. *Molecular Electronic Structure Theory*. Wiley, 2000.

[64] P. Schwerdtfeger (Editor). *Relativistic Electronic Structure Theory*. Elsevier Science, 2004.

[65] K.G. Dyall and Jr. K. Faegri. *Introduction to Relativistic Quantum Chemistry*. Oxford, 2007.

[66] I.P. Grant. *Relativistic Quantum Theory of Atoms and Molecules*. Springer, 2006.

[67] M. Reiher and A. Wolf. *Relativistic Quantum Chemistry: The Fundamental Theory of Molecular Science*. Wiley-VCH, 2009.

[68] B. Swirles. The relativistic self-consistent field. *Proc. Roy. Soc. Lond.*, A152:625, 1935.

[69] C. Collins, K.G. Dyall, and H.F. Schaefer III. Relativistic and correlation effects in CuH, AgH, and AuH: Comparison of various relativistic methods. *J. Chem. Phys.*, 102:2024, 1995.

[70] A relativistic ab initio electronic structure program, release 3.1, written by T. Saue, T. Enevoldsen, T. Helgaker, H.J.Aa. Jensen, J.K. Laerdahl, K. Ruud, J. Thyssen and L. Visscher. see `http://dirac.chem.sdu.dk`; T. Saue, K. Fægri, Jr., T. Helgaker, and O. Gropen. *Mol. Phys.*, 91:937, 1997.

[71] R.E. Stanton and S. Havriliak. Kinetic balance: A partial solution to the problem of variational safety in Dirac calculations. *J. Chem. Phys.*, 81:1910, 1984.

[72] J. Cizek. On the correlation problem in atomic and molecular systems. calculation of wavefunction components in ursell-type expansion using quantum-field theoretical methods. *J. Chem. Phys.*, 45:4256, 1966.

[73] J. Cizek. On the use of the cluster expansion and the technique of diagrams in calculations of correlation effects in atoms and molecules. *Adv. Chem. Phys.*, 14:35, 1969.

[74] J. Cizek and J. Paldus. Correlation problems in atomic and molecular systems. iii. rederivation of the coupled-pair many-electron theory using the traditional quantum chemical methods. *Int. J. Quantum Chem.*, 5:359, 1971.

[75] R.J. Bartlett and M. Musia. Coupled-cluster theory in quantum chemistry. *Rev. Mod. Phys.*, 79:291, 2007.

[76] L. Visscher, K.G. Dyall, and T.J. Lee. Kramers restricted closed-shell CCSD theory. *Int. J. Quantum Chem. Symp.*, 29:411, 1995.

[77] P. Hohenberg and W. Kohn. Inhomogeneous electron gas. *Phys. Rev.*, 136:B864, 1964.

[78] M. Holthausen W. Koch. *A Chemist's Guide to Density Functional Theory.* Wiley, 2001.

[79] A.K. Rajagopal and J. Callaway. Inhomogeneous electron gas. *Phys. Rev. B*, 7:1912, 1973.

[80] A.K. Rajagopal. Inhomogeneous relativistic electron gas. *J. Phys. C*, 11:L943, 1978.

[81] A.H. Macdonald and S.H. Vosko. A relativistic density functional formalism. *J. Phys. C*, 12:2977, 1979.

[82] M. Mayer, O.D. Häberlen, and N. Rösch. Relevance of relativistic exchange-correlation functionals and of finite nuclei in molecular density-functional calculations. *Phys. Rev. A*, 54:4775, 1996.

[83] S. Varga, E. Engel, W.D. Sepp, and B. Fricke. Systematic study of the Ib diatomic molecules Cu_2, Ag_2, and Au_2 using advanced relativistic density functionals. *Phys. Rev. A*, 59:4288, 1999.

[84] S. Varga, B. Fricke, H. Nakamatsu, T. Mukoyama, J. Anton, D. Geschke, A. Heitmann, and E. Engel und T. Bastug. Four-component relativistic density functional calculations of heavy diatomic molecules. *J. Chem. Phys.*, 112:3499, 2000.

[85] P.J. Mohr, G. Plunien, and G. Soff. QED corrections in heavy atoms. *Phys. Rep.*, 293:227, 1998.

[86] W.R. Johnson and G. Soff. Dirac-Fock using different nuclear charge distributions. *At. Data Nucl. Data Tabl.*, 33:405, 1985.

[87] I. Lindgren, H. Persson, S. Salomonson, V. Karasiev, L. Labzowsky, A. Mitrushenkov, and M. Tokman. Second-order QED corrections for few-electron heavy ions: reducible Breit-Coulomb correction and mixed self-energy-vacuum polarization correction. *J. Phys. B*, 26:L503, 1993.

[88] H. Persson, I. Lindgren, S. Salomonson, and P. Sunnergren. Accurate vacuum-polarization calculations. *Phys. Rev. A*, 48:2772, 1993.

[89] H. Persson, I. Lindgren, S. Salomonson, and P. Sunnergren. A new approach to the electron self energy calculation. *Phys. Scr. T*, 46:125, 1993.

[90] J. Schweppe, A. Belkacem, L. Blumenfield, N. Claytor, B. Feinberg, H. Goulda, V.E. Koster, L. Levy, S. Misawa, J.R. Mowat, and M.H. Prior. Measurement of the Lamb shift in lithiumlike uranium (U^{89+}). *Phys. Rev. Lett.*, 66:1434, 1991.

[91] G. Gabrielse, D. Hanneke, T. Kinoshita, M. Nio, and B. Odom. New determination of the fine structure constant from the electron g value and QED. *Phys. Rev. Lett.*, 97:030802, 2006.

[92] S. Laporta. Analytical value of some sixth-order graphs to the electron g-2 in QED. *Phys. Rev. D*, 47:4793, 1993.

[93] T. Aoyama, M. Hayakawa, T. Kinoshita, and M. Nio. Revised value of the eighth-order QED contribution to the anomalous magnetic moment of the electron. *Phys. Rev. D*, 77:053012, 2008.

[94] U. Kaldor, E. Eliav, , and A. Landau. *in Theoretical Chemistry and Physics of Heavy and Superheavy Elements, (ed. U. Kaldor and S. Wilson)*. Kluwer Academic Publishers, 2003.

[95] U. Kaldor, E. Eliav, , and A. Landau. *in Recent Advances in Relativistic Molecular Theory, (ed. K. Hirao and Y. Ishikawa*. World Scientific, 2004.

[96] G. Breit. The effect of retardation on the interaction of two electrons. *Phys. Rev.*, 34:553, 1929.

[97] H.A. Bethe. The electromagnetic shift of energy levels. *Phys. Rev.*, 72:339, 1947.

[98] P. Pyykkö, M. Tokman, and L.N. Labzowsky. Estimated valence-level Lamb shifts for group 1 and group 11 metal atoms. *Phys. Rev. A*, 57:R689, 1998.

[99] L.N. Labzowsky, I. Goidenko, M. Tokman, and P. Pyykkö. Calculated self-energy contributions for an ns valence electron using the multiple-commutator method. *Phys. Rev. A*, 59:2707, 1999.

[100] E. M. Lifschitz L. D. Landau. *Quantenelektrodynamik*. Akademie Verlag Berlin, 1989.

[101] N.N. Bogoljubov and D.W. Sirkov. *Quantenfelder*. VEB Deutscher Verlag der Wissenschaften, 1984.

[102] P.J. Mohr. Self-energy correction to one-electron energy levels in a strong Coulomb field. *Phys. Rev. A*, 46:4421, 1992.

[103] P.J. Mohr and Y.K. Kim. Self-energy of excited states in a strong Coulomb field. *Phys. Rev. A*, 45:2727, 1992.

[104] K.G. Dyall, I.P. Grant, C.T. Johnson, F.A. Parpia, and E.P. Plummer. GRASP: A general-purpose relativistic atomic structure program. *Comput. Phys. Commun.*, 55:425, 1989.

[105] C.C. Lu, T.A. Carlson, F.B. Malik, T.C. Tucker, and C.W. Nestor. Relativistic Hartree-Fock-Slater eigenvalues, radial expectation values, and potentials for atoms, $2 \leq Z \leq 126$. *At. Data Nucl. Data Tables*, 3:1, 1968.

[106] D. Andrae. Finite nuclear charge density distributions in electronic structure calculations for atoms and molecules. *Phys. Rep.*, 336:413, 2000.

[107] M. Eides, H. Grotch, and V.A. Shelyuto. Theory of light hydrogenlike atoms. *Phys. Rep.*, 342:63, 2001.

[108] G. Breit. The fine structure of He as a test of the spin interactions of two electrons. *Phys. Rev.*, 36:383, 1930.

[109] G. Breit. Dirac's equation and the spin-spin interactions of two electrons. *Phys. Rev.*, 39:616, 1932.

[110] E.H. Wichmann and N.M. Kroll. Vacuum polarization in a strong Coulomb field. *Phys. Rev.*, 101:843, 1956.

[111] G. Källen and A. Sabry. . *Mat. Fys. Medd. Dan. Vid. Selsk.*, 29:17, 1955.

[112] P.J. Mohr. Self-energy radiative corrections in hydrogen-like systems. *Ann. Phys. (NY)*, 88:26, 1974.

[113] P.J. Mohr. Numerical evaluation of the 1 $S_{1/2}$-state radiative level shift. *Ann. Phys. (NY)*, 88:52, 1974.

[114] L. Labzowsky, I. Goidenko, M Tokman, and P Pyykkö. Calculated self-energy contributions for an ns valence electron using the multiple-commutator method. *Phys. Rev. A*, 59:2707, 1999.

[115] E. Eliav, U. Kaldor, P. Schwerdtfeger, B. Hess, and Y. Ishikawa. Ground state electron configuration of element 111. *Phys. Rev. Lett*, 73:3203, 1994.

[116] P. Indelicato, J. P. Santos, S. Boucard, and J.-P. Desclaux. QED and relativistic corrections in superheavy elements. *Eur. Phys. J. D*, 45:155, 2007.

[117] P. Indelicato, O. Gorveix, and J. P. Desclaux. Multiconfigurational Dirac-Fock studies of two-electron ions. II. Radiative corrections and comparison with experiment. *J. Phys. B: At. Mol. Opt. Phys.*, 20:651, 1987.

[118] B. Ravaine A. Derevianko and W. R. Johnson. Relaxation effect and radiative corrections in many-electron atoms. *Phys. Rev. A*, 69:054502, 2004.

[119] E. Lindroth, A.-M. Mårtensson-Pendrill, A. Ynnerman, and Per Öster. Self-consistent treatment of the Breit interaction, with application to the electric dipole moment in thallium. *J. Phys. B: At. Mol. Opt. Phys.*, 22:2447, 1989.

[120] Y.-K. Kim. Relativistic self-consistent-field theory for closed-shell atoms. *Phys. Rev.*, 154:17, 1967.

[121] T. Kagawa. Relativistic Hartree-Fock-Roothaan theory for open-shell atoms. *Phys. Rev. A*, 12:2245, 1980.

[122] H. Quiney, I.P. Grant, and S. Wilson. The Dirac equation in the algebraic approximation. V. self-consistent studies of the Breit interaction. *J. Phys. B*, 20:1413, 1987.

[123] I.P. Grant. Relativistic self-consistent fields. *Proc. R. Soc. A*, 262:555, 1961.

[124] Y. Ishikawa, H.M. Quiney, and G. L. Malli. Dirac-Fock-Breit self-consistent-field method: Gaussian basis-set calculations on many-electron atoms. *Phys. Rev. A*, 43:3270, 1991.

[125] T. A. Koopmans. Über die Zuordnung von Wellenfunktionen und Eigenwerten zu den einzelnen Elektronen eines Atoms. *Physica*, 1:104, 1933.

[126] M. Pernpointner. The effect of the Gaunt interaction on the electric field gradient. *J. Phys. B: At. Mol. Phys.*, 35:383, 2002.

[127] M. Pernpointner. The effect of the Gaunt interaction on the molecular ionization spectra of CO, H_2S and TlH. *J. Phys. B: At. Mol. Phys.*, 38:1955, 2005.

[128] E. Eliav, U. Kaldor, and Y. Ishikawa. Spin dynamics of a model singlet ground-state system. *Phys. Rev. Lett.*, 49:1724, 1994.

[129] C.E. Moore. *Atomic Energy Levels.* Natl. Bur. Stand. Ref. Data Ser., Nat. Bur. Stand. (U.S.) Circ. No. NSRDS-NBS 35 (U.S. GPO, Washington, D.C., 1971.

[130] A. Ghiorso, S.G. Thompson, G.H. Higgins, G.T. Seaborg, M.H. Studier, P.R. Fields, S.M. Fried, H. Diamond, J.F. Mech, G.L. Pyle, J.R. Huizenga, A. Hirsch, W.M. Manning, C.I. Browne, H.L. Smith, and R.W. Spence. New elements Einsteinium and Fermium, atomic numbers 99 and 100. *Phys. Rev.*, 99:1048, 1955.

[131] S. Hofmann, V. Ninov, F.P. Heßberger, P. Armbruster, H. Folger, G. Münzenberg, H.J. Schött, A.G. Popeko, A.V. Yeremin, S. Saro, R. Janik, and M. Leino. The new element 112. *Z. Phys. A*, 354:229, 1996.

[132] S. Hofmann, F.P. Heßberger, D. Ackermann, G. Münzenberg, S. Antalic, P. Cagarda, B. Kindler, J. Ko jouharova, M. Leino, B. Lommel, R. Mann, A. G. Popeko, S. Reshitko, S. Saro, J. Uusitalo, and A. V. Yeremin. New results on elements 111 and 112. *Eur. Phys. J. A*, 14:147, 2002.

[133] S. Hofmann. New elements - approaching Z=114. *Rep. Prog. Phys.*, 61:639, 1998.

[134] C. Samanta, P.R. Chowdhurya, and D.N. Basu. Predictions of alpha decay half lives of heavy and superheavy elements. *Nucl. Phys. A*, 789:142, 2007.

[135] P.R. Chowdhurya, C. Samanta, and D.N. Basu. Search for long lived heaviest nuclei beyond the valley of stability. *Phys. Rev. C*, 77:044603, 2008.

[136] C. Rauth, D. Ackermann, K. Blaum, M. Block, A. Chaudhuri, S. Eliseev Z. Di, R. Ferrer, D. Habs, F. Herfurth, F.P. Heßberger, S. Hofmann, H.-J. Kluge, G. Maero, A. Martin, G. Marx, M. Mukherjee, J.B. Neumayr, W.R. Plaß, S. Rahaman, D. Rodriguez, C. Scheidenberger, L. Schweikhard, P.G. Thirolf, G. Vorobjev, and C. Weber. First Penning trap mass measurements beyond the proton drip line. *Phys. Rev. Lett.*, 100:012501, 2008.

[137] J.V. Kratz. *Chemsitry of Transactinides Handbook of Nuclear Chemsitry, Vol. 2, pp. 323-395.* Kluwer Academic Publishers, 2003.

[138] T.A. Carlson and Jr. C.W. Nestor. Calculation of K and L X-rays for elements of Z = 95 to 130. *At. Data Nucl. Data Tables*, 19:153, 1977.

[139] N. Gaston, P. Schwerdtfeger, and W. Nazarewicz. Ionization potentials of internal conversion electrons for the superheavy elements 112, 114, 116, and 118. *Phys. Rev. A*, 66:062505, 2002.

[140] I. Goidenko, I. Tupitsyn, and G. Plunien. QED corrections and the chemical properties of Eka-Hg. *Eur. Phys. J. D*, 45:171, 2007.

[141] R. Hofstadter. Nuclear and nucleon scattering of high-energy electrons. *Ann. Rev. Nucl. Sci.*, 7:231, 1957.

[142] K. T. Cheng, W. R. Johnson, and J. Sapirstein. Lamb-shift calculations for non-Coulomb potentials. *Phys. Rev. A*, 47:1817, 1993.

[143] D.R. Lide (ed). *CRC Handbook of Chemistry and Physics (63rd edition).* CRC press, 1983.

[144] Y. Watanabe and H. Tatewaki. Correlation energies for He isoelectronic sequence with Z=2-116 from four-component relativistic configuration interactions. *J. Chem. Phys.*, 123:074322, 2005.

[145] F.P. Heßberger, S. Hofmann, D. Ackermann, S. Antalic, B. Kindler, I. Kojouharov, P. Kuusiniemi, M. Leino, B. Lommel, R. Mann, K. Nishio, A.G. Popeko, B. Sulignano, S. Saro, B. Streicher, M. Venhart, and A.V. Yeremin.

Alpha-gamma decay studies of ^{255}Rf, ^{251}No and ^{247}Fm. *Eur. Phys. J.*, A30:561, 2006.

[146] K.D. Bonin and V.V. Kresin. *Electric-Dipole Polarizabilities of Atoms, Molecules and Clusters*. World Scientific, 1997.

[147] J. M. Amini and H. Gould. High precision measurement of the static dipole polarizability of cesium. *Phys. Rev. Lett.*, 91:153001, 2003.

[148] W. de Heer, P. Milani, and A. Châtelain. Nonjellium-to-jellium transition in aluminum cluster polarizabilities. *Phys. Rev. Lett.*, 63:2834, 1989.

[149] M. Broyer, R. Antoine, I. Compagnon, D. Rayane, and P. Dugourd. From clusters to biomolecules: electric dipole, structure and dynamics. *Phys. Scr.*, 76:C135, 2007.

[150] S. Schäfer, M. Mehring, R. Schäfer, and P. Schwerdtfeger. Polarizabilities of Ba and Ba_2: Comparison of molecular beam experiments with relativistic quantum chemistry. *Phys. Rev. A*, 76:052515, 2007.

[151] C.R. Ekstrom, J. Schmiedmayer, M. S. Chapman, T. R. Hammond, and D. E. Pritchard. Measurement of the electric polarizability of sodium with an atom interferometer. *Phys. Rev. A*, 51:3883, 1995.

[152] I.S. Lim, M. Pernpointner, M. Seth, J.K. Laerdahl, P. Schwerdtfeger, P. Neogrady, and M. Urban. Relativistic coupled-cluster static dipole polarizabilities of the alkali metals from Li to element 119. *Phys. Rev. A*, 60:2822, 1999.

[153] I.S. Lim and P. Schwerdtfeger. Four-component and scalar relativistic Douglas-Kroll calculations for static dipole polarizabilities of the alkaline-earth-metal elements and their ions from Ca^n to Ra^n ($n = 0, +1, +2$). *Phys. Rev. A*, 70:062501, 2004.

[154] P. Schwerdtfeger. *in Computational Aspects of Electric Polarizability Calculations: Atoms, Molecules and Clusters, ed. G. Maroulis*. IOS Press, 2006.

[155] T. Fleig and A. Sadlej. Electric dipole polarizabilities of the halogen atoms in $^2P_{1/2}$ and $^2P_{3/2}$ states: Scalar relativistic and two-component configuration-interaction calculations. *Phys. Rev. A*, 65:032506, 2002.

[156] D.R. Lide (ed). *CRC Handbook of Chemistry and Physics (82rd edition)*. CRC press, 2002.

[157] T. Fleig. Spin-orbit-resolved static polarizabilities of group-13 atoms: Four-component relativistic configuration interaction and coupled-cluster calculations. *Phys. Rev. A*, 72:052506, 2005.

[158] V. Pershina, A. Borschevsky, and E. Eliavand U. Kaldor. Prediction of the adsorption behavior of elements 112 and 114 on inert surfaces from ab initio Dirac-Coulomb atomic calculations. *J. Chem. Phys.*, 128:024707, 2008.

[159] A.J. Sadlej, M. Urban, and O. Gropen. Relativistic and electron-correlation contributions to the dipole polarizability of the alkaline-earth-metal atoms Ca, Sr, and Ba. *Phys. Rev. A*, 44:5547, 1991.

[160] J.P. Desclaux, L. Laaksonen, and P. Pyykkö. Finite-difference Dirac-Fock. Calculations of electric dipole polarizabilities for $(ns)^1$ and $(ns)^2$ atoms. *J. Phys. B*, 14:419, 1981.

[161] L.T. Sin Fai Lam. Relativistic effects in static dipole polarisabilities. *J. Phys. B*, 37:3543, 1981.

[162] M. Seth, P. Schwerdtfeger, and M. Dolg. The chemistry of superheavy elements I. pseudopotentials for 111 and 112 and relativistic coupled-cluster calculations for $(112)H^+$, $(112)F_2$, and $(112)F_4$. *J. Chem. Phys.*, 106:3623, 1997.

[163] T.M. Miller and B. Bederson. Atomic and molecular polarizabilities. A review of recent advances. *Adv. At. Mol. Phys.*, 13:1, 1977.

[164] T.M. Miller and B. Bederson. Electric dipole polarizability measurements. *Adv. At. Mol. Phys.*, 25:37, 1988.

[165] S. Schäfer, S. Heiles, J. A. Becker, and R. Schäfer. Electric deflection studies on lead clusters. *J. Chem. Phys.*, 129:044304, 2008.

[166] M.J. Frisch, G.W. Trucks, H.B. Schlegel, G. E. Scuseria, M.A. Robb, J.R. Cheeseman, J. A. Montgomery Jr., T. Vreven, K. N. Kudin, J.C. Burant, J.M. Millam, S. S. Iyengar, J. Tomasi, V. Barone, B. Mennucci, M. Cossi,

G. Scalmani, N. Rega, G. A. Petersson, H. Nakatsuji, M. Hada, M. Ehara, K. Toyota, R. Fukuda, J. Hasegawa, M. Ishida, T. Nakajima, Y. Honda, O. Kitao, H. Nakai, M. Klene, X. Li, J. E. Knox, H. P. Hratchian, J.B. Cross, V. Bakken, C. Adamo, J. Jaramillo, R. Gomperts, R. E. Stratmann, O. Yazyev, A. J. Austin, R. Cammi, C. Pomelli, J. W. Ochterski, P. Y. Ayala, K. Morokuma, G. A. Voth, P. Salvador, J. J. Dannenberg, V. G. Zakrzewski, S. Dapprich, A.D. Daniels, M. C. Strain, O. Farkas, D. K. Malick, A. D. Rabuck, K. Raghavachari, J.B. Foresman, J. V. Ortiz, Q. Cui, A. G. Baboul, S. Clifford, J. Cioslowski, B.B. Stefanov, G. Liu, A. Liashenko, P. Piskorz, I. Komaromi, R.L. Martin, D.J. Fox, T. Keith, M. A. Al-Laham, C. Y. Peng, A. Nanayakkara, M. Challacombe, P.M.W. Gill, B. Johnson, W. Chen, M.W. Wong, C. Gonzalez, and J.A. Pople. *Program Gaussian 03*, revision c.03. *Gaussian, Inc., Wallingford, CT*, 2004.

[167] M. Douglas and N.M. Kroll. Quantum electrodynamical corrections to the fine structure of helium. *Ann. Phys. (N.Y.)*, 82:89, 1974.

[168] B.A. Hess. Relativistic electronic-structure calculations employing a two-component no-pair formalism with external-field projection operators. *Phys. Rev. A*, 33:3742, 1986.

[169] A. Wolf, M. Reiher, and B.A. Hess. *in Relativistic Electronic Structure Theory, Part 1: Fundamentals,*. edited by *P. Schwerdtfeger*. Elsevier Science, 2002.

[170] S.H. Vosko, L. Wilk, and M. Nusair. Accurate spin-dependent electron liquid correlation energies for local spin density calculations: a critical analysis. *Can. J. Phys.*, 58:1200, 1980.

[171] J.P. Perdew, K. Burke, and M. Ernzerhof. Generalized gradient approximation made simple. *Phys. Rev. Lett.*, 77:3865, 1996.

[172] C. Lee, W. Yang, and R.G. Parr. Development of the colle-salvetti correlation-energy formula into a functional of the electron density. *Phys. Rev. B*, 37:785, 1988.

[173] A.D. Becke. Density-functional thermochemistry III. The role of exact exchange. *J. Chem. Phys.*, 98:5648, 1993.

[174] A.D. Becke. Exploring the limits of gradient corrections in density functional theory. *J. Comput. Chem.*, 20:63, 1999.

[175] D.E. Woon and Jr. T.H. Dunning. Accurate correlation consistent basis sets for molecular core-valence correlation effects. the second row atoms Al - Ar, and the first row atoms B - Ne revisted. *J. Chem. Phys.*, 103:4572, 1993.

[176] K.A. Peterson and Jr. T.H. Dunning. Gaussian basis sets for use in correlated molecular calculations V. Core-valence basis sets for Boron through Neon. *J. Chem. Phys.*, 117:10548, 2002.

[177] J. Koput and K.A. Peterson. The ab initio potential energy surface and vibrational-rotational energy levels of $X^2\Sigma^+$ CaOH. *J. Phys. Chem. A*, 106:9595, 2002.

[178] K.G. Dyall. Relativistic quadruple-zeta and revised triple-zeta and double-zeta basis sets for the 4p, 5p, and 6p elements. *Theor. Chem. Acc.*, 115:441, 2006.

[179] K. Faegri. Relativistic gaussian basis sets for the elements K - Uuo. *Theor. Chem. Acc.*, 105:252, 2001.

[180] C. Møller. Über den Stoß zweier Teilchen unter Berücksichtigung der Retardation der Kräfte. *Z. Phys.*, 70:786, 1931.

[181] J.P. Perdew and L. A. Cole. On the local density approximation for Breit interaction. *J. Phys. C*, 15:L905, 1982.

[182] T.M. Miller H.L. Schwartz and B. Bederson. Measurement of the static electric dipole polarizabilities of Barium and Strontium. *Phys. Rev. A*, 10:1924, 1974.

[183] A.K. Das and A.J. Thakkar. Static response properties of second-period atoms: Coupled-cluster calculations. *J. Phys. B*, 31:2215, 1998.

[184] C. Lupinetti and A. J. Thakkar. Polarizabilities of the alkali anions: Li^- to Fr^-. *J. Chem. Phys.*, 122:044301, 2005.

[185] J. Stiehler and J. Hinze. Calculation of static polarizabilities and hyperpolarizabilities for the atoms He through Kr with a numerical RHF method. *J. Phys. B*, 28:4055, 1995.

[186] M.J. Stott and E. Zaremba. Linear-response theory within the density-functional formalism: Application to atomic polarizabilities. *Phys. Rev. A*, 21:12, 1980.

[187] D. Gugan and G.W. Michel. Improved dipole moments by combining short-range gradient-corrected density-functional theory with long-range wave-function methods. *Phys. Rev. A*, 76:032507, 2007.

[188] S. Hofmann, V. Ninov, F.P. Heßberger, P. Armbruster, H. Folger, G. Münzenberger, H. J. Schött, A. G. Popeko, A. V. Yeremin, A. N. Andreyev, S. Śaro, R. Janik, and M. Leino. The new element 111. *Z. Phys. A*, 350:281, 1995.

[189] Yu. Ts. Oganessian, V. K. Utyonkov, Yu. V. Lobanov, F. Sh. Abdullin, A. N. Polyakov, I. V. Shirokovsky, Yu. S. Tsyganov, G. G. Gulbekian, S. L. Bogomolov, B. N. Gikal, A. N. Mezentsev, S. Iliev, V. G. Subbotin, A. M. Sukhov, O. V. Ivanov, G. V. Buklanov, K. Subotic, M. G. Itkis, K. J. Moody, J. F. Wild, N. J. Stoyer, M. A. Stoyer, R. W. Lougheed, C. A. Laue, Ye. A. Karelin, and A. N. Tatarinov. Observation of the decay of $^{292}116$. *Phys. Rev. C*, 63:011301, 2000.

[190] Yu. Ts. Oganessian, V. K. Utyonkoy, Yu. V. Lobanov, F. Sh. Abdullin, A. N. Polyakov, I. V. Shirokovsky, Yu. S. Tsyganov, G. G. Gulbekian, S. L. Bogomolov, A. N. Mezentsev, S. Iliev, V. G. Subbotin, A. M. Sukhov, A. A. Voinov, G. V. Buklanov, K. Subotic, V. I. Zagrebaev, M. G. Itkis, J. B. Patin, K. J. Moody, J. F. Wild, M. A. Stoyer, N. J. Stoyer, D. A. Shaughnessy, J. M. Kenneally, and R. W. Lougheed. Experiments on the synthesis of element 115 in the reaction ^{243}Am(^{48}Ca,xn)$^{291-x}115$. *Phys. Rev. C*, 69:021601, 2004.

[191] Yu. Ts. Oganessian, V. K. Utyonkov, Yu. V. Lobanov, F. Sh. Abdullin, A. N. Polyakov, I. V. Shirokovsky, Yu. S. Tsyganov, G. G. Gulbekian, S. L. Bogomolov, B. N. Gikal, A. N. Mezentsev, S. Iliev, V. G. Subbotin, A. M. Sukhov, A. A. Voinov, G. V. Buklanov, K. Subotic, V. I. Zagrebaev, M. G.

Itkis, J. B. Patin, K. J. Moody nad J. F. Wild, M. A. Stoyer, N. J. Stoyer, D. A. Shaughnessy, J. M. Kenneally, P. A. Wilk, R. W. Lougheed, R. I. Ilkaev, , and S. P. Vesnovskii. Measurements of cross sections and decay properties of the isotopes of elements 112, 114, and 116 produced in the fusion reactions ^{233,238}U, ^{242}Pu, and ^{248}Cm + ^{48}Ca. *Phys. Rev. C*, 70:064609, 2004.

[192] Yu. Ts. Oganessian, V. K. Utyonkov, Yu. V. Lobanov, F. Sh. Abdullin, A. N. Polyakov, I. V. Shirokovsky, Yu. S. Tsyganov, G. G. Gulbekian, S. L. Bogomolov, B. N. Gikal, A. N. Mezentsev, S. Iliev, V. G. Subbotin, A. M. Sukhov, A. A. Voinov, G. V. Buklanov, K. Subotic, V. I. Zagrebaev, M. G. Itkis, J. B. Patin, K. J. Moody, J. F. Wild, M. A. Stoyer, N. J. Stoyer, D. A. Shaughnessy, J. M. Kenneally, and R. W. Lougheed. Measurements of cross sections for the fusion-evaporation reactions ^{244}Pu(^{48}Ca,xn)$^{292-x}$114 and ^{245}Cm(^{48}Ca,xn)$^{293-x}$116. *Phys. Rev. C*, 69:054607, 2004.

[193] Yu. Ts. Oganessian, V. K. Utyonkov, Yu. V. Lobanov, F. Sh. Abdullin, A. N. Polyakov, R. N. Sagaidak, I. V. Shirokovsky, Yu. S. Tsyganov, A. A. Voinov, G. G. Gulbekian, S. L. Bogomolov, B. N. Gikal, A. N. Mezentsev, S. Iliev, V. G. Subbotin, A. M. Sukhov, K. Subotic, V. I. Zagrebaev, G. K. Vostokin, , M. G. Itkis, K. J. Moody, J. B. Patin, D. A. Shaughnessy, M. A. Stoyer, N. J. Stoyer, P. A. Wilk, J. M. Kenneally, J. H. Landrum, J. F. Wild, and R. W. Lougheed. Synthesis of the isotopes of elements 118 and 116 in the ^{249}Cf and ^{245}Cm + ^{48}Ca fusion reactions. *Phys. Rev. C*, 74:044602, 2006.

[194] P. R. Chowdhury, C. Samanta, and D. N. Basu. Nuclear half-lives for α-radioactivity of elements with $100 \leq Z \leq 130$. *At. Data Nucl. Data Tables*, 94:781, 2008.

[195] A. T. Kruppa, M. Bender, W. Nazarewicz, P.-G. Reinhard, T. Vertse, and S. Ćwiok. Shell corrections of superheavy nuclei in self-consistent calculations. *Phys. Rev. C*, 61:034313, 2000.

[196] M. Schädel. Chemistry of superheavy elements. *Angew. Chem. Int. Ed.*, 45:368, 2006.

[197] Ch. E. Düllmann, W. Brüchle, R. Dressler, K. Eberhardt, B. Eichler, R. Eichler, H. W. Gäggeler, T. N. Ginter, F. Glaus, K. E. Gregorich, D. C. Hoffman, E. Jäger, D. T. Jost, U. W. Kirbach, D. M. Leek, H. Nitsche, J. B. Patin, V. Pershina, D. Piguet, Z. Qin, M. Schädel, B. Schausten, E. Schimpf, H.-J. Schött, S. Soverna, R. Sudowe, P. Thörle, S. N. Timokhin, N. Trautmann, A. Türler, A. Vahle, G. Wirth, A. B. Yakushev, and P. M. Zielinski. Chemical investigation of Hassium (element 108). *Nature*, 418:859, 2002.

[198] R. Eichler, W. Brüchle, R. Buda, S. Bürger, R. Dressler, Ch. E. Düllmann, J. Dvorak, K. Eberhardt, B. Eichler, C.M.Folden III, H. W. Gäggeler, K. E. Gregorich, F. Haenssler, D. C. Hoffman, H. Hummrich, E. Jäger, J. V. Kratz, B. Kuczewski, D. Liebe, D. Nayak, H. Nitsche, D. Piguet, Z. Qin, U. Rieth, M. Schädel, B. Schausten, E. Schimpf, A. Semchenkov, S. Soverna, R. Sudowe, N. Trautmann, P. Thörle, A. Türler, B. Wierczinski, N. Wiehl, P.A. Wilk, G. Wirth, A. B. Yakushev, and A. von Zweidorf. Attempts to chemically investigate element 112. *Radiochim. Acta*, 94:181, 2006.

[199] R. Eichler, N.V. Aksenov, A.V. Belozerov, G.A. Bozhikov, V.I. Chepigin, R. Dressler, S.N. Dmitriev, H.W. Gäggeler, V.A. Gorshkov, F. Haenssler, M.G. Itkis, V.Ya. Lebedev, A. Laube, O.N. Malyshev, Yu.Ts. Oganessian, O.V. Petrushkin, D. Piguet, P. Rasmussen, S.V. Shishkin, A.V. Shutov, A.I. Svirikhin, E.E. Tereshatov, G.K. Vostokin, M.Wegrzecki, and A.V. Yeremin. Chemical characterization of element 112. *Nature*, 447:72, 2007.

[200] H. W. Gäggeler, W. Brüchle, Ch. E. Dülmann, R. Dressler, K. Eberhardt, B. Eichler, R. Eichler, C.M. Folden, T. N. Ginter, F. Glaus, K. E. Gregorich, F. Haenssler, D. C. Hoffman, E. Jäger, D. T. Jost, U. W. Kirbach, J.V. Kratz, H. Nitsche, J. B. Patin, V. Pershina, D. Piguet, Z. Qin, U. Rieth, M. Schädel, E. Schimpf, B. Schausten, S. Soverna, R. Sudowe, P. Thörle, N. Trautmann, A. Türler, A. Vahle, P.A. Wilk, G. Wirth, A. B. Yakushev, , and A. von Zweidorf. Chemical and nuclear studies of Hassium and element 112. *Nucl. Phys. A*, 734:208, 2004.

[201] A.B. Yakushev, I. Zvara, Yu.Ts. Oganessian, A.V. Belozerov, S.N. Dmitriev, B. Eichler, S. Hübener, A. Türler EA. Sokol, A.V.Yeremin, G.V.

Buklanov, M.L. Chelnokov, V.I. Chepigin, V.A. Gorshkov, A.V. Gulyaev, V.Ya. Lebedev, O.N. Malyshev, A.G. Popeko, S. Soverna, Z. Szeglowski, S.N. Timokhin, S.P. Tretyakova, V.M. Vasko, and M.G. Itkis. Chemical identification and properties of element 112. *Nucl. Phys. A*, 734:204, 2004.

[202] M. Sewtz, H. Backe, A. Dretzke, G. Kube, W. Lauth, P. Schwamb, K. Eberhardt, C. Grüning, P. Thörle, N. Trautmann, P. Kunz, J. Lassen, G. Passler, C. Z. Dong, S. Fritzsche, and R. G. Haire. First observation of atomic levels for the element fermium (Z=100). *Phys. Rev. Lett.*, 90:163002, 2003.

[203] D. C. Hoffman. Atom-at-a-time studies of the transactinide elements. *J. Radioanalyt. Nucl. Chem.*, 276:525, 2008.

[204] M. Roberts, P. Taylor, G. P. Barwood, P. Gill, H. A. Klein, and W. R. C. Rowley. Observation of an electric octupole transition in a single ion. *Phys. Rev. Lett.*, 78:1876, 1997.

[205] U. Hechtfischer, Z. Amitay, P. Forck, M. Lange, J. Linkemann, M. Schmitt, U. Schramm, D. Schwalm, R. Wester, D. Zajfman, and A. Wolf. Near-threshold photodissociation of cold CH^+ in a storage ring. *Phys. Rev. Lett.*, 80:2809, 1998.

[206] K. Mølhave and M. Drewsen. Formation of translationally cold MgH^+ and MgD^+ molecules in an ion trap. *Phys. Rev. A*, 62:011401(R), 2000.

[207] M. Drewsen, A. Mortensen, R. Martinussen, P. Staanum, and J. L. Sørensen. Nondestructive identification of cold and extremely localized single molecular ions. *Phys. Rev. Lett.*, 93:243201, 2004.

[208] K. Højbjerre, D. Offenberg, C. Z. Bisgaard, H. Stapelfeldt, P. F. Staanum, A. Mortensen, and M. Drewse. Consecutive photodissociation of a single complex molecular ion. *Phys. Rev. A*, 77:030702(R), 2008.

[209] R. Eichler, W. Brüchle, R. Dressler, Ch. E. Düllmann, B. Eichler, H. W. Gäggeler, K. E. Gregorich, D. C. Hoffman, S. Hübener, D. T. Jost, U. W. Kirbach, C. A. Laue, V. M. Lavanchy, H. Nitsche, J. B. Patin, D. Piguet, M. Schädel, D. A. Shaughnessy, D. A. Strellis, S. Taut, L. Tobler, Y. S.

Tsyganov, A. Türler, A. Vahle, P. A. Wilk, and A. B. Yakushev. Chemical characterization of Bohrium (element 107). *Nature*, 407:63, 2000.

[210] P. Schwerdtfeger and M. Seth. *in: P. von R. Schleyer, N. L. Allinger, T. Clark, J. Gasteiger, P.A. Kollmann (et.), Encyclopedia of Computational Chemistry*. Wiley-VCH, 1998.

[211] B. Fricke. Superheavy elements a prediction of their chemical and physical properties. *Struct. Bonding*, 21:90, 1975.

[212] V. Pershina. Theoretical predictions of properties and chemical behavior of superheavy elements. *J. Nucl. Radiochem. Sci.*, 3:137, 2002.

[213] V. Pershina. *in Relativistic Electronic Structure Theory. Part 2. Applications. P. Schwerdtfeger (Ed.)*. Elsevier, Amsterdam, 2004.

[214] M. Seth, K. Faegri, and P. Schwerdtfeger. The stability of the oxidation state +4 in group 14 compounds from carbon to element 114. *Angew. Chem.*, 37:2493, 1998.

[215] N. Gaston, I. Opahle, H. W. Gäggeler, and P. Schwerdtfeger. Is Eka-Mercury (element 112) a group 12 metal? *Angew. Chem. Int. Ed.*, 46:1663, 2007.

[216] V. Pershina, W.-D. Sepp, T. Bastug, B. Fricke, and G. V. Ionova. Relativistic effects in physics and chemistry of element 105. III. Electronic structure of hahnium oxyhalides as analogs of group 5 elements oxyhalides. *J. Chem. Phys.*, 97:1123, 1992.

[217] V. Pershina. Electronic structure and properties of the transactinides and their compounds. *Chem. Rev.*, 96:1977, 1997.

[218] P. Schwerdtfeger. *in Strength from Weakness: Structural Consequences of Weak Interactions in Molecules, Supermolecules, and Crystals, A. Domenicano, I. Hargittai (eds.), NATO Science Series*. Kluwer, Dordrecht, 2002.

[219] V. Pershina and T. Bastug. Relativistic effects on experimentally studied gas-phase properties of the heaviest elements. *Chem. Phys.*, 311:139, 2005.

[220] V. Pershinaa, T. Bastug, and B. Fricke. Relativistic effects on the electronic structure and volatility of group-8 tetroxides MO_4, where M=Ru, Os, and element 108, Hs. *J. Chem. Phys.*, 122:124301, 2005.

[221] P. Schwerdtfeger. *in Progress in Theoretical Chemistry and Physics - Theoretical chemistry and physics of heavy and superheavy elements U. Kaldor, S. Wilson (eds.)*. Kluwer Academic, 2003.

[222] W. Liu and C. van Wüllen. Spectroscopic constants of Gold and Eka-Gold (element 111) diatomic compounds: The importance of spin-orbit coupling. *J. Chem. Phys.*, 110:3730, 1999.

[223] J. Anton, B. Fricke, and P. Schwerdtfeger. Non-collinear and collinear four-component relativistic molecular density functional calculations. *Chem. Phys.*, 311:97, 2005.

[224] R. Wesendrup, J. K. Laerdahl, and P. Schwerdtfeger. Relativistic effects in Gold chemistry. VI. Coupled-cluster calculations for the isoelectronic series $AuPt^-$, Au_2 and $AuHg^+$. *J. Chem. Phys.*, 110:9457, 1999.

[225] P. Schwerdtfeger, J. R. Brown, J. K. Laerdahl, and H. Stoll. The accuracy of the pseudopotential approximation. III. A comparison between pseudopotential and all-electron methods for Au and AuH. *J. Chem. Phys.*, 113:7110, 2000.

[226] M. Seth, P. Schwerdtfeger, M. Dolg, K. Faegri, B. A. Hess, and U. Kaldor. Large relativistic effects in molecular properties of the hydride of superheavy element 111. *Chem. Phys. Lett.*, 250:461, 1996.

[227] M. Seth and P. Schwerdtfeger. A comparison of relativistic and electron correlation effects for (111)F, (111)H and (111)Li. *Chem. Phys. Lett.*, 318:314, 2000.

[228] Y.-K. Han and K. Hirao. Two-component coupled-cluster calculations for the hydride of element 111: On the performance of relativistic effective core potentials. *Chem. Phys. Lett.*, 328:453, 2000.

[229] M. Dolg, H. Stoll, M. Seth, and P. Schwerdtfeger. On the performance of energy-consistent spin-orbit pseudopotentials: (111)H revisited. *Chem. Phys. Lett.*, 345:490, 2001.

[230] P. Pyykkö and M. Atsumi. Molecular single-bond covalent radii for elements 1 - 118. *Chem. Eur. J.*, 15:186, 2009.

[231] T. Nakajima and K. Hirao. Numerical illustration of third-order DouglasKroll method: Atomic and molecular properties of superheavy element 112. *Chem. Phys. Lett.*, 329:511, 2000.

[232] C.S. Nash. Atomic and molecular properties of elements 112, 114, and 118. *J. Phys. Chem. A*, 109:3493, 2005.

[233] N. S. Mosyagin, T. A. Isaev, and A. V. Titov. Is E112 a relatively inert element? Benchmark relativistic correlation study of spectroscopic constants in E112H and its cation. *J. Chem. Phys.*, 124:224302, 2006.

[234] M. Seth, P. Schwerdtfeger, and K. Faegri. The chemistry of superheavy elements. III. Theoretical studies on element 113 compounds. *J. Chem. Phys.*, 111:6422, 2001.

[235] Y.-K. Han, C. Bae, S.-K. Son, and Y. S. Lee. Spin-orbit effects on the transactinide p-block element monohydrides MH (M = element 113-118). *J. Chem. Phys.*, 112:2684, 2000.

[236] Y. J. Choi, Y.-K. Han, and Y. S. Lee. The convergence of spinorbit configuration interaction calculations for TlH and (113)H. *J. Chem. Phys.*, 115:3448, 2001.

[237] Y. J. Choi and Y. S. Lee. Spinorbit density functional theory calculations for heavy metal monohydrides. *J. Chem. Phys.*, 119:2014, 2003.

[238] D. Peng, W. Liu, Y. Xiao, and L. Cheng. Making four- and two-component relativistic density functional methods fully equivalent based on the idea of from atoms to molecule. *J. Chem. Phys.*, 127:104106, 2007.

[239] A. Landau, E. Eliav, Y. Ishikawa, and U. Kaldor. Benchmark calculations of electron affinities of the alkali atoms Sodium to Eka-Francium (element 119). *J. Chem. Phys.*, 115:2389, 2001.

[240] I. Lim, J. K. Laerdahl, and P. Schwerdtfeger. Fully relativistic coupled-cluster static dipole polarizabilities of the positively charged alkali ions from Li^+ to 119^+. *J. Chem. Phys.*, 116:172, 2002.

[241] I. S. Lim, P. Schwerdtfeger, B. Metz, and H. Stoll. All-electron and relativistic pseudopotential studies for the group 1 element polarizabilities from K to element 119. *J. Chem. Phys.*, 122:104103, 2005.

[242] T. H. Dinh, V. A. Dzuba, V. V. Flambaum, and J. S. M. Ginges. Calculations of the spectra of superheavy elements Z=119 and Z=120^{+}. *Phys. Rev. A*, 78:022507, 2008.

[243] K. G. Dyall. An exact separation of the spin-free and spin-dependent terms of the Dirac-Coulomb-Breit Hamiltonian. *J. Chem. Phys.*, 100:2118, 1994.

[244] L. Visscher, T. J. Lee, and K. G. Dyall. Formulation and implementation of a relativistic unrestricted coupled-cluster method including noniterative connected triples. *J. Chem. Phys.*, 105:8769, 1996.

[245] L. Visscher, P. J. C. Aerts, O. Visser, and W. C. Nieuwpoort. Kinetic balance in contracted basis sets for relativistic calculations. *Int. J. Quantum Chem. Symp.*, 25:131, 1991.

[246] L. Visscher and K. G. Dyall. Dirac-Fock atomic electronic structure calculations using different nuclear charge distributions. *At. Data Nucl. Data Tables*, 67:207, 1997.

[247] Jr. T.H. Dunning. Gaussian basis sets for use in correlated molecular calculations. I. The atoms Boron through Neon and Hydrogen. *J. Chem. Phys.*, 90:1007, 1989.

[248] R. A. Kendall, T. H. Dunning, and R. J. Harrison. Electron affinities of the first-row atoms revisited. Systematic basis sets and wave functions. *J. Chem. Phys.*, 96:6796, 1992.

[249] K. Dyall and K. Faegri Jr. Kinetic balance and variational bounds failure in the solution of the Dirac equation in a finite Gaussian basis set. *Chem. Phys. Lett.*, 174:25, 1990.

[250] S. F. Boys and F. Bernardi. The calculation of small molecular interactions by the differences of separate total energies. some procedures with reduced errors. *Mol. Phys.*, 19:533, 1970.

[251] U. Kaldor. The Fock-space coupled-cluster method: Theory and application. *Theor. Chim. Acta*, 80:427, 1991.

[252] A. Landau, E. Eliav, and U. Kaldor. Intermediate Hamiltonian Fock-space coupled-cluster method. *Chem. Phys. Lett.*, 313:399, 1999.

[253] E. Eliav, U. Kaldor, P.Schwerdtfeger, B.Hess, and Y.Ishikawa. Ground state electron configuration of element 111. *Phys. Rev. Lett.*, 73:3203, 1994.

[254] G. Brown and D. G. Ravenhall. On the interaction of two electrons. *Proc. R. Soc. A*, 208:552, 1951.

[255] J.P. Desclaux. Relativistic dirac-fock expectation values for atoms with Z = 1 to Z = 120. *At. Data Nucl. Data Tables*, 12:311, 1973.

[256] P. Schwerdtfeger and M. Seth. *in The Encyclopedia of Computational Chemistry (P. von R. Schleyer, N. L.Allinger, T. Clark, J. Gasteiger, P. Kollman, H. F. Schaefer III (Eds.)*. Wiley, New York, 1998.

[257] P. Pyykkö and J. P. Desclaux. Relativity and the periodic system of elements. *Acc. Chem. Res.*, 12:276, 1979.

[258] M. Seth, M. Dolg, P. Fulde, and P. Schwerdtfeger. Lanthanide and actinide contractions: Relativistic and shell structure effects. *J. Am. Chem. Soc.*, 117:6597, 1995.

[259] J. Autschbach, S. Siekierski, M. Seth, P. Schwerdtfeger, and W. H. E. Schwarz. The dependence of relativistic effects on the electronic configurations in the atoms of the d- and f-block elements. *J. Comput. Chem.*, 23:804, 2002.

[260] E. Eliav, U. Kaldor, Y. Ishikawa, M. Seth, and P. Pyykkö. Calculated energy levels of Thallium and Eka-Thallium (element 113). *Phys. Rev. A*, 53:3926, 1996.

[261] P. Pyykkö. Dirac-Fock one-centre calculations. Part 7. Divalent systems MH^+ and MH_2 (M = Be, Mg, Ca, Sr, Ba, Ra, Zn, Cd, Hg, Yb and No). *J. Chem. Soc., Faraday Trans. II*, 75:1256, 1978.

[262] P. Pyykkö, J. G. Snijders, and E. J. Baerends. On the effect of d-orbitals on relativistic bond-length contractions. *Chem. Phys. Lett.*, 83:432, 1981.

[263] C.E. Moore. *Atomic Energy Levels*. Natl. Bur. Stand. (U.S.) Circ. No. 467; U.S. GPO: Washington D.C., 1958.

[264] P. Schwerdtfeger, M. Dolg, W. H. E.Schwarz, G. A. Bowmaker, and P.D.W. Boyd. Relativistic effects in Gold chemistry. I. Diatomic Gold compounds. *J. Chem. Phys.*, 91:1762, 1989.

[265] K.P. Huber and G. Herzberg. *Molecular Spectra and Molecular Structure Constants of Diatomic Molecules*. Van Nostrand, 1979.

[266] A.J. Sadlej and M. Urban. Medium-size polarized basis sets for high-level-correlated calculations of molecular electric properties. III. Alkali (Li, Na, K, Rb) and alkaline-earth (Be, Mg, Ca, Sr) atoms. *J. Mol. Struct.*, 234:147, 1991.

[267] A.S.P. Gomes and L. Visscher. The influence of core-correlation on the spectroscopic constants of HAt. *Chem. Phys. Lett.*, 399:1, 2004.

[268] J.P. Perdew and S. Kurth. *A primer in density functional theory. In: C. Fiolhais, F. Nogueria, M. Marques (eds.), Lecture Notes in Physics, Vol.620*. Springer, 2003.

[269] S. Kristyán and P. Pulay. Can (semi)local density functional theories account for the london dispersion forces? *Chem. Phys. Lett.*, 229:175, 1994.

[270] W. Kohn, Y. Meir, and D.E. Makarov. Van der Waals energies in density functional theory. *Phys. Rev. Lett.*, 80:4153, 1998.

[271] J.A. Alonso and A. Mananes. Long-range Van der Waals interactions in density functional theory. *Theor. Chem. Acc.*, 117:467, 2007.

[272] M. Cococcioni and S. de Gironcoli. Linear response approach to the calculation of the effective interaction parameters in the LDA + U method. *Phys. Rev. B*, 71:035105, 2005.

[273] J.N. Harvey. *in Structure and Bonding, edited by N. Kaltsoyannis and J.E. McGrady*. Springer, 2004.

[274] Y. Nakao, K. Hirao, and T. Taketsugu. Theoretical study of first-row transition metal oxide cations. *J. Chem. Phys.*, 114:7935, 2001.

[275] S. Patchkovskii and T. Ziegler. Improving difficult reaction barriers with self-interaction corrected density functional theory. *J. Chem. Phys.*, 116:7806, 2002.

[276] J.W. Song, T. Hirosawa, T. Tsuneda, and K. Hirao. Long-range corrected density functional calculations of chemical reactions: Redetermination of parameter. *J. Chem. Phys.*, 126:154105, 2007.

[277] Z.-L. Cai, M.J. Crossley, J.R. Reimers, R. Kobayashi, and R.D. Amos. Density functional theory for charge transfer: The nature of the n-bands of porphyrins and chlorophylls revealed through CAM-B3LYP, CASPT2, and SAC-CI calculations. *J. Phys. Chem. B*, 110:15624, 2006.

[278] P. Schwerdtfeger, M. Pernpointner, and J.K. Laerdahl. The accuracy of current density functionals for the calculation of electric field gradients: A comparison with ab initio methods for HCl and CuCl. *J. Chem. Phys.*, 111:3357, 1999.

[279] E. van Lenthe and E.J. Baerends. Density funtional calculations of nuclear quadupole coupling constants in the zero-order regular approximation for relativistic effects. *J. Chem. Phys.*, 112:8279, 2000.

[280] P. Schwerdtfeger, M. Pernpointner, and W. Nazarewicz. *Theory and Applications. In: M. Kaupp, M. Bühl, V. G. Malkin (ed.), Calculation of NMR and EPR Parameters.* Wiley-VCH, 2004.

[281] P. Blaha, K. Schwarz, and P. Novak. Electric field gradients in cuprates: Does LDA+U give the correct charge distribution? *Int. J. Quantum Chem.*, 101:550, 2005.

[282] E.T. Yanai, D.P. Tew, and N.C. Handy. A new hybrid exchange-correlation functional using the Coulomb-attenuating method (CAM-B3LYP). *Chem. Phys. Lett.*, 393:51, 2004.

[283] H. Sekino, Y. Maeda, M. Kamiya, and K. Hirao. Polarizability and second hyperpolarizability evaluation of long molecules by the density functional theory with long-range correction. *J. Chem. Phys.*, 126:014107, 2007.

[284] P. Schwerdtfeger, T. Söhnel, M. Pernpointner, J.K. Laerdahl, and F.E. Wagner. Comparison of ab initio and density functional calculations of electric field gradients: The ^{57}Fe nuclear quadrupole moment from Mõssbauer data. *J. Chem. Phys.*, 115:5913, 2001.

[285] G. Martinez-Pinedo, E. Caurier, K. Langanke, W. Nazarewicz, T. Söhnel, and P. Schwerdtfeger. The nuclear quadrupole moment of ^{57}Fe from microscopic nuclear and atomic calculations. *Phys. Rev. Lett.*, 87:062701, 2001.

[286] R. Bast and P. Schwerdtfeger. The accuracy of current density functionals for electric field gradients. test calculations for ScX, CuX and GaX (X=F, Cl, Br, I, H and Li). *J. Chem. Phys.*, 119:5988, 2003.

[287] E. Goll, H. Stoll, C. Thierfelder, and P. Schwerdtfeger. Improved dipole moments by combining short-range gradient-corrected density-functional theory with long-range wave-function methods. *Phys. Rev. A*, 76:032507, 2007.

[288] M.J.G. Peach, T. Helgaker, P. Salek, T.W. Keal, O.B. Lutnæs, D.J. Tozer, and N.C. Handy. Assessment of a Coulomb-attenuated exchange-correlation energy functional. *Phys. Chem. Chem. Phys.*, 8:558, 2006.

[289] H. Stoll and A. Savin. *in Density Functional Methods in Physics, edited by R. Dreizler and J. da Providencia*. Plenum, 1985.

[290] E.A.C. Lucken. *Nuclear Quadrupole Coupling Constants*. Academic Press, 1969.

[291] D.E. Woon and Jr. T.H. Dunning. Gaussian basis sets for use in correlated molecular calculations. III. The atoms Aluminum through Argon. *J. Chem. Phys.*, 98:1358, 1993.

[292] A.K. Wilson, D.E. Woon, K.A. Peterson, and Jr. T.H. Dunning. Gaussian basis sets for use in correlated molecular calculations. IX. The atoms Gallium through Krypton. *J. Chem. Phys.*, 110:7667, 1999.

[293] C.J. Evans and M.C.L. Gerry. The pure rotational spectra of AuCl and AuBr. *J. Mol. Spectr.*, 203:105, 2000.

[294] L.M. Reynolds, C.J. Evans, and M.C.L. Gerry. The pure rotational spectrum of AuI. *J. Mol. Spectr.*, 205:344, 2001.

[295] T. Okabayashi, E.Y. Okabayashi, M. Tanimoto, T. Furuya, and S. Saito. Rotational spectroscopy of AuH and AuD in the $^1\Sigma^+$ electronic ground state. *Chem. Phys. Lett.*, 422:58, 2006.

[296] C.J. Evans, L.M. Reynard, and M.C.L. Gerry. Pure rotational spectra, structures, and hyperfine constants of OC-AuX (X = F, Cl, Br). *Inorg. Chem.*, 40:6123, 2001.

[297] N.R. Walker, S.G. Francis, S.L. Matthews, J.J. Rowlands, and A.C. Legon. Microwave spectrum and structure of carbonyl Gold iodide, OCAuI. *Mol. Phys.*, 104:3329, 2006.

[298] N.R. Walker and M.C.L. Gerry. Microwave spectra, geometries, and hyperfine constants of OCCuX (X = F, Cl, Br). *Inorg. Chem.*, 40:6158, 2001.

[299] S.G. Batten and A.C. Legon. OCCuI synthesized by reaction of laser-ablated Cu with a $CH_3I/CO/Ar$ mixture and characterised by pulsed-jet, fourier-transform microwave spectroscopy. *Chem. Phys. Lett.*, 422:192, 2006.

[300] L. Belpassi, F. Tarantelli, A. Sgamellotti, H.M. Quiney, J.N.P. van Stralen, and L. Visscher. Nuclear electric quadrupole moment of Gold. *J. Chem. Phys.*, 126:064314, 2007.

[301] W.H. Press, S.A. Teukolsky, W.T. Vettering, and B.P. Flannery. *Numerical recepies in Fortran 77*. Cambridge University Press, 1992.

[302] P. Pyykkö. *Nuclear quadrupole moments, Report Huki 1-92, Helsinki, available from* `http://www.shef.ac.uk/uni/academic/A-C/chem/web-elements/`. , 1992.

[303] R.J. Powers, P. Martin, G.H. Miller, R.E. Welsh, and D.A. Jenkins. Muonic ^{197}Au: A test of the weak-coupling model. *Nucl. Phys. A*, 230:413, 1974.

[304] W.M. Itano. Quadrupole moments and hyperfine constants of metastable states of Ca^+, Sr^+, Ba^+, Yb^+, Hg^+, and Au. *Phys. Rev. A*, 73:022510, 2006.

[305] P. Palade, F.E. Wagner, A.D. Jianu, and G. Filoti. Electronic properties of Gold-Aluminium intermetallic compounds. *J. Alloys Compounds*, 353:23, 2003.

[306] C. Clavaguéra, J.-P. Dognon, V. Kellö, P. Pyykkö, A.J. Sadlej, and P. Schwerdtfeger. *to be published*.

[307] H. Yakobi, E. Eliav, and U. Kaldor. Nuclear quadrupole moment of ^{197}Au from high-accuracy atomic calculations. *J. Chem. Phys.*, 126:184305, 2007.

[308] J. Thyssen, J.K. Laerdahl, and P. Schwerdtfeger. Fully relativistic coupled-cluster treatment for parity-violating energy differences in molecules. *Phys. Rev. Lett.*, 85:3105, 2000.

[309] C. Thierfelder, P. Schwerdtfeger, and T. Saue. ^{63}Cu and ^{197}Ag nuclear quadrupole moments form four-component relativistic density functional calculations. *Phys. Rev A*, 76:034502, 2007.

[310] M. Maggiore. *A Modern Introduction to Quantum Field Theory*. Oxford Press, 2005.